Modulation of El Niño - Southern Oscillation and its impacts by the mean climate state

Paloma Trascasa-Castro

School of Earth and Environment

University of Leeds

A thesis submitted for the degree of

Doctor of Philosophy

August 2023

Para Fina, mi madre.

Saliendo del baño, Joaquín Sorolla (1915).

Declaration

I confirm that the work submitted in this thesis is my own, except where work which has formed part of jointly-authored publications has been included. My contributions to jointly-authored papers and that of the other authors is explicitly indicated below. I confirm also that appropriate credit has been given within this thesis where reference has been made to the work of others.

The majority of the research included in the thesis, in Chapters 2 and 3, has been peer-reviewed and published. The remaining research in Chapter 4 has been prepared for submission to a peer-reviewed journal. This thesis is published using the University of Leeds alternative thesis format, which allows the research within it to be readily identified and accessed.

Chapter 2 has been published in Geophysical Research Letters as the following:

Trascasa-Castro, P., Ruprich-Robert, Y., Castruccio, F., Maycock, A. C. (2021). Warm phase of AMV damps ENSO through weakened thermocline feedback. *Geophysical Research Letters, 48(23), e2021GL096149.*
https://doi.org/10.1029/2021GL096149

The author contributions to this work are:

Paloma Trascasa-Castro: Original paper idea, performed the analysis, made the plots, wrote the paper. **Yohan Ruprich-Robert**: Development of idea. Active participation, results discussion and contribution to writing the paper. **Amanda Maycock**: Development of idea. Active participation, results discussion and contribution to writing up the paper. **Fred Castruccio**: Run the idealised AMV simulations with the NCAR-CESM1 model whose output we analysed.

Chapter 3 has been published in Environmental Research Letters as the following:

Trascasa-Castro, P., Maycock, A. C., Ruprich-Robert, Y., Turco, M., Staten, P. W. (2023). Atlantic Multidecadal Variability modulates the climate impacts of El Niño-Southern Oscillation in Australia. *Environmental Research Letters. 18*. https://doi.org/10.1088/1748-9326/ace920

The author contributions to this work are:

Paloma Trascasa-Castro: Original paper idea, performed most of the analysis, made the plots and wrote the paper. **Amanda Maycock**: Development of idea. Active participation, results discussion and contribution to writing up the paper. **Yohan Ruprich-Robert**: Development of idea. Active participation, results discussion and contribution to writing up the paper. **Marco Turco**: Performed the analysis to estimate the empirical relationship between the Standardised Precipitation Evapotranspiration index and Burned Area over Southeastern Australia. Revised the manuscript and provided comments before submitting it. **Paul Staten**: Provided and assisted with the code to separate the Walker and Hadley circulation components. Revised the manuscript and provided comments before submitting it.

The work in **Chapter 4** of the thesis is prepared as a manuscript to be submitted to Journal of Climate as follows: Trascasa-Castro, P., Ruprich-Robert, Y and Maycock, A. Future climate response to very strong El Niño events.

The author contributions to this work are:

Paloma Trascasa-Castro: Original idea, run the simulations with the EC-Earth3-CC model, analysed the output and wrote the chapter. **Yohan Ruprich-Robert**: Development of idea. Provided training to run the model, assisted in the experimental design, results discussion. **Amanda Maycock**: Development of idea. Assisted in the experimental design, results discussion.

Acknowledgements

As Jack the Ripper said, let's go by parts.

First and foremost I want to thank my advisors Prof Amanda Maycock and Dr Yohan Ruprich-Robert for their invaluable guidance, patience and contribution to this doctoral thesis, which is the result of many many hours discussing cool science. Amanda, a massive thank you for giving me all the opportunities and trust you have given me since we met back in 2017. Thanks for all the doors you opened for me and for your encouragement to present at all the conferences I attended. I admire your infinite curiosity about science in general and your work as a world-leading researcher on climate change. Yohan, merci beaucoup for your empathy, for all your formulas and full whiteboards, your help running EC-Earth and your patience those days when I was extra stubborn and got tempted to go back to my swimming pool and work as a lifeguard again. I have never seen an advisor spending so much time with their students, and I really appreciate that.

Thanks to my thesis examiners, Mat Collins and Ian Brooks, for an interesting discussion during the viva and for providing useful and constructive feedback. Thanks to my teachers, who helped me being here today. Thanks to Elena Ibáñez for seeing beyond this clown at school. Thanks to Germán Poveda at the Universidad Nacional de Colombia (Medellín) for introducing me to the beautiful world of ENSO. Thanks to Felipe Fernández and Fernando Allende at the Universidad Autónoma de Madrid for your guidance in the last steps of my undergraduate degree, and to Jose Antonio López Díaz for your kindness and everything you taught me during my internship at

AEMet. Thanks to Ryan Neely and the MRes lecturers at the University of Leeds for helping me build the foundations of my research skills. Thanks to the inspiring women I had the opportunity to meet throughout my PhD and discuss science, specially Nicola Maher, Antonietta Capotondi, Froila Palmeiro and Marta Martín del Rey.

I would like to thank the Physical Climate Change group at Leeds for their feedback and interest in my work, specially Piers, Lauren, Ruza, Alex and Chris. It has been a true privilege to grow surrounded by such an amazing team of top scientists. Thanks Richard Rigby for all your technical help. Thanks to Andreas for the tips and our meals at Mediterranean time. Thanks to my friends in Leeds, Yvan and Molly for the walks, the fun and not-so-fun moments; Christine, Will, Essie, Tom, Chetan, Michael, Laura, Jorge, Rashmi, Liam, Alberto, Lamprini and Marcos, for being part of such an important chapter of my life. Thank you Bianca for dreaming with me in the exciting times of The Climate Press.

Moving now to the south, I would like to thank the Climate Variability and Change and Earth System Services group at the Barcelona Supercomputing Center for your warm welcome. Thanks to Kim, Eric, Pierre Antoine and Marga for their technical support. Thanks Marco Turco for the discussions about fires. Special thanks go to Andrea, Vero, Eneko and Aude for making every day beautiful at work. Thanks to my flatmates, a mi cronopio Juan, to Dani and María for your cheerleading. Thanks to Julia, for all the laughs, the conferences, the surprises, the songs, you are always so far and yet so close. Thanks to all my friends at BSC, specially Euli, Raquel, Pep, Carlos, Jaume, Cris, Elisa, Saskia, Alba, Albert, Amanda, Bernat, Bala, Bianca, Gert, Lluis, Kat, Nadia, Martín, Nuria, Stella, Ángel and Carmen... thanks for the beers, the calçots, the guitar, and the climbing, for making me feel at home from day 1. Aleks, you have filled these last months with excitement, care, fun, support, beautiful

energy, mountains and beach. I can't wait for all the adventures to come. Merci per tot, compinche.

Gracias a mis amigos de Madrid, en especial a Bolita, Sonia, Pedro, Juanma, Barbi, Barrio y Javi, y a mis amigos de la UAM, por las rutas, los ánimos y el interés constante en lo que estaba haciendo. Gracias Adri, por el hilo invisible que nos mantiene cerca a la distancia.

Like The Beatles said: "I got by with a (*not so*) little help from my friends".

Finally, I would like to thank my family for their inconditional love and support. Gracias a mi abuelita María, por cuidarme desde las alturas. Gracias a toda la familia Castro, a mis primos, titas y sobre todo a mi tito Miguelín y a mi tita Carmela, por leereos mis artículos. Gracias de todo corazón a mis hermanos, Ángel, Rodrigo y Fina (¡feliz cumpleaños!), os siento siempre a mi lado, también a mis cuñados Aurélie, Mariana y Zamo. Gracias a mis sobrinos Natalia y Rubén, por inyectarme felicidad pura por un tubo, sois las flores que siempre quise en mi jardín.

Por último, gracias mamá por tu alegría, tus inventos, los tuppers, por apoyar siempre mis ideas locas, mis viajes, por venir a verme a todas partes. Por todas las noches sin dormir, por las lágrimas en los aeropuertos, este trabajo va por tí.

Abstract

This doctoral thesis aims to understand how changes in the background climate state can affect the dynamics and regional impacts of El Niño-Southern Oscillation (ENSO). Given the global reach of ENSO teleconnections, it is key to understand how natural and anthropogenic sources of climate variability modulate its dynamics, in order to improve the resilience of ecosystems and populations to ENSO impacts. Climate interactions between the Atlantic and Pacific Oceans at different timescales modulate the tropical Pacific mean state and ENSO variability. Firstly I use the NCAR-CESM1 model to investigate how Atlantic Multidecadal Variability (AMV) modulates ENSO. Under warm AMV conditions (AMV+), ENSO variability weakens, relative to AMV-. In AMV+, the thermocline is less reactive to surface wind stress anomalies, which are more confined over the western equatorial Pacific. Building on the first results chapter, I explore the AMV modulation of ENSO impacts over Australia in austral summer, and find that AMV strengthens the climate response to ENSO in western Australia and weakens it over the east. AMV alters the Hadley circulation response to ENSO, ultimately modulating its extratropical teleconnections. Finally, a set of pacemaker simulations are performed with the EC-Earth3-CC model to understand how the impacts of very strong El Niño, such as the ones observed in 1982/83, 1997/98 and 2015/16 would manifest in a future warmer climate. The simulations reveal that the impacts of extreme El Niño events will amplify in the future in some regions, including North America and Australia, where the cold and hot anomalies during winter and summer, respectively, will get amplified during very strong El Niño events. In other regions, like Southern Africa and southeastern South America, shifts in atmospheric circulation lead to a weakening of the simulated impacts of very strong El Niño events. Overall, this thesis has further demonstrated that both ENSO variability and teleconnections are sensitive to changes in the background climate state induced by AMV and anthropogenic emissions of greenhouse gases.

Abbreviations

AMOC	Atlantic Meridional Overturning Circulation
AMV	Atlantic Multidecadal Variability
BA	Burned Area
BJ	Bjerknes Stability index
CGCM	Coupled General Circulation Model
CMIP	Climate Model Intercomparison Project
CP	Central Pacific
DCPP	Decadal Climate Prediction Project
DO	Delayed Oscillator
EP	Eastern Pacific
ENSO	El Niño Southern Oscillation
GHG	Greenhouse gas
IPCC	Intergovernmental Panel on Climate Change
ITCZ	Intertropical Convergence Zone
NAO	North Atlantic Oscillation
NPO	North Pacific Oscillation
PNA	Pacific North American
PSA	Pacific South American
RO	Recharge Oscillator
SPCZ	South Pacific Convergence Zone
SPEI	Standardized Precipitation Evapotranspiration Index
SSP	Shared Socioeconomic Pathway
SST	Sea Surface Temperature
TNA	Tropical North Atlantic

Contents

List of Figures

Chapter 1

Introduction

Surely in Meteorology, as in Astronomy, the thing to hunt down is a cycle, and if that is not to be found in the temperate zone, then go to the frigid zones or the torrid zones to look for it, and if found, then above all things and in whatever manner, lay hold to it, study it, record it and see what it means.

The Meteorology of the future, Norman Lockyer.

1.1. Motivation

Despite the very large dimensionality and chaotic nature of Earth's climate system, there are many emergent quasi-periodic seesaws and oscillations that manifest as internal climate variability. Many of these internal 'modes of variability' emerge as a result of tight coupling between components of the climate system.

This thesis focuses on El Niño-Southern Oscillation (ENSO), arguably the most well known example of coupling between the ocean and the atmosphere. ENSO is a natural climate phenomenon that manifests primarily in the equatorial Pacific Ocean and leads to global-scale effects, from suppressing the Indian Monsoon rainfall (Kumar et al., 1999) to weakening the stratospheric polar vortex (Ineson and Scaife, 2009) during El Niño (its warm phase), to flooding in Australia during La Niña (its cold phase) (Chung and Power, 2017), among many other impacts on ecosystems and populations.

Natural modes of climate variability can interfere with each other at different timescales (Elsbury et al., 2019; Muñoz et al., 2015). The fact that ENSO excites other modes of variability is well known (Chang et al., 2006). In the last decades, several studies have demonstrated the bidirectional nature of these interactions, with Atlantic (Rodríguez-Fonseca et al., 2009; Ruprich-Robert et al., 2021), and Indian (Kug and Kang, 2006) Ocean modes feeding back to the Pacific by driving changes in atmospheric circulation (Cai et al., 2019). Historical records allow us to gain a general picture of the global impacts of El Niño and La Niña (see Fig. 1.4). However, there is a large diversity in ENSO events in terms of their development, dynamics, magnitude, spatial location of anomalous sea surface temperatures (SSTs) and regional teleconnections. Teleconnections refer to a robust and significant response to a specific mode of climate variability (in this case ENSO) in locations outside the forcing region (the equatorial Pacific Ocean). Ocean basins outside the tropical Pacific play a role, for instance in the duration and amplitude of ENSO, as it has been suggested in the context of the last three-year La Niña event (2020-2022) (Hasan et al., 2022); and also in the

modulation of ENSO-related droughts in the Amazon (Jimenez et al., 2019).

In particular, the role of Atlantic Multidecadal Variability (AMV) as a potential modulator of ENSO variability has gained attention in the recent years (Dong and Sutton, 2007; Levine et al., 2017). Understanding the mechanisms by which AMV modulates ENSO variability and teleconnections offers the potential to improve ENSO forecasts as well as understand sources of variability in ENSO teleconnections.

In addition to the effects of natural phenomena, external forcings also drive changes in the global climate system. Due to human activities, the Earth's temperature has increased by 1.1°C since the 1850s (Arias et al., 2021). Should the planet continue to warm under rising greenhouse gases, the spatial structure, amplitude and frequency of ENSO events is expected to change in the future (Cai et al., 2022; Collins et al., 2010; Maher et al., 2023). The hydrological cycle also responds to an increase in temperature in the atmosphere (following the Clausius-Clapeyron relationship from a thermodynamic perspective), altering future ENSO teleconnections across the planet (Johnson et al., 2022; McGregor et al., 2022; Müller and Roeckner, 2006).

Most climate models project a weakening of the Walker circulation as a response to greenhouse gas forcing (Vecchi and Soden, 2007), manifested by the eastern equatorial Pacific warming at a faster rate than the western Pacific. This change in the background climate state is expected to increase the frequency of extreme El Niño events (Cai et al., 2014; Heede and Fedorov, 2023b), although the time of emergence of such response is a matter of disagreement within models (Heede and Fedorov, 2023a). Interestingly, the signature of global warming on ENSO-related precipitation would emerge decades earlier than ENSO-SST themselves (Ying et al., 2022), which means that ENSO teleconnections might change in the future even if ENSO itself does not change. Global impacts associated with El Niño and La Niña are projected to intensify in the future (Johnson et al., 2022; McGregor et al., 2014; Perry et al., 2017), exposing a larger proportion of the Earth's population to severe climate hazards.

Understanding how changes in the background climate state, driven by either natural modes of variability or by climate change, alter ENSO is key to improving its predictability and eventually its impacts on populations. This thesis aims to first understand the mechanisms by which Atlantic Multidecadal Variability affects ENSO dynamics, with a later focus on the ENSO teleconnection to Australia, a region heavily impacted by ENSO. Then, given the severity of the climate impacts that very strong El Niño events have driven in the past, the thesis aims to understand if and how the global climate response to these events could change in a warmer climate.

1.2. El Niño-Southern Oscillation

1.2.1. ENSO history

Rasmusson and Wallace (1983) compared the study of ENSO to the assembly of a jigsaw puzzle. Since the first signs of what we would call today an ENSO event around 4500 years ago, until the last "triple-dip" La Niña (2020-2023), our way of observing, understanding, forecasting and experiencing ENSO events has evolved by leaps and bounds.

Evidence from oxygen isotopes, corals, tree rings and historical records captured by historians, geographers, sailors, anglers and farmers in different parts of the world narrate a story about the footprint that ENSO left in the past, even before being catalogued or recognized as a cyclic phenomenon. ENSO records provide insightful testimonies to understand the socioeconomic impact that changes in temperature and precipitation patterns caused to human civilizations across the world.

The history of our civilisation has been shaped by climate conditions, including strong El Niño years that drove severe socieconomic impacts and forced settlements to adapt to them, migrate or collapse, like it was suggested with the Maya civilization (Grove and Adamson, 2018). In the last centuries and even millennia,

societies relied heavily on agriculture and were vulnerable to changes in weather and climate conditions, such as the delay or strength of the rainy season and extreme precipitation and temperature events.

In the late 19th century, peruvian fishermen identified a warm current that brought different fish and other animal species (Fig. 1.1) and precipitation off the coast of Peru, a normally dry region. This current appeared around Christmas time and was named "El Niño", which in Spanish it means "the boy child". Since it was thought to be a phenomenon with limited local reach, El Niño did not call a lot of attention within the scientific community at that time.

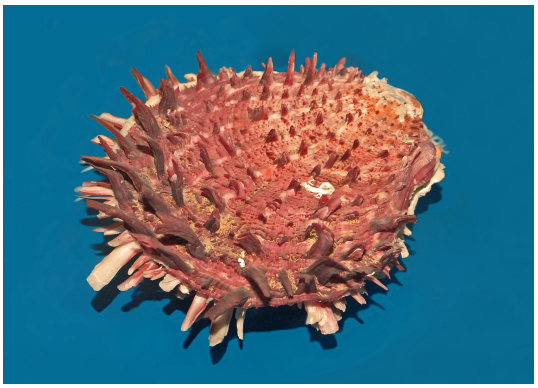

Figure 1.1: The Spondylus, or thorny oyster, is typical of warm waters. When it showed up in the coast, Peruvians knew that El Niño was coming. Picture by Hectonichus (CC BY-SA 3.0).

In 1897, the Swedish meteorologist Hugo Hildebrand was searching for what he called 'atmospheric centers of action', or pairs of regions with opposite sign pressure perturbation that were thought to be interconnected, including Sydney (Australia) and Buenos Aires (Argentina). In the early years of the 20th century, Norman Lockyer and his son, both British scientists, noticed another atmospheric pressure 'see-saw' between Argentina and India. During the First World War, the British mathematician Gilbert Walker was named head of the Indian Meteorological department. Together with his team of junior meteorologists, Walker found 20 locations or 'centres of action' across the world that could potentially influence weather patterns in remote locations, including the North Atlantic Oscillation (NAO) and the North Pacific Oscillation (NPO). This was

the first time that the scientific community considered the possibility of climate interactions between remote locations.

Hendrik Berlage also started to compile information on atmospheric pressure between Jakarta in Indonesia and 2 stations over the eastern Pacific (EP) (Santiago and Easter Island) after discovering that both locations were part of an atmospheric see-saw with pressure of opposite sign, what later would be called the "Southern Oscillation". The civil war in Indonesia in the late 1940s destroyed all the available records and the western Pacific station was moved to Darwin in Australia up to today, being the other side of the see-saw the French Polinesian island of Tahiti in the central equatorial Pacific Ocean.

In the late 1950s, a scientific alliance organized by the governments of Peru, Ecuador and Colombia took part on the "El Niño project", with the aim of understanding the mechanisms of the El Niño current and testing the theories suggested by the Swedish meteorologist Jacob Bjerknes. In his work, Bjerknes identified the link between tropical Pacific wind stress driven by the strong easterlies named as "trade winds" and SSTs along the equator (Bjerknes, 1969). By 1969, Bjerknes had already tied up several loose ends by acknowledging the relationship between the Southern Oscillation and SSTs in the central-eastern equatorial Pacific (see Fig.1.2).

Another key point of Bjerknes' work is that it first recognises the tight connection between the ocean and atmosphere within the tropical Pacific, and recognises the Walker and Hadley overturning circulations. In terms of the origin of El Niño current, there was still some disagreement within the scientific community at that time. Bjerknes suggested that the origin of the El Niño current was in the EP, a theory that was refuted years later by Klaus Wyrtki, who suggest that the ocean processes triggering El Niño events were based at the western side of the equatorial Pacific. Wyrtki (1985) noted that prior to an El Niño event, there was an accumulation of warm water over the western equatorial Pacific (a recharge of upper ocean heat content), and that this heat excess over the western Pacific was recovered after an El Niño event as the eastern Pacific "discharged" warm waters

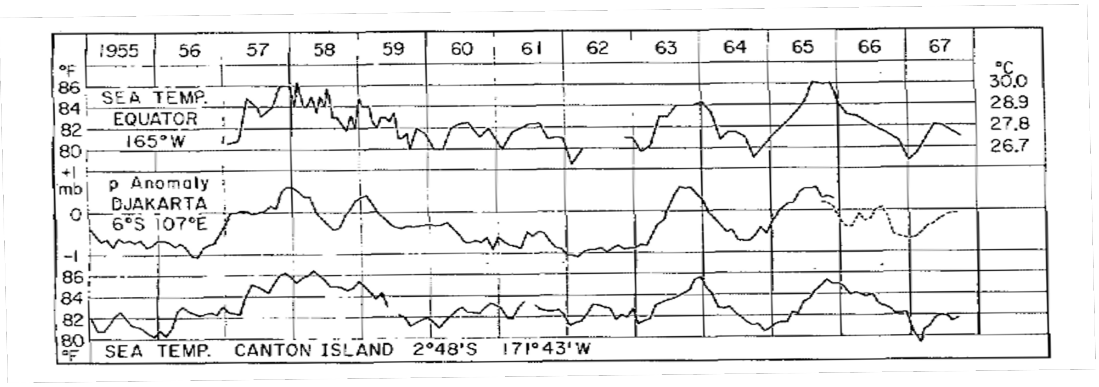

Figure 1.2: The Southern Oscillation from 1955 to 1967 represented by 6-mo overlapping averages of Djakarta monthly pressure anomalies. Dashed curve based on Singapore data. On same time scale: sea temperature at the Equator at approximately 165°W, and sea temperature by monthly averages at Canton Island. Taken from Bjerknes (1969).

towards the western margin.

Despite the increasing interest and resource investment in the study of El Niño, especially by the United States and Australia, there was a key moment that shook up the scientific community and reminded them that there was still a lot to do in terms of ENSO prediction. The El Niño event of 1982/83 was one of the strongest on record, with SST anomalies in the eastern equatorial Pacific reaching 2.2°C in boreal winter. This event was poorly forecasted, partially due to the eruption of the El Chichón volcano in Mexico in March of 1982, which impaired the ability of satellites to measure sea level height and identify warming in the central and EP Ocean. Not only did the scientific community fail to predict this particular El Niño event, but they refused to acknowledge that El Niño was coming despite the clear signs of warming over EP. Wyrtki even said "To call this El Niño would be child abuse!", as he sustained his theory of El Niño events originating in the western equatorial Pacific and the 1982/83 event was a canonical classic EP El Niño event.

The climate impacts of this event were devastating, including severe droughts

in northeast Brazil, southeast Asia and Australia, the West African Sahel and Southern Africa, and heavy flooding in Peru, Bolivia and Ecuador (Glantz, 2001; Glynn, 1990), leading to damage to infrastructures and food insecurity. The failure of predicting the strong El Niño event in 1982/83 was nevertheless what the scientific community needed to understand the need to improve ENSO prediction capability.

With this aim, the Tropical Ocean and Global Atmosphere programme (TOGA) kicked off in 1985, consisting of a joint international scientific effort to improve the prediction of ENSO by tightly observing the tropical Pacific ocean and atmosphere (McPhaden et al., 1998). The TOGA project also enhanced the understanding of La Niña events (as the American climatologist George Philander coined the counter-phase of El Niño), as such conditions were previously catalogued as "extreme-normal" periods given the fact that La Niña consists of a strengthening of the normal atmosphere and ocean conditions in the equatorial Pacific. TOGA came to an end in 1994 after being a successful 10-year project that allowed to predict and monitor the 1997/98 El Niño and advancing significantly our knowledge on ENSO dynamics (McPhaden et al., 2010).

1.2.2. ENSO characteristics

In the equatorial Pacific Ocean basin, trade winds blow from east to west, inducing wind stress onto the surface of the ocean and leading to accumulation of warm waters over the west Pacific 'warm pool', an area on the western equatorial Pacific where climatological SSTs lie above 28°C, triggering deep convection in the atmosphere and feeding the ascending branch of the Pacific Walker cell (Graham and Barnett, 1987). Over this area, the trades meet the westerly wind flow from the Indian Ocean, leading to convergence and rising of air masses. This ascent is enhanced by the release of latent heat from the condensation of water within ascending plumes in the western equatorial Pacific, leading to deep convection. In the upper troposphere, wind diverges zonally towards the EP, closing the Pacific Walker cell as shown in Fig. 1.3 (top). In a similar way, over the western Pacific upper troposphere, wind diverges polewards and transports air masses towards

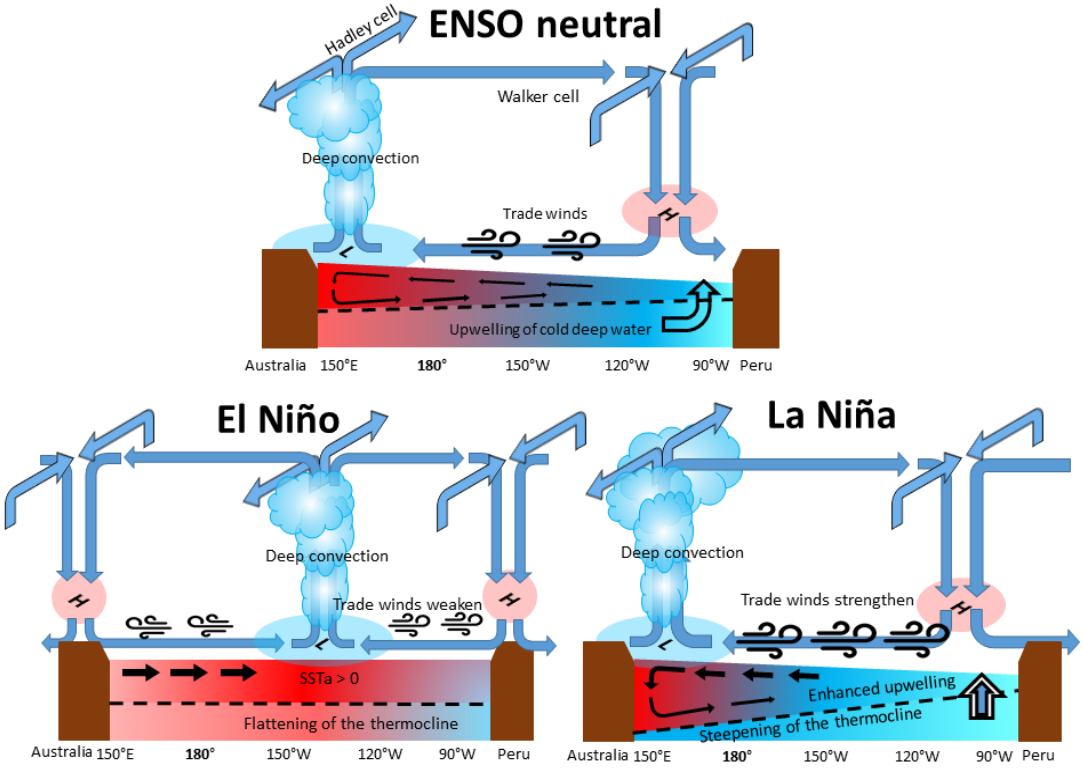

Figure 1.3: Schematic of ENSO-neutral (top), El Niño (bottom left) and La Niña (bottom right) conditions. Cross section of the equatorial Pacific at the equator between the coasts of Australia and Peru.

the extratropics through the Hadley circulation. In the EP, there is meridional and zonal wind convergence in the upper troposphere and consequently divergence and subsidence at the surface, reinforcing high-pressure conditions off the coast of South America.

In the upper ocean, the layer separating the warm surface waters from the colder deep abyssal waters is known as the thermocline. It is often characterised by the 20°C isotherm, and is deeper in the western Pacific than in the East. Contributing to a sharp east-west SST gradient across the equatorial Pacific, cold deep waters ascend in the EP creating a 'cold tongue' at the surface.

During El Niño (Fig. 1.3, bottom left), the Walker circulation weakens. Trade winds lose strength and lead to eastward ocean currents at the surface that advect warm water from the warm pool towards the central equatorial Pacific. Positive SST anomalies lead to a flattening of the equatorial Pacific thermocline, that hinders the upwelling of cold deep waters over the EP, further reinforcing the positive SST anomaly at the surface. The area of deep convection and precipitation anomalies is shifted towards the central equatorial Pacific, leading to dry anomalies over the Maritime continent.

La Niña events (Fig. 1.3, bottom right) are characterised by a strengthening of the climatological Walker circulation over the tropical Pacific. Trade winds strengthen and enhance westward advection of waters, increasing SSTs over the warm pool as well as sea surface height. The increase in warm water volume over the western Pacific deepens the thermocline, which slope sharpens due to the enhanced upwelling of cold waters over the EP. These changes in ocean heat content result in negative SST anomalies over the central and eastern equatorial Pacific and a more pronounced east-west SST gradient. Deep convection is enhanced over the warm pool, driving positive precipitation anomalies in the Maritime continent and surrounding areas. Changes in the position of SST anomalies alter thermodynamic fluxes and consequently the poleward energy transport via altering the propagation of Rossby waves.

1.2.3. ENSO teleconnections

The tropical Pacific atmosphere and ocean are tightly coupled, and feedback processes continuously transfer energy from the ocean to the atmosphere and vice versa. SST changes lead to convergence and ascent of air at the surface of the ocean, and consequently precipitation changes. Changes in precipitation and deep convection during ENSO events lead to anomalous latent heating that in turn excites equatorial Kelvin and Rossby waves (Gill, 1980), propagating ENSO signal through the tropics and intro the extratropics. Shifts in the location of deep convection alters the Walker circulation, and has extratropical reach through the Hadley circulation (Trenberth et al., 1998).

ENSO-driven changes in convection and upper-level divergence excite anomalous trains of planetary Rossby waves that propagate the ENSO signal to the extratropics (Hoskins and Karoly, 1981) via the Pacific North American (PNA; (Müller and Roeckner, 2006)) and Pacific South American (PSA, (Mo and Higgins, 1998)) patterns; and even the polar stratosphere (Mezzina et al., 2022). The propagation of ENSO signal to the extratropics depends on the background state. For example, Hardiman et al. (2019) found that the stratospheric pathway of ENSO teleconnection to Europe is suppressed when the stratospheric polar vortex is strong; Lee et al. (2009) made a link between barotropic background westerlies and the propagation of ENSO signal; and Yeh et al. (2018) hypothesised about the impacts of background warming on ENSO teleconnections.

The global reach of ENSO impacts is well known. Figure 1.4 shows temperature (1.4a) and precipitation (1.4b) anomalies regressed onto SST anomalies in the Niño 3.4 region (5°N–5°S, 170°W–120°W) from November to January. This figure assumes symmetry between the climate responses to El Niño and La Niña, meaning that the amplitude and spatial location of El Niño and La Niña impacts are equivalent but opposite in sign. However, that condition is not met in regions such as Australia (Chung and Power, 2017), Europe (López-Parages et al., 2016; Trascasa-Castro et al., 2019), North America (Hoerling et al., 1997) and the Indian Ocean Hong et al. (2010).

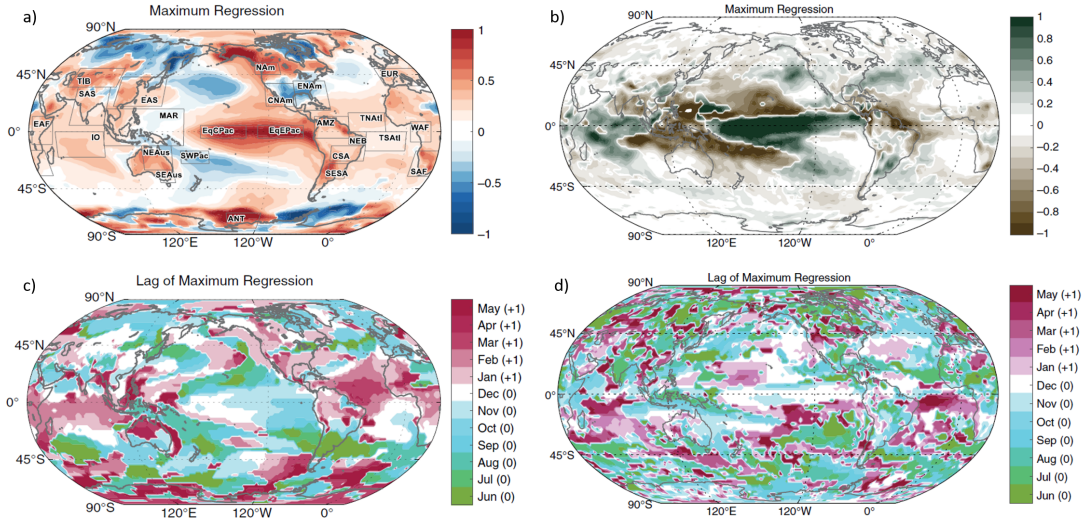

Figure 1.4: ENSO temperature (a, c) and precipitation (b, d) response. Maximum regression of 3-month mean air temperature (°C STD^{-1}) (a) and precipitation (mm day^{-1} STD^{-1}) (b) anomaly onto Nov-to-Jan Niño-3.4 index. (c, d) Month of maximum regression. The numbers 0 and +1 in the color bar labels indicate the years of ENSO development and decaying phase, respectively. Niño-3.4 index based on the HadISST data. Air temperature and precipitation from NCEP/NCAR (Dec 1948 to Nov 2017; (Kalnay et al., 1996). Figure taken from Taschetto et al. (2020).

The temporality of ENSO impacts also varies, with some regions being affected most strongly by ENSO even before it reaches its mature phase. Figs. 1.4c and d shows the month of maximum regression of ENSO temperature and precipitation anomalies, respectively. From June to August during the developing phase of ENSO (JJA0), the Maritime continent already sees an increase in precipitation during La Niña and the opposite during El Niño, due to the zonal shift in the Pacific Walker cell (Hendon, 2003). In the same season, South Eastern South America experiences changes in surface temperature (Barros et al., 2002), and during El Niño, India receives less rainfall as a result of the well-known suppression of the Indian summer monsoon (Kumar et al., 1999). In Australia, La Niña leads to above normal precipitation and higher risk of flooding over the country in austral spring (from September to November) (Chung and Power, 2017), whereas during El Niño there are hotter and drier conditions that increase the risk of wildfires (Abram et al., 2021).

From December to February, El Niño reduces the amount of precipitation during the rainy season in southern Africa (Ratnam et al., 2014). The North Atlantic Oscillation (NAO) is the dominant mode of winter climate variability over the North Atlantic-European sector. Its relationship with ENSO consists of a weakening of the Icelandic low and Azores high during El Niño winters, leading to a more negative NAO index and colder winters in northern Europe (Jiménez-Esteve and Domeisen, 2018). With some months of delay after the peak of ENSO, El Niño increases precipitation rates East Africa's 'short' and 'long rains' seasons (Nicholson and Kim, 1997; Palmer et al., 2023). During summer, El Niño is known to strengthen the North American Monsoon (NAM) system and lead to more precipitation over the United States, while the opposite climate response is expected during La Niña (Higgins et al., 1999).

1.3. ENSO theory

The 1980s were key for the development of theories that explained that atmosphere and ocean feedbacks are responsible for ENSO growth and decay. They

were based on the equatorial Pacific as a coupled system in a constant transition towards an "unreachable" equilibrium state. Although simple in nature, the theories of the delayed (Suarez and Schopf, 1988), wave (Jin, 1997a), recharge (Jin, 1996, 1997a) and advective-reflective oscillators (Picaut et al., 1997) aimed to summarise and quantify the observed physical processes during ENSO events as a forecasting tool.

Cane et al. (1986) used a deterministic numerical model capturing the main coupled dynamics in the tropical Pacific to develop a forecasting tool to predict ENSO events in advance. They tested their model with observations of El Niño events since 1970 and suggested that the buildup of warm SST anomalies preceding an El Niño could be forecasted more than a year in advance. This statement was optimistic at the time and remains so nowadays, as ENSO events are hard to predict with reasonable skill at more than 14 months in lead time (Gonzalez and Goddard, 2016). The main challenge in predicting the growth of ENSO lies within the loss of autocorrelation in the tropical Pacific processes in boreal summer (Mukhin et al., 2021) that leads to forecast errors (Jin et al., 2008). The noise in the tropical Pacific is larger than the SST anomaly associated with ENSO in boreal spring, when ENSO decays, reducing the predictability skill of ENSO in the following months (Lai et al., 2018).

The Cane-Zebiak (CZ, (Cane and Zebiak, 1985)) model was pioneering in the coupled instability theory of ENSO dynamics (Fedorov and Philander, 2000; Gill, 1985), and explained SST anomalies based on climatological SSTs, surface winds and thermocline depths. They concluded that ENSO is indeed an oscillation restricted to the tropical Pacific with no influence from the extratropics. They differenciate between the surface layer of the ocean, which reacts strongly to wind stress, and the upper ocean heat content which determines the interannual variability of ENSO.

A synchronous line of ENSO research was the development of simple conceptual models. The first model was the Delayed Oscillator (Battisti and Hirst, 1989; Suarez and Schopf, 1988), and proposes two mechanisms to explain ENSO growth

and decay phases. The equatorial East-West SST gradient decreases when SSTs are anomalously warm over the eastern equatorial Pacific, reducing the strength of the Walker circulation and hence the trade winds. Less easterly wind forcing further enhances the positive SST anomaly over the EP given by the eastward migration of warm water across the equatorial Pacific. This process is known as the positive Bjerknes feedback (Bjerknes, 1969), and is suggested to be the cause of ENSO growth in the Delayed Oscillator theory framework.

Once ENSO peaks, wind stress over the central equatorial Pacific triggers an eastward downwelling Kelvin wave and an westward upwelling Rossby wave. Rossby waves are reflected as upwelling Kelvin waves and propagates back to the EP, which helps dissipating the accumulation of heat in the upper ocean and favours ENSO phase transition. Overall, ocean dynamics dominate in the phase of ENSO decay, while its periodicity is determined by the time waves take to propagate.

Years later, Jin (1996, 1997a,b) developed the Recharged Oscillator (RO) theory. Positive SST anomalies over the western and central equatorial Pacific cause westerly wind forcing that enhances the meridional transport or "discharge" of warm waters that occur during an El Niño event (Fig.1.5a). As a result of wind stress forcing and the meridional discharge of warm waters, the thermocline flattens across the equatorial Pacific, and the SST damping over the EP reduces the SST anomaly (Fig.1.5b). The anomalous shallow thermocline over the EP allows upwelling of cold deep waters, leading to negative SST anomalies (Fig.1.5c). Trade wind stress strengthens due to cold SST anomalies, advecting warm waters towards the warm pool which eventually deepen the WP thermocline. Easterly wind forcing enhances the equatorward advection or "recharge" of warm waters (Fig.1.5c), and bring the equatorial Pacific to another neutral state before trade winds weaken again and warm waters are advected to the EP (Fig.1.5a). The main mechanism allowing the ENSO phase transition in the RO framework is the recharge/discharge of warm waters outside/towards the equatorial Pacific driven by the equatorial Pacific wind stress curl and location (Jin et al., 2020). It paves the way for the formulation of the Bjerknes Stability (BJ) index shown in eq. 1.1.

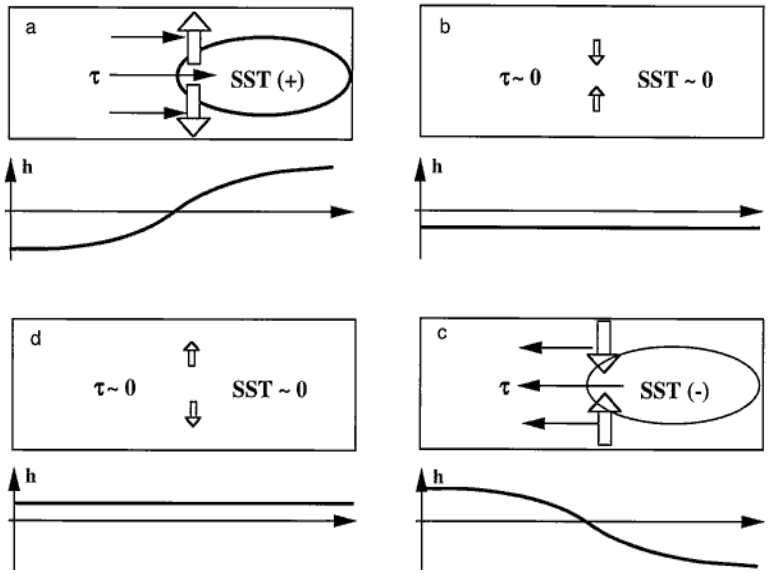

Figure 1.5: Schematic panels of the four phases of the recharge oscillator: (a) the warm phase, (b) the warm to cold transition phase, (c) the cold phase, and (d) the cold to warm transition phase. The rectangular box represents the equatorial Pacific basin, the elliptical circle represents the SST anomaly, the thin and filled arrows represent wind stress anomaly associated with the SST anomaly, and the thick unfilled arrows represent the recharge/discharge of equatorial heat content. Each panel also shows the distribution of the thermocline depth anomaly (h) along the equator. Taken from Jin (1997a).

$$2BJ = -\left[a_1\frac{\langle\Delta\bar{u}\rangle_E}{L_x} + a_2\frac{\langle\Delta\bar{v}\rangle_E}{L_y}\right]_{CD} - [\alpha_s]_{TD} + \left[\mu_a\beta_u\langle-\frac{\delta\bar{T}}{\delta x}\rangle_E\right]_{ZA} + \left[\mu_a\beta_w\langle-\frac{\delta\bar{T}}{\delta z}\rangle_E\right]_{EK} + \left[\mu_a\beta_h\langle-\frac{\bar{w}}{H_1}\rangle_E a_h\right]_{TC} \quad (1.1)$$

Built upon the basis of the recharged Oscillator, the BJ index was first introduced by Jin et al. (2006), and captures the main atmosphere and ocean processes responsible for ENSO growth rate. It represents the competition of five coupled feedbacks, which damp (current damping and thermodynamic feedbacks) or enhance (zonal advective, Ekman and thermocline feedbacks) the development of SST anomalies in the EP to eventually grow into an ENSO event.

The current damping feedback (CD in eq. 1.1, Fig. 1.6a) accounts for zonal ($a_1\frac{\langle\Delta\bar{u}\rangle_E}{L_x}$) and meridional ($a_2\frac{\langle\Delta\bar{v}\rangle_E}{L_y}$) gradients of absolute SST values in the EP. Secondly, the thermodynamic (TD, α_s, Fig. 1.6b) feedback accounts for the exchange of heat between the ocean and the atmosphere, including latent and sensible heat fluxes as well as longwave and shortwave radiation fluxes at the surface. This feedback is very strong during boreal spring and summer, and it is highly dependent on the type of clouds above the eastern equatorial Pacific and the position of the Walker cell.

The zonal advective (ZA, Fig. 1.6c) feedback accounts for the effect of wind stress across the equatorial Pacific on EP SSTs ($\mu_a\beta_u$) and climatological zonal SST gradients ($\frac{\delta\bar{T}}{\delta x}$). The Ekman (EK, Fig. 1.6d) feedback relates to the upwelling of cold water favoured by the wind ($\mu_a\beta_w$) and accounts for the climatological temperature gradient from the ocean surface to a depth of 50m ($\frac{\delta\bar{T}}{\delta z}$). Finally, the thermocline feedback (TH, Fig. 1.6d) captures the SST response to wind stress (μ_a), the sensitivity of the thermocline slope to equatorial wind stress (β_h) and the climatological upwelling of cold water in the uppermost 50 m of the ocean, all of these variables contributing to the redistribution of upper ocean heat content.

ENSO feedbacks follow a seasonal cycle, with the damping feedbacks being strongest

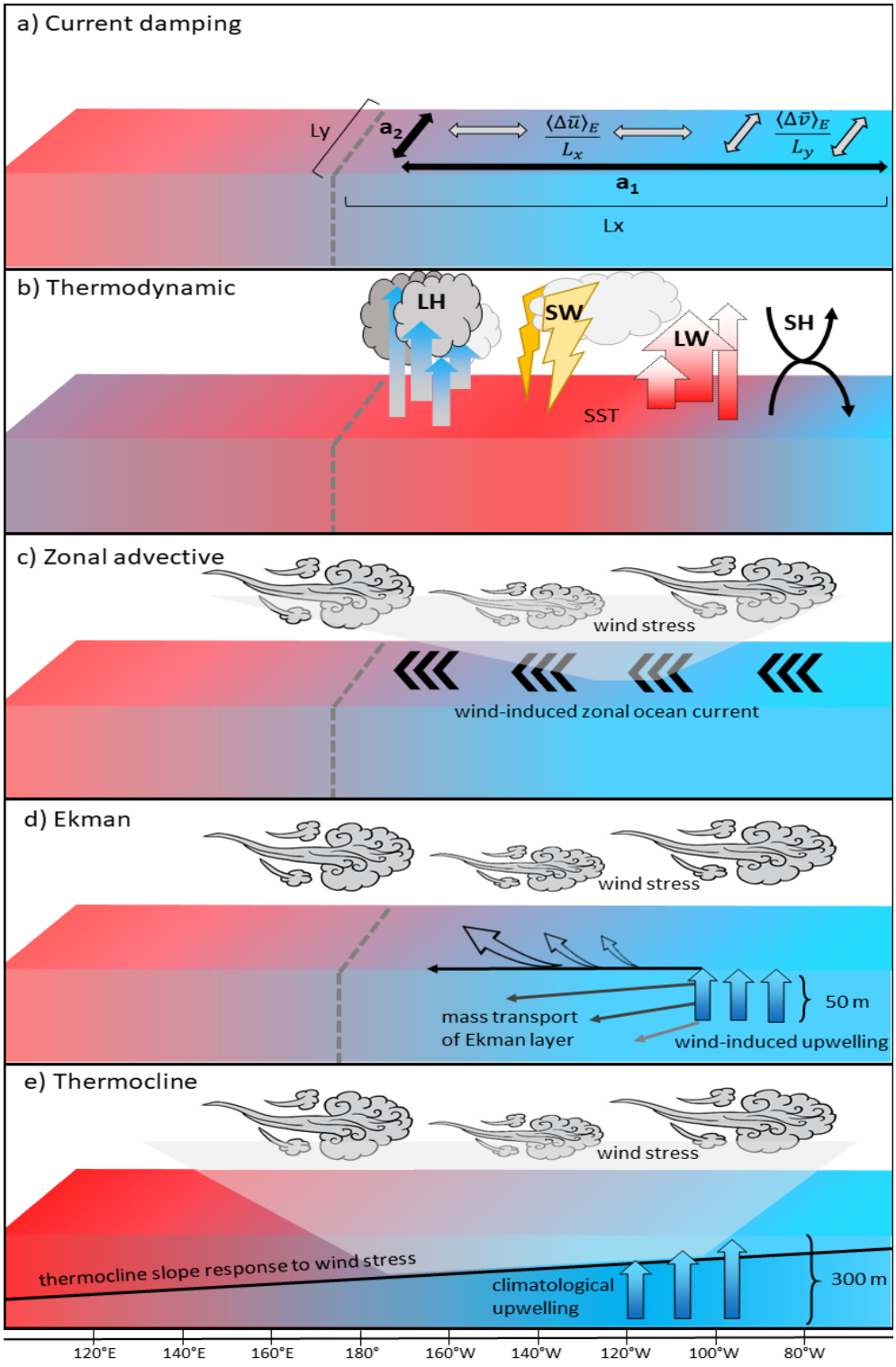

Figure 1.6: Schematic of the feedbacks included in the BJ index calculation: a) current damping, b) thermodynamic, c) zonal advective, d) Ekman and e) thermocline.

in late boreal spring and the positive feedbacks (zonal advective, Ekman and thermocline) peaking in late boreal autumn (see Fig. 2.2 in Chapter 2). The BJ index is computed over two main areas, the whole equatorial Pacific or the eastern equatorial Pacific (denoted with an "E" in eq.1.1). Both areas extend in latitude from 5°N to 5°S, and the longitudinal boundary that separates WP from EP can be either a fixed threshold (160°W , (Jin et al., 2006); 180°E , (Ferrett and Collins, 2019) or estimated by regressing ocean heat content anomalies onto the timeseries of the first empirical orthogonal function (EOF) of anomalous SSTs across the equatorial Pacific (Kim and Jin, 2011; Kim et al., 2014). It has been widely used to compare ENSO behaviour in different climate models (Bellenger et al., 2014; Kim et al., 2014), time periods (Kim and Jin, 2011) and background states (Levine et al., 2017).

Along with the advantages that the BJ index provides for the comprehension of the main processes responsible for ENSO dynamics, it is important to highlight that the cost of its simplicity carries several limitations. This fact arises from the large variability in the value of the BJ index and the individual feedbacks between different General Circulation Models (GCMs) (Kim et al., 2014). The cause of such a big diversity can be the different background states in the models (Fedorov, 2002). Comparisons between the strength of the feedbacks in models and atmosphere-ocean reanalyses reveal that the there is an important underestimation of the thermocline feedback in the former group (Jin and An, 1999) compared to the latter (Lübbecke and Mcphaden, 2013).

A most striking aspect of the BJ index is the assumption of linear relationships between variables. For instance, climate models largely underestimate the shortwave radiation response to changes in SSTs in the equatorial Pacific (Lloyd et al., 2012), and it is the largest contributor of intermodel spread in the representation of the thermodynamic feedback (Lloyd et al., 2009). This is partly due to the poor representation of tropical clouds in GCMs (Bony and Dufresne, 2005). Nonlinearities in the equatorial wind stress response to EP SSTs (μ_a) are also a limiting factor that adds uncertainty to the interpretation of the BJ index (Graham et al., 2014; Wang and McPhaden, 2000).

1.3.1. ENSO diversity and nonlinearity

Despite the well known mechanistic theories to explain the existence of ENSO, it is a fact that every ENSO event is unique. The spatial structure of SST anomalies, intensity, duration and evolution vary from event to event. The most obvious way to appreciate ENSO diversity is by looking at the areas of maximum SST anomalies during ENSO events in the historical record.

Historically, several attempts to capture different ENSO "flavours" have been made, for example by classifying ENSO events as Central Pacific (CP) or EP depending on where their maximum SST anomaly lies within the equatorial Pacific Ocean (Niño4 (5°N-5°S, 160°E-150°W) for CP and Niño3 (5°N-5°S, 150°W-90°W) for EP). Fig.1.7 illustrates the diversity of El Niño events in terms of the longitudinal extent of their SST anomalies. Nevertheless, even within the EP type events, there is a massive range of values. By looking at the amplitude of the blue and red lines, one can also see that EP El Niño events are significantly stronger than CP events. EP and CP ENSO events can trigger a significantly different climate response in several regions, such as South America (Cai et al., 2020), Australia (Taschetto and England, 2009) and Antarctica (Zhang et al., 2021).

The magnitude of the climate response to ENSO can show nonlinear behaviour, it does not simply scale with the amplitude of Niño3.4 SST anomalies (Hoerling et al., 1997). Nonlinearities in ENSO teleconnections arise from the fact that ENSO-related precipitation anomalies do not scale linearly with SST anomalies in the equatorial Pacific (He et al., 2018). Due to the nonlinear nature of ENSO teleconnections, very strong events deserve careful attention as they have the potential to cause devastating impacts on ecosystems and society (Casselman et al., 2023; Dewitte and Takahashi, 2019; Santoso et al., 2015). The three strongest El Niño events of the last decades occurred in 1982/83, 1997/98 and 2015/16, reaching a maximum SST anomaly of 2.43°C, 2.42°C and 2.57°C, respectively, relative to the 1981-2010 period. The first two ones were catalogued as "canonical El Niño", since they developed over the eastern equatorial Pacific, however the 2015/16 event had hints of an El Niño "modoki", or CP El Niño (Santoso et al., 2017). Very strong El Niño events, also called "extreme El Niño"

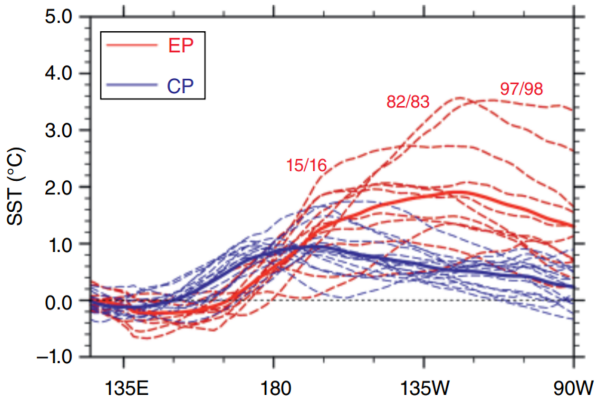

Figure 1.7: Equatorial SST anomaly profiles averaged over 2°S-2°N during winter (DJF) for CP (blue) and EP (red) El Niño events over the period January 1951–December 2017. Thin dashed lines show the profiles of individual events, while the thick red and blue solid lines indicate the composite profiles for EP and CP El Niño events, respectively. Monthly SST data were obtained from the NOAA Extended Reconstructed SST dataset version 5 (ERSSTv5; (Huang et al., 2017)). Anomalies were computed relative to the 1951–2017 climatology, and linearly detrended prior to the profile calculation. The extreme events of 1982–1983, 1997–1998, and 2015–2016 are labeled. Taken from Capotondi et al. (2020).

have different precursors than "regular" El Niño events (Chen et al., 2016) based on differences in zonal current and thermocline depth anomalies. One key difference between the 2015/16 El Niño and the other two extreme events is that warm SST anomalies were already present in the winter of 2014, although they never fully developed into an El Niño. The other two extreme El Niño winters were preceded by La Niña winters.

Finding sources of ENSO predictability is a key challenge for the scientific community. Some sources are well known and local such as upper ocean heat content or westerly wind bursts. Others, however, have their origin outside the tropical Pacific Ocean and it was not until the last years when they attracted attention. All these precursors are dynamical processes that occur in the atmosphere and the ocean before the onset of an ENSO event, favouring its development. The predominant precursor and the one that was recognized earliest is the build-up of upper ocean heat content anomalies across the equatorial Pacific (Cane et al., 1986; Wyrtki, 1985). The integrated warm water volume index (Meinen and

McPhaden, 2000) is widely used as a proxy for upper ocean heat content and usually precedes SST anomalies in the Niño3.4 region up to one year in advance. Westerly wind bursts are short-lived, surface westerly wind events in the western equatorial Pacific ocean that enhance the eastward propagation of warm waters leading to an El Niño event via eastward propagating Kelvin waves.

1.4. Internal and external drivers of ENSO variability

Since the second half of the 19$^{\text{th}}$ century, anthropogenic emissions of greenhouse gases (GHG) have caused a rise of 1.1°C in the global mean surface temperature (Arias et al., 2021). The atmosphere's capacity of holding water increases by 7% every degree Celsius of warming, according to the Clausius-Clapeyron relationship. Such changes in the hydrological cycle and the Earth's energy balance mean a transition towards a new climate state. The study of natural modes of climate variability such as ENSO, require a careful distinction between natural or anthropogenic processes that have the ability to alter ENSO dynamics by modulating the background state of the climate. We understand by ENSO variability the deviations from an SST value averaged over time, and usually over the Niño3.4 region. In the last decades, identifying and understanding potential drivers of ENSO variability in the tropics and extratropics has gained special attention, since they represent a source of skill in ENSO predictions.

1.4.1. Pantropical climate interactions

The global reach of ENSO impacts is well known (Taschetto et al., 2020); however, it was not until the recent past when the scientific community started to investigate the influence of other modes of climate variability on ENSO. In particular, an increasing number of studies based on observational evidence point towards the interaction between tropical oceans as a source of predictability of the main ocean modes at different timescales. The ascending branch of the Walker cell over the tropical Pacific warm pool diverges in the upper troposphere and transports air westwards towards the Indian Ocean and eastwards across the

equatorial Pacific, creating a tight link between the two oceans.

Changes to the Walker circulation result in shifts in the main modes of variability over the tropical oceans. El Niño events frequently trigger a positive Indian Ocean Dipole (IOD) phase (Fig. 1.8b and c), (Xie et al., 2002)), characterised by anomalous warm SSTs over the western Indian Ocean and cold SSTs over the east. In a similar manner, and since IOD events can occur independent of ENSO (Fischer et al., 2005), changes associated with IOD events are also known to influence ENSO dynamics (Kug and Kang, 2006; Saji et al., 1999) at interannual timescales. In a similar way, warming over the Indian Ocean associated with the Indian Ocean Basin Mode (IOBM) involves the development of easterlies over the western equatorial Pacific that enhances the transition from El Niño to La Niña (Okumura et al., 2011) and El Niño conditions enhance warm IOBM (1.8d), e)) at the same time as ENSO peaks.

We cannot dig into interbasin climate interactions without including the Atlantic Ocean. Interactions between the Atlantic and Pacific Oceans occur at different timescales. Observational (Ham et al., 2013; Martin-Rey et al., 2014; Rodríguez-Fonseca et al., 2009) and modelling (Ham and Kug, 2015; Keenlyside et al., 2013; Polo et al., 2014) studies provide evidence on the influence of the tropical North Atlantic (TNA) on ENSO variability. This demonstrates the bidirectional nature of the Pacific-Atlantic relationship, since prior to the 21th century the influence of the Atlantic on the tropical Pacific and ENSO was not known nor understood (Sutton et al., 2000).

Warm SSTs in the tropical North Atlantic during boreal summer strengthen the ascending branch of the Atlantic Walker cell, eventually leading to enhanced subsidence and strengthening of the trade winds over the central equatorial Pacific in the following winter, favouring the development of La Niña-like conditions (Fig. 1.8d and e).

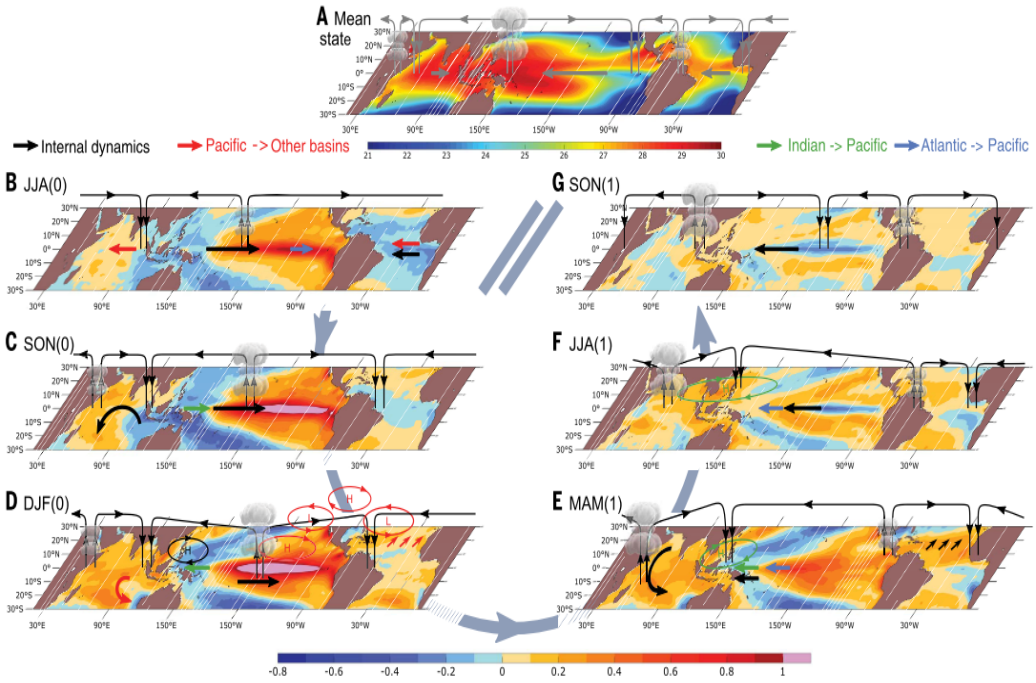

Figure 1.8: Tropical basin interactions from JJA prior to the peak of an El Niño event (B) to SON of the following year, shown as local SST anomalies regressed onto the DJF Niño3.4 index. H, regions of anomalously high surface pressure; L, regions of anomalously low surface pressure. Taken from Cai et al. (2019).

1.4.2. Atlantic Multidecadal Variability

In the last years, it has become evident that climate variability outside the tropical Pacific can affect on ENSO. At longer timescales, observational evidence suggests a warming trend in the North Atlantic Ocean contributed to the consistent tropical Pacific cooling observed from 1990 to 2010 (McGregor et al., 2014). During this period, there was a slowdown of the global warming trend, also called global warming 'hiatus' (Kosaka and Xie, 2013; McGregor et al., 2014).

Atlantic Multidecadal Variability consists of North Atlantic basinwide SST anomalies (Zhang et al., 2019) that fluctuate from positive to negative at multidecadal timescales, with each phase lasting for a few decades (Knight et al., 2006). A positive AMV phase (AMV+) display a horseshoe like pattern of warm anoma-

lies that are maximum in the subpolar gyre. Modelling studies were also able to reproduce a cooling in the tropical Pacific as a response to the positive phase of AMV (Ruprich-Robert et al., 2017).

AMV is known to affect surface climate conditions in remote locations. Over Africa, warm AMV conditions lead to increased rainfall over the Sahel (Mohino et al., 2011; Wang et al., 2012; Zhang and Delworth, 2006). By exciting the Atlantic Meridional Mode (AMM), shifting the Intertropical Convergence Zone (ITCZ) meridionally and modulating wind shear in the Atlantic hurricane development region, AMV+ enhances hurricane activity at decadal timescales (Sutton and Hodson, 2007; Vimont and Kossin, 2007). Over North America, warm AMV conditions enhance the frequency of drought periods (McCabe et al., 2004). Sutton and Dong (2012) linked the positive phase of AMV observed during the 1990s with persistent wet summers in Northern Europe and anomalous hot and dry summers over the Mediterranean region, where Qasmi et al. (2021) also reported an increase in the occurrence of heatwaves under warm AMV conditions.

There is observational and modelled evidence of the link between AMV and the Atlantic Meridional Overturning Circulation (AMOC) (Zhang et al., 2019). The AMOC consists of a large-scale ocean circulation across the Atlantic Ocean that transports heat from South to North in the western Atlantic margin through shallow currents and cold waters towards the South via deep currents that originate in the deep water formation areas in the subpolar North Atlantic. Model prediction studies highlight the importance of correctly initializing the ocean to capture the AMOC variability to effectively reproduce SST variability over the subpolar gyre region (Yeager and Robson, 2017).

Also, some studies identify a role for external forcings in AMV, such as those that point towards anthropogenic aerosols, more specifically their indirect effect. The main hypothesis is that due to the reduction of atmospheric concentration of anthropogenic aerosols which act as cloud concentration nuclei, there is less reflection of incoming shortwave radiation, which gets absorbed by the surface of the ocean.

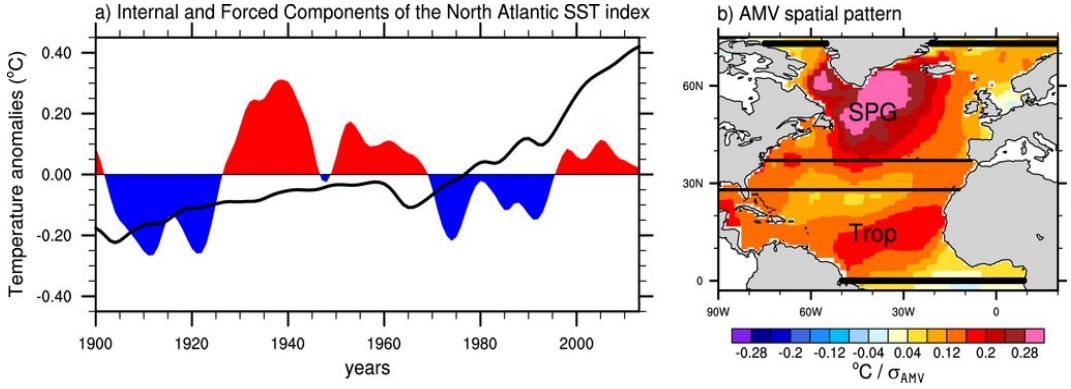

Figure 1.9: Internal (red and blue) vs external (black line) components of the observed North Atlantic SST decadal variability following the Ting et al. (2009) definition. (b) Regression map of the observed annual mean SST (ERSST.v3; Smith et al. (2008) on the internal component of the North Atlantic SST index (i.e., the AMV index; units are degrees Celsius per std dev of AMV index). Both SST field and AMV index time series have been low-pass filtered prior to computing the regression, using a Lanczos filter (21 weights with a 10-yr cutoff period). The black latitude lines in (b) show the subpolar and tropical domains used for the SPG-AMV and Trop-AMV experiments (see section 2b). Taken from Ruprich-Robert et al. (2017).

Watanabe and Tatebe (2019) suggest that changes in the emission and atmospheric concentration of anthropogenic sulphate aerosols explain up to 63% of SST variations associated with AMV, in agreement with Murphy et al. (2017) who highlighted the need to consider external forcings in modelling studies to properly capture the amplitude and periodicity of the observed AMV. Nevertheless, some studies suggest that the dependence of AMV variability on external or internal forcings is time dependent, with internal forcing dominating from preindustrial times to the first half of the 20$^{\text{th}}$ century, whereas external drivers explain most of AMV variability since 1950 (Bellomo et al., 2018). Given the relatively short observational record, modelling studies provide larger sampling to disentangle the origin of AMV variability between external and internal drivers. Nevertheless, Coupled General Circulation Models (CGCMs) probably fail to estimate the real strength of the aerosol forcing due to the poor representation of aerosol-cloud interactions in climate models (Murphy et al., 2017).

Idealised AMV simulations agree in the cooling of the equatorial Pacific as a

response to the warm AMV phase (Ruprich-Robert et al., 2021), which in turn has global-side effects. Nevertheless, O'Reilly et al. (2023) looked at this effect with coupled models and suggest that idealised experiments with SST restoring in the North Atlantic overestimate the global response to AMV. Given the AMV modulation of tropical Pacific mean state SSTs, there is special interest in finding out whether AMV modulates ENSO variability at multidecadal timescales and in case it does, understand the mechanism behind such teleconnection.

The mechanism by which anomalous warm SSTs drive tropical Pacific cooling consists of an intensification of deep convection in the tropical Altantic and consequently upper level mass divergence, altering the Walker circulation (Dong and Sutton, 2007; Ham and Kug, 2015; Martin-Rey et al., 2014). This anomaly is followed by an enhancement of the descending branch of the Walker cell over the CP that increases wind stress, and westward ocean currents and allows the accumulation of warm water over the warm pool, deepening the western Pacific thermocline.

Due to the relatively short observational records, and the disagreement between modelling studies, there is still some uncertainty in the mechanisms by which AMV might modulate ENSO variability. Several modelling studies agree in that ENSO variability decreases under warm AMV conditions (Dong and Sutton, 2007; Hu and Fedorov, 2018; Levine et al., 2017). Dong and Sutton (2007) suggests that the deepening of the western Pacific thermocline propagates to the EP, leading to a reduction of the thermocline slope and a weakening ENSO growth rate.

Given the short observational records, modelling studies have attempted to understand the dynamics and mechanisms of AMV teleconnections by using idealized simulations where a fixed AMV pattern based on observations is imposed onto climatological SSTs for a number of years to obtain robust information on AMV impacts. For example, the Decadal Climate Prediction Project (DCPP, (Boer et al., 2016)) aims to understand the mechanisms by which internal climate variability such as AMV affect global climate and trends.

1.5. El Niño and global warming

1.5.1. Changes to the tropical Pacific mean state

Due to anthropogenic emissions of greenhouse gases (GHG) since preindustrial times, the temperature of the planet has risen by 1.1°C (Arias et al., 2021). This warming is not homogeneous in space, global land areas are warming faster than the ocean (1.59°C and 0.88°C, respectively). Understanding if and how ENSO itself and its teleconnections will change in a warmer climate is challenging and urgent given the global reach of ENSO impacts.

The Sixth Assessment Report (AR6) of the Intergovernmental Panel on Climate Change (IPCC) highlights the uncertainty in changes to ENSO SST variability in a warmer planet (Masson-Delmotte et al., 2021) due to low agreement between CMIP6 models, in agreement with previous findings from the IPCC's Fifth Assessment Report (AR5) using CMIP5 models (Christensen et al., 2013). There is, however, robust evidence for an enhancement of the precipitation variability driven by ENSO in all possible scenarios of future warming (Lee et al., 2021; Yun et al., 2021), regardless of whether ENSO-SST variability changes or not, as well as an intensification of ENSO impacts.

After the publication of AR6, new studies have shed the light on an increase in ENSO SST variability under climate change scenarios. On one hand, a number of studies suggest an enhanced east-west SST gradient in the tropical Pacific in response to increasing concentrations of greenhouse gases in the atmosphere (Cane et al., 1986) due to enhanced upwelling over the EP that further reinforces the Bjerknes feedback. Callahan et al. (2021) used long run simulations from the Pliocene, and suggest that increasing CO_2 concentrations weaken ENSO variability, in agreement with Wengel et al. (2021) who tested this hypothesis with very high model resolution.

Cai et al. (2022) compared the 20th and 21st centuries with an ensemble of up to 43 CMIP6 models (the size is scenario-dependent) and found a strengthening of

ENSO variability in the later period. The largest increase is found in the most aggressive Shared Socioeconomic Pathway scenario (SSP5-8.5), with a multimodel mean increase of 16.1% in the 21st century relative to the 20th century. The work from Heede and Fedorov (2023b) agrees with Cai et al. (2022), and highlights that uncertainty in the projections of ENSO variability is driven by inter-model differences. Overall, most CMIP models agree on a weakening of the Walker circulation due to the fact that specific humidity increases at a faster rate than precipitation in a warmer atmosphere, slowing down the zonal overturning circulation in the tropics (Liu et al., 2005; Vecchi et al., 2006). This involves reduced east-west SST gradient in the equatorial Pacific due to the faster warming rate of the EP (Xie et al., 2010), that consequently leads to a shift of ENSO-related precipitation anomalies towards the eastern equatorial Pacific (McGregor et al., 2022), given the nonlinear nature of the atmospheric response to SSTs (Cai et al., 2021). Also, due to background warming, EP-type El Niño events are expected to increase in frequency (Cai et al., 2014; Heede and Fedorov, 2023b), which historically correspond to extreme El Niño events.

Large ensemble simulations from both CMIP5 and CMIP6 models project a decrease in the zonal equatorial Pacific SST gradient, and display a large model agreement on the increase in the Niño3.4 SST variability, especially over the central equatorial Pacific towards the end of the 21st century (Maher et al., 2023). Maher et al. (2023) also highlight the inter-model differences in the time of emergence of SST changes in the equatorial Pacific, which can be robustly differenciated from internal variability with a sufficiently large sample size.

In contrast to what is simulated in many GCMs and according to observations, there has been a strengthening of the Walker circulation from the early 1980s (Hu and Fedorov, 2018; McGregor et al., 2014), evident by a strengthening of the cross-equatorial trade winds triggering cold SST anomalies in the equatorial Pacific. It must be highlighted that climate models have overall failed to capture observed SST trends in the equatorial Pacific in the last decades (see Fig. 1.10, (Heede and Fedorov, 2023a)), with the zonal SST anomalies being largely

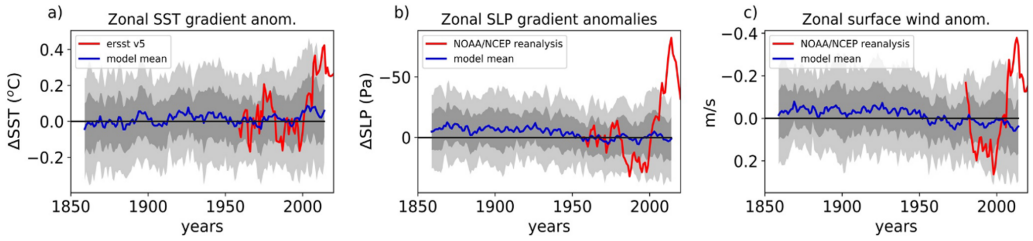

Figure 1.10: Observed and simulated historical variations in the east–west SST gradient, SLP gradient and zonal surface winds along the equator. Anomalies relative to a baseline are plotted. Observations are in red; a multi-model mean of CMIP6 models is in blue. The model spread across the 40 CMIP6 models is indicated by dark and light gray shadings (one and two standard deviations, respectively). A 10-year running mean is applied before calculating the spread. Baseline values were computed for each model and the observations, and then subtracted from the data. The baseline calculations cover the period from 1950 to 1970 for SST and SLP gradients and from 1980 to 1985 for zonal surface wind anomalies as the wind data is less reliable prior to this period. Taken from Heede and Fedorov (2023a).

overestimated relative to observations, which lie outside the range of model simulations (Lee et al., 2022). This suggests caution is required when interpreting projections of future changes in ENSO variability made with models that cannot capture changes in the past.

A relatively small number of models, however, are able to reproduce the observed recent tropical Pacific cooling trend by capturing the ocean thermostat mechanism proposed by Clement et al. (1996). This set of models project a transient response to greenhouse forcing consisting of a strengthening of the Walker circulation and a trend towards a La Niña-like pattern that delays the projected slowdown of the Walker circulation (Heede and Fedorov, 2021, 2023a; Lu et al., 2021; Ying et al., 2022), which might explain the different time of emergence of changes to ENSO variability reported by Maher et al. (2023).

In addition to changes in the mean zonal-SST gradient in the Pacific, in order to understand future changes to ENSO teleconnections, one must take into account that tropical precipitation is enhanced by the background warming, and this might alter the precipitation sensitivity to ENSO-SSTs in the tropical Pacific.

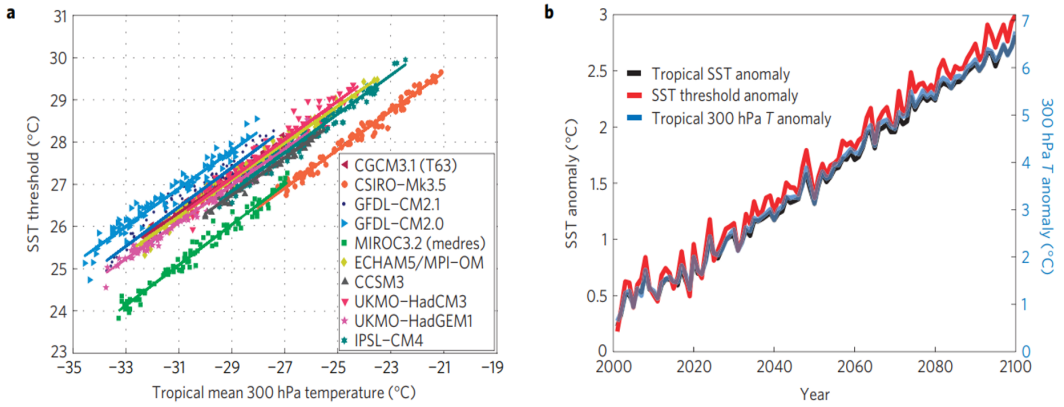

Figure 1.11: **a**, Scatter plot of SST threshold versus tropical mean 300hPa temperature with regression lines for each of ten CMIP3 models under emissions scenario A1B in simulations of the twenty-first century. **b**, Ensemble mean tropical mean SST (black), SST threshold for convection (red) and tropical mean 300 hPa temperature (blue) anomaly time series for the CMIP3 models. Anomalies are relative to the 1961–1990 climatology. The left y axis corresponds to the tropical mean SST and SST threshold, whereas the right y axis corresponds to the 300 hPa temperature. The scaling for the 300 hPa temperature (right y axis) corresponds approximately to that of MALR adjustment of the tropical mean SST (left y axis). Taken from Johnson and Xie (2010).

Changes in convection and upper level divergence directly implies shifts in ENSO extratropical teleconnections.

Atmospheric deep convection mostly happens over regions where climatological SSTs surpass 26°-28°C. In the tropics, equatorial waves smooth horizontal temperature gradients in the troposphere (Sobel et al., 2001), however the boundary layer moist static energy is directly proportional to local SST changes, hence any perturbation in atmospheric instability is dependent on local SST changes over the tropical oceans. Observations show that the minimum SST value needed to trigger deep convection, what we know as convective threshold, in the tropics has increased by 0.1°C per decade since 1980 (Johnson and Xie, 2010), alongside tropical climatological SSTs in the tropics. They link the increase in the SST-convective threshold to an increase in 300hPa temperature (see Fig. 1.11, as convective instability in the tropics is determined by SST changes, and highlight the dependence of tropical Pacific precipitation both on SSTs and atmospheric stability (He et al., 2017).

Despite the uncertainties around future changes in ENSO variability, there is some agreement in the increase in ENSO-related precipitation variability (Heede and Fedorov, 2023b). In fact, Ying et al. (2022) suggest that changes in precipitation variability driven by ENSO will emerge by 2040, decades before any signature of climate change is distinguishable in ENSO-related SSTs. This has direct implications On ENSO remote impacts, that might experience changes even before changes in ENSO variability emerge.

A number of studies have explored future changes to ENSO teleconnections using climate model simulations and different global warming scenarios. Changes in atmospheric circulation in a warmer world, driven by an overall increase in global mean surface temperature and a tropical Pacific atmosphere loaded with extra moisture, are expected to alter the dynamics of ENSO teleconnections. For example, Power and Delage (2018) suggest an amplification of ENSO-driven precipitation variability by 15-20% in areas already experiencing precipitation anomalies during El Niño. The amplitude and spatial pattern of future ENSO

teleconnections will depend on the rate of global warming and SST changes in the tropical Pacific and other ocean basins (Taschetto et al., 2020). CMIP models project an intensification of ENSO teleconnections as a result of the eastward shift of tropical Pacific precipitation (Cai et al., 2021; McGregor et al., 2022; Yun et al., 2021).

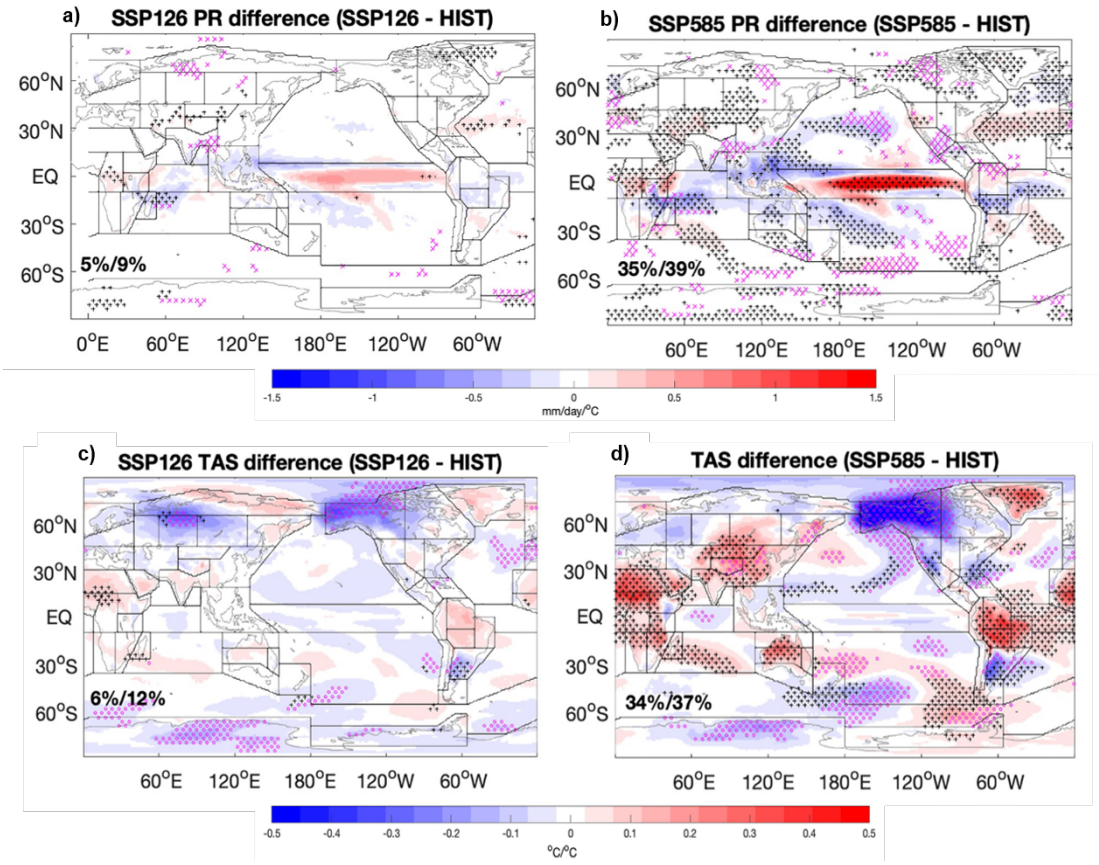

Figure 1.12: Global December-February precipitation (top, PR) and surface temperature (bottom, TAS) teleconnections of ENSO, measured as anomalous change per SST change in the Niño3.4 region; mm day^{-1} °C^{-1} (top) and °C^{-1} (bottom). The least and most aggressive global warming scenarios are shown in the left and right columns, with SSP1-2.6 and SSP5-8.5 (left and right columns, respectively) anomalies in the 2081-2100 period relative to the 1950-2014 period. The AR6 regions are overlaid. Black (purple) stippling indicates projected statistical significant teleconnection amplification (dampening). Numbers displayed in the bottom left of panels represent the percentage global area (left) and global land area (right) displaying significant changes. Taken from McGregor et al. (2022).

McGregor et al. (2022) analysed a suite of 52 CMIP6 models to evaluate changes in future ENSO teleconnection in 4 different Shared Socioeconomic Pathways (SSPs): SSP1-2.6, SSP2-4.5, SSP3-7.0 and SSP5-8.5, with radiative forcing values by the end of the century of 2.6, 4.5, 7.0 and 8.5 W m^{-2}, respectively. They found future changes in the climate response to ENSO in half of the world's regions under the most aggressive global warming scenario (SSP5-8.5), despite uncertainties in the magnitude and timing of changes in ENSO variability (Lee et al., 2021).

Some example of areas where the boreal winter climate response to ENSO (Fig. 1.12b, d) amplifies include the equatorial Pacific, the South American Monsoon region, California and some parts of Canada, Australia, Central and Eastern Africa, the Arabian Peninsula, West Central Asia and Tibet, Greenland and the North Atlantic, in agreement with Perry et al. (2017). The link between El Niño (La Niña) and a negative (positive) NAO is also expected to strengthen in the future (Drouard and Cassou, 2019; Johnson et al., 2022). Other areas, however, display a significant weakening of future ENSO teleconnections, such as Southern Central America, Northern South America, the Mediterranean and the Bengal Gulf for precipitation and a striking weakening of the temperature reponse to ENSO over Northwest of the United States and Antarctica. A weakening of North American response to El Niño in future climates has been reported (Beverley et al., 2021), due to a shift in ENSO-related precipitation in future climates.

According to McGregor et al. (2022), the amplitude and statistical significance of changes in ENSO anomalies scale with the rate of global warming. Comparing the SSP1-2.6 and SSP5-8.5 scenarios, the percentage of areas (considering both land and ocean areas) with a significant precipitation response to ENSO increases from 9% to 35%, and from 12% to 37% when it comes to surface temperature changes.

Understanding how the tropical Pacific mean state impacts on ENSO global teleconnections is key to understand future changes in surface impacts driven by El Niño and La Niña around the world. Despite the invaluable progress made in

ENSO prediction, the truth is that societies around the world still struggle to adapt to strong events and mitigate their impacts.

This thesis aims to advance of the role of background climate state in altering ENSO and its teleconnections, separating mean state changes driven by internal decadal climate variability and from the externally forced global warming signal.

1.6. Aims and objectives

The general objective of this thesis is to advance our knowledge on how changes in the background climate state driven by natural variability (AMV) or anthropogenic emissions of greenhouse gases modulate ENSO and its teleconnections. The specific objectives are addressed in the results chapters and follow the gaps identified in the previous section:

1. Understand the mechanisms by which Atlantic Multidecadal Variability drives changes in the tropical Pacific mean state and therefore ENSO variability. To address this scientific question, we use output of idealised AMV simulations to robustly isolate the AMV modulation of ENSO from the direct AMV response.

2. Quantify the AMV modulation of the surface climate response to ENSO in Australia, including changes to mean and extreme temperature and precipitation impacts as well as extreme events such as wildfires that represent a dangerous risk for society.

3. Investigate how changes in the tropical Pacific mean state in a warmer climate affect the surface climate response to very strong El Niño events globally. To achieve this goal, we ran and compared a set of Global Climate Model pacemaker experiments with SST anomaly patterns corresponding to 3 strong El Niño events from observations and added these anomalies to mean background corresponding to present and future conditions.

1.7. Thesis structure

This thesis is structured as follows:

- Chapter 1: Introduction
- Chapter 2: Results. Warm phase of AMV damps ENSO through weakened thermocline feedback
- Chapter 3: Results. Atlantic Multidecadal Variability modulates the climate impacts of El Niño–Southern Oscillation in Australia.
- Chapter 4: Results. Future climate response to very strong El Niño events.
- Chapter 5: Conclusions: Key findings and future work.

References

N. J. Abram, B. J. Henley, A. S. Gupta, T. J. R. Lippmann, H. Clarke, A. J. Dowdy, J. J. Sharples, R. H. Nolan, T. Zhang, M. J. Wooster, J. B. Wurtzel, K. J. Meissner, A. J. Pitman, A. M. Ukkola, B. P. Murphy, N. J. Tapper, and M. M. Boer. Connections of climate change and variability to large and extreme forest fires in southeast australia. *Communications Earth Environment*, 2: 8, 2021. ISSN 2662-4435. doi: 10.1038/s43247-020-00065-8. URL https://doi.org/10.1038/s43247-020-00065-8. 14

P. A. Arias, N. Bellouin, E. Coppola, R. Jones, G. Krinner, J. Marotzke, V. Naik, M. Palmer, G.-K. Plattner, J. Rogelj, M. Rojas, J. Sillmann, T. Storelvmo, P. Thorne, B. Trewin, K. A. Rao, B. Adhikary, R. Allan, K. Armour, G. Bala, R. Barimalala, S. Berger, J. Canadell, C. Cassou, A. Cherchi, W. Collins, W. Collins, S. Connors, S. Corti, F. Cruz, F. Dentener, C. Dereczynski, A. D. Luca, A. D. Niang, F. Doblas-Reyes, A. Dosio, H. Douville, F. Engelbrecht, V. Eyring, E. Fischer, P. Forster, B. Fox-Kemper, J. Fuglestvedt, J. Fyfe, N. Gillett, L. Goldfarb, I. Gorodetskaya, J. Gutierrez, R. Hamdi, E. Hawkins, H. Hewitt, P. Hope, A. Islam, C. Jones, D. Kaufman, R. Kopp, Y. Kosaka,

J. Kossin, S. Krakovska, J.-Y. Lee, J. Li, T. Mauritsen, T. Maycock, M. Meinshausen, S.-K. Min, P. Monteiro, T. Ngo-Duc, F. Otto, I. Pinto, A. Pirani, K. Raghavan, R. Ranasinghe, A. Ruane, L. Ruiz, J.-B. Sallée, B. Samset, S. Sathyendranath, S. Seneviratne, A. Sörensson, S. Szopa, I. Takayabu, A.-M. Tréguier, B. van den Hurk, R. Vautard, K. von Schuckmann, S. Zaehle, X. Zhang, and K. Zickfeld. Climate change 2021: The physical science basis. contribution of working group i to the sixth assessment report of the intergovernmental panel on climate change. *Cambridge University Press*, 2021. doi: 10.1017/9781009157896.002. 4, 23, 29

V. R. Barros, A. M. Grimm, and M. E. Doyle. Relationship between temperature and circulation in southeastern south america and its influence from el niño and la niña events. *Journal of the Meteorological Society of Japan. Ser. II*, 80:21–32, 2002. doi: 10.2151/jmsj.80.21. 14

D. S. Battisti and A. C. Hirst. Interannual variability in a tropical atmosphere–ocean model: Influence of the basic state, ocean geometry and nonlinearity. *Journal of Atmospheric Sciences*, 46:1687 – 1712, 1989. doi: https://doi.org/10.1175/1520-0469(1989)046<1687:IVIATA>2.0.CO;2. URL https://journals.ametsoc.org/view/journals/atsc/46/12/1520-0469_1989_046_1687_iviata_2_0_co_2.xml. 15

H. Bellenger, E. Guilyardi, J. Leloup, M. Lengaigne, and J. Vialard. Enso representation in climate models: from cmip3 to cmip5. *Climate Dynamics*, 42: 1999–2018, 2014. ISSN 1432-0894. doi: 10.1007/s00382-013-1783-z. URL https://doi.org/10.1007/s00382-013-1783-z. 20

K. Bellomo, L. N. Murphy, M. A. Cane, A. C. Clement, and L. M. Polvani. Historical forcings as main drivers of the atlantic multidecadal variability in the cesm large ensemble. *Climate Dynamics*, 50:3687–3698, 2018. ISSN 1432-0894. doi: 10.1007/s00382-017-3834-3. URL https://doi.org/10.1007/s00382-017-3834-3. 27

J. D. Beverley, M. Collins, F. H. Lambert, and R. Chadwick. Future changes to el niño teleconnections over the north pacific and north america. *Journal of Climate*, 34:6191 – 6205, 2021. doi: https://doi.org/10.1175/

JCLI-D-20-0877.1. URL https://journals.ametsoc.org/view/journals/clim/34/15/JCLI-D-20-0877.1.xml. 35

J. Bjerknes. Atmospheric teleconnections from the equatorial pacific. *Monthly Weather Review*, 97:163 – 172, 1969. doi: https://doi.org/10.1175/1520-0493(1969)097<0163:ATFTEP>2.3.CO;2. URL https://journals.ametsoc.org/view/journals/mwre/97/3/1520-0493_1969_097_0163_atftep_2_3_co_2.xml. 7, 8, 16

G. J. Boer, D. M. Smith, C. Cassou, F. Doblas-Reyes, G. Danabasoglu, B. Kirtman, Y. Kushnir, M. Kimoto, G. A. Meehl, R. Msadek, W. A. Mueller, K. E. Taylor, F. Zwiers, M. Rixen, Y. Ruprich-Robert, and R. Eade. The decadal climate prediction project (dcpp) contribution to cmip6. *Geoscientific Model Development*, 9:3751–3777, 2016. doi: 10.5194/gmd-9-3751-2016. URL https://gmd.copernicus.org/articles/9/3751/2016/. 28

S. Bony and J. L. Dufresne. Marine boundary layer clouds at the heart of tropical cloud feedback uncertainties in climate models. *Geophysical Research Letters*, 32:1–4, 5 2005. ISSN 00948276. doi: 10.1029/2005GL023851. 20

W. Cai, S. Borlace, M. Lengaigne, P. van Rensch, M. Collins, G. Vecchi, A. Timmermann, A. Santoso, M. J. McPhaden, L. Wu, M. H. England, G. Wang, E. Guilyardi, and F.-F. Jin. Increasing frequency of extreme el niño events due to greenhouse warming. *Nature Climate Change*, 4:111–116, 2014. ISSN 1758-6798. doi: 10.1038/nclimate2100. URL https://doi.org/10.1038/nclimate2100. 4, 30

W. Cai, L. Wu, M. Lengaigne, T. Li, S. McGregor, J.-S. Kug, J.-Y. Yu, M. F. Stuecker, A. Santoso, X. Li, Y.-G. Ham, Y. Chikamoto, B. Ng, M. J. McPhaden, Y. Du, D. Dommenget, F. Jia, J. B. Kajtar, N. Keenlyside, X. Lin, J.-J. Luo, M. Martín-Rey, Y. Ruprich-Robert, G. Wang, S.-P. Xie, Y. Yang, S. M. Kang, J.-Y. Choi, B. Gan, G.-I. Kim, C.-E. Kim, S. Kim, J.-H. Kim, and P. Chang. Pantropical climate interactions. *Science*, 363:eaav4236, 2019. doi: 10.1126/science.aav4236. URL https://www.science.org/doi/abs/10.1126/science.aav4236. 3, 25

REFERENCES

W. Cai, B. Ng, T. Geng, L. Wu, A. Santoso, and M. J. McPhaden. Butterfly effect and a self-modulating el niño response to global warming. *Nature*, 585: 68–73, 5 2020. ISSN 14764687. doi: 10.1038/s41586-020-2641-x. 21

W. Cai, A. Santoso, M. Collins, B. Dewitte, C. Karamperidou, J.-S. Kug, M. Lengaigne, M. J. McPhaden, M. F. Stuecker, A. S. Taschetto, A. Timmermann, L. Wu, S.-W. Yeh, G. Wang, B. Ng, F. Jia, Y. Yang, J. Ying, X.-T. Zheng, T. Bayr, J. R. Brown, A. Capotondi, K. M. Cobb, B. Gan, T. Geng, Y.-G. Ham, F.-F. Jin, H.-S. Jo, X. Li, X. Lin, S. McGregor, J.-H. Park, K. Stein, K. Yang, L. Zhang, and W. Zhong. Changing el niño–southern oscillation in a warming climate. *Nature Reviews Earth Environment 2021*, pages 1–17, 5 2021. ISSN 2662-138X. doi: 10.1038/s43017-021-00199-z. URL https://www.nature.com/articles/s43017-021-00199-z. 30, 34

W. Cai, B. Ng, G. Wang, A. Santoso, L. Wu, and K. Yang. Increased enso sea surface temperature variability under four ipcc emission scenarios. *Nature Climate Change*, 12:228–231, 2022. ISSN 1758-6798. doi: 10.1038/s41558-022-01282-z. URL https://doi.org/10.1038/s41558-022-01282-z. 4, 29, 30

C. W. Callahan, C. Chen, M. Rugenstein, J. Bloch-Johnson, S. Yang, and E. J. Moyer. Robust decrease in el niño/southern oscillation amplitude under long-term warming. *Nature Climate Change 2021 11:9*, 11:752–757, 5 2021. ISSN 1758-6798. doi: 10.1038/s41558-021-01099-2. URL https://www.nature.com/articles/s41558-021-01099-2. 29

M. A. Cane and S. E. Zebiak. A theory for el nixf1;o and the southern oscillation. *Science*, 228:1085–1087, 1985. doi: 10.1126/science.228.4703.1085. URL https://www.science.org/doi/abs/10.1126/science.228.4703.1085. 15

M. A. Cane, S. E. Zebiak, and S. C. Dolan. Experimental forecasts of el niño. *Nature*, 321:827–832, 1986. ISSN 1476-4687. doi: 10.1038/321827a0. URL https://doi.org/10.1038/321827a0. 15, 22, 29

A. Capotondi, A. T. Wittenberg, J.-S. Kug, K. Takahashi, and M. J. McPhaden. Enso diversity, 2020. URL https://agupubs.onlinelibrary.wiley.com/doi/abs/10.1002/9781119548164.ch4. 22

J. W. Casselman, J. F. Lübbecke, T. Bayr, W. Huo, S. Wahl, and D. I. V. Domeisen. The teleconnection of extreme el niño–southern oscillation (enso) events to the tropical north atlantic in coupled climate models. *Weather and Climate Dynamics*, 4:471–487, 2023. doi: 10.5194/wcd-4-471-2023. URL https://wcd.copernicus.org/articles/4/471/2023/. 21

P. Chang, T. Yamagata, P. Schopf, S. K. Behera, J. Carton, W. S. Kessler, G. Meyers, T. Qu, F. Schott, S. Shetye, and S.-P. Xie. Climate fluctuations of tropical coupled systems—the role of ocean dynamics. *Journal of Climate*, 19:5122 – 5174, 2006. doi: https://doi.org/10.1175/JCLI3903.1. URL https://journals.ametsoc.org/view/journals/clim/19/20/jcli3903.1.xml. 3

Y. Chen, D. C. Morton, N. Andela, L. Giglio, and J. T. Randerson. How much global burned area can be forecast on seasonal time scales using sea surface temperatures? *Environ. Res. Lett*, 11:45001, 2016. doi: 10.1088/1748-9326/11/4/045001. 22

J. H. Christensen, K. K. Kanikicharla, E. Aldrian, S. I. An, I. F. A. Cavalcanti, M. D. Castro, W. Dong, P. Goswami, A. Hall, J. K. Kanyanga, and Others. Climate phenomena and their relevance for future regional climate change. *Climate Change 2013 the Physical Science Basis: Working Group I Contribution to the Fifth Assessment Report of the Intergovernmental Panel on Climate Change*, pages 1217–1308, 2013. 29

C. T. Y. Chung and S. B. Power. The non-linear impact of el niño, la niña and the southern oscillation on seasonal and regional australian precipitation. *Journal of Southern Hemisphere Earth Systems Science*, 67:25–45, 2017. ISSN 22065865. doi: 10.22499/3.6701.003. 3, 12, 14

A. C. Clement, R. Seager, M. A. Cane, and S. E. Zebiak. An ocean dynamical thermostat. *Journal of Climate*, 9:2190 – 2196, 1996. doi: https://doi.org/10.1175/1520-0442(1996)009<2190:AODT>2.0.CO;2. URL https://journals.ametsoc.org/view/journals/clim/9/9/1520-0442_1996_009_2190_aodt_2_0_co_2.xml. 31

REFERENCES

M. Collins, S.-I. An, W. Cai, A. Ganachaud, E. Guilyardi, F.-F. Jin, M. Jochum, M. Lengaigne, S. Power, A. Timmermann, G. Vecchi, and A. Wittenberg. The impact of global warming on the tropical pacific ocean and el niño. *Nature Geoscience*, 3:391–397, 2010. ISSN 1752-0908. doi: 10.1038/ngeo868. URL https://doi.org/10.1038/ngeo868. 4

B. Dewitte and K. Takahashi. Chapter 6 - extreme el niño events. *Tropical Extremes*, pages 165–201, 2019. doi: https://doi.org/10.1016/B978-0-12-809248-4.00006-6. URL https://www.sciencedirect.com/science/article/pii/B9780128092484000066. 21

B. Dong and R. T. Sutton. Enhancement of enso variability by a weakened atlantic thermohaline circulation in a coupled gcm. *Journal of Climate*, 20: 4920 – 4939, 2007. doi: https://doi.org/10.1175/JCLI4284.1. URL https://journals.ametsoc.org/view/journals/clim/20/19/jcli4284.1.xml. 4, 28

M. Drouard and C. Cassou. A modeling- and process-oriented study to investigate the projected change of enso-forced wintertime teleconnectivity in a warmer world. *Journal of Climate*, 32:8047 – 8068, 2019. doi: https://doi.org/10.1175/JCLI-D-18-0803.1. URL https://journals.ametsoc.org/view/journals/clim/32/23/jcli-d-18-0803.1.xml. 35

D. Elsbury, Y. Peings, D. Saint-Martin, H. Douville, and G. Magnusdottir. The atmospheric response to positive ipv, positive amv, and their combination in boreal winter. *Journal of Climate*, 32:4193 – 4213, 2019. doi: https://doi.org/10.1175/JCLI-D-18-0422.1. URL https://journals.ametsoc.org/view/journals/clim/32/14/jcli-d-18-0422.1.xml. 3

A. V. Fedorov. The response of the coupled tropical ocean–atmosphere to westerly wind bursts. *J. R. Meteorol. Soc*, 128:1–23, 2002. 20

A. V. Fedorov and S. G. Philander. A stability analysis of tropical ocean-atmosphere interactions: Bridging measurements and theory for el niño, 2000. 15

S. Ferrett and M. Collins. Enso feedbacks and their relationships with the mean state in a flux adjusted ensemble. *Climate Dynamics*, 52:7189–7208, 5 2019. ISSN 14320894. doi: 10.1007/s00382-016-3270-9. URL https://doi.org/10.1007/s00382-016-3270-9. 20

A. S. Fischer, P. Terray, E. Guilyardi, S. Gualdi, and P. Delecluse. Two independent triggers for the indian ocean dipole/zonal mode in a coupled gcm. *Journal of Climate*, 18:3428 – 3449, 2005. doi: https://doi.org/10.1175/JCLI3478.1. URL https://journals.ametsoc.org/view/journals/clim/18/17/jcli3478.1.xml. 24

A. E. Gill. Some simple solutions for heat-induced tropical circulation. *Quarterly Journal of the Royal Meteorological Society*, 106:447–462, 1980. doi: https://doi.org/10.1002/qj.49710644905. URL https://rmets.onlinelibrary.wiley.com/doi/abs/10.1002/qj.49710644905. 12

A. E. Gill. Chapter 22 elements of coupled ocean-atmosphere models for the tropics, 1985. ISSN 0422-9894. URL https://www.sciencedirect.com/science/article/pii/S0422989408707189. 15

M. Glantz. Currents of change: Impacts of el niño and la niña on climate and society. *Disaster Prevention and Management: An International Journal*, 10:197–199, 1 2001. ISSN 0965-3562. doi: 10.1108/dpm.2001.10.3.197.5. URL https://doi.org/10.1108/dpm.2001.10.3.197.5. 9

P. W. Glynn. *Global ecological consequences of the 1982-83 El Nino-Southern Oscillation / edited by P.W. Glynn.* Elsevier, 1990. ISBN 0444883037 (alkaline paper). Includes bibliographical references and indexes. 9

P. L. M. Gonzalez and L. Goddard. Long-lead enso predictability from cmip5 decadal hindcasts. *Climate Dynamics*, 46:3127–3147, 2016. ISSN 1432-0894. doi: 10.1007/s00382-015-2757-0. URL https://doi.org/10.1007/s00382-015-2757-0. 15

REFERENCES

F. S. Graham, J. N. Brown, C. Langlais, S. J. Marsland, A. T. Wittenberg, and N. J. Holbrook. Effectiveness of the bjerknes stability index in representing ocean dynamics. *Climate Dynamics*, 43:2399–2414, 2014. ISSN 1432-0894. doi: 10.1007/s00382-014-2062-3. URL https://doi.org/10.1007/s00382-014-2062-3. 20

N. E. Graham and T. P. Barnett. Sea surface temperature, surface wind divergence, and convection over tropical oceans. *Science*, 238:657–659, 5 1987. ISSN 00368075. doi: 10.1126/SCIENCE.238.4827.657. URL https://www.science.org/doi/10.1126/science.238.4827.657. 9

R. Grove and G. Adamson. El niño in world history. 2018. doi: 10.1057/978-1-137-45740-0. URL https://link.springer.com/10.1057/978-1-137-45740-0. 5

Y.-G. Ham and J.-S. Kug. Role of north tropical atlantic sst on the enso simulated using cmip3 and cmip5 models. *Climate Dynamics*, 45:3103–3117, 2015. ISSN 1432-0894. doi: 10.1007/s00382-015-2527-z. URL https://doi.org/10.1007/s00382-015-2527-z. 24, 28

Y.-G. Ham, J.-S. Kug, J.-Y. Park, and F.-F. Jin. Sea surface temperature in the north tropical atlantic as a trigger for el niño/southern oscillation events. *Nature Geoscience*, 6:112–116, 2013. ISSN 1752-0908. doi: 10.1038/ngeo1686. URL https://doi.org/10.1038/ngeo1686. 24

S. C. Hardiman, N. J. Dunstone, A. A. Scaife, D. M. Smith, S. Ineson, J. Lim, and D. Fereday. The impact of strong el niño and la niña events on the north atlantic. *Geophysical Research Letters*, 46:2874–2883, 3 2019. ISSN 19448007. doi: 10.1029/2018GL081776. 12

N. A. Hasan, Y. Chikamoto, and M. J. McPhaden. The influence of tropical basin interactions on the 2020–2022 double-dip la niña. *Frontiers in Climate*, 4, 2022. ISSN 2624-9553. doi: 10.3389/fclim.2022.1001174. URL https://www.frontiersin.org/articles/10.3389/fclim.2022.1001174. 3

J. He, C. Deser, and B. J. Soden. Atmospheric and oceanic origins of tropical precipitation variability. *Journal of Climate*, 30:3197 – 3217, 2017. doi: https://doi.org/10.1175/JCLI-D-16-0714.1. URL https://journals.ametsoc.org/view/journals/clim/30/9/jcli-d-16-0714.1.xml. 33

J. He, N. C. Johnson, G. A. Vecchi, B. Kirtman, A. T. Wittenberg, and S. Sturm. Precipitation sensitivity to local variations in tropical sea surface temperature. *Journal of Climate*, 31:9225–9238, 5 2018. ISSN 0894-8755. doi: 10.1175/JCLI-D-18-0262.1. URL https://journals.ametsoc.org/view/journals/clim/31/22/jcli-d-18-0262.1.xml. 21

U. K. Heede and A. V. Fedorov. Eastern equatorial pacific warming delayed by aerosols and thermostat response to co2 increase. *Nature Climate Change*, 11:696–703, 2021. ISSN 1758-6798. doi: 10.1038/s41558-021-01101-x. URL https://doi.org/10.1038/s41558-021-01101-x. 31

U. K. Heede and A. V. Fedorov. Colder eastern equatorial pacific and stronger walker circulation in the early 21st century: Separating the forced response to global warming from natural variability. *Geophysical Research Letters*, 50, 5 2023a. ISSN 19448007. doi: 10.1029/2022GL101020. 4, 30, 31

U. K. Heede and A. V. Fedorov. Towards understanding the robust strengthening of enso and more frequent extreme el niño events in cmip6 global warming simulations. *Climate Dynamics*, 61:3047–3060, 2023b. ISSN 1432-0894. doi: 10.1007/s00382-023-06856-x. URL https://doi.org/10.1007/s00382-023-06856-x. 4, 30, 33

H. H. Hendon. Indonesian rainfall variability: Impacts of enso and local air–sea interaction. *Journal of Climate*, 16:1775 – 1790, 2003. doi: https://doi.org/10.1175/1520-0442(2003)016<1775:IRVIOE>2.0.CO;2. URL https://journals.ametsoc.org/view/journals/clim/16/11/1520-0442_2003_016_1775_irvioe_2.0.co_2.xml. 14

R. W. Higgins, Y. Chen, and A. V. Douglas. Interannual variability of the north american warm season precipitation regime. *Journal of Climate*, 12:653 – 680, 1999. doi: https://doi.org/10.1175/1520-0442(1999)012<0653:IVOTNA>

2.0.CO;2. URL https://journals.ametsoc.org/view/journals/clim/12/3/1520-0442_1999_012_0653_ivotna_2.0.co_2.xml. 14

M. P. Hoerling, A. Kumar, and M. Zhong. El niño, la niña, and the nonlinearity of their teleconnections. *Journal of Climate*, 10:1769 – 1786, 1997. doi: https://doi.org/10.1175/1520-0442(1997)010<1769:ENOLNA>2.0.CO;2. URL https://journals.ametsoc.org/view/journals/clim/10/8/1520-0442_1997_010_1769_enolna_2.0.co_2.xml. 12, 21

C.-C. Hong, T. Li, LinHo, and Y.-C. Chen. Asymmetry of the indian ocean basinwide sst anomalies: Roles of enso and iod. *Journal of Climate*, 23:3563 – 3576, 2010. doi: https://doi.org/10.1175/2010JCLI3320.1. URL https://journals.ametsoc.org/view/journals/clim/23/13/2010jcli3320.1.xml. 12

B. J. Hoskins and D. J. Karoly. The steady linear response of a spherical atmosphere to thermal and orographic forcing. *http://dx.doi.org/10.1175/1520-0469(1981)038<1179:TSLROA>2.0.CO;2*, 5 1981. doi: 10.1175/1520-0469(1981)038<1179:TSLROA>2.0.CO;2. 12

S. Hu and A. V. Fedorov. Cross-equatorial winds control el niño diversity and change. *Nature Climate Change*, 8:798–802, 9 2018. ISSN 17586798. doi: 10.1038/s41558-018-0248-0. URL https://doi.org/10.1038/s41558-018-0248-0. 28, 30

B. Huang, P. W. Thorne, V. F. Banzon, T. Boyer, G. Chepurin, J. H. Lawrimore, M. J. Menne, T. M. Smith, R. S. Vose, and H. M. Zhang. Extended reconstructed sea surface temperature, version 5 (ersstv5): Upgrades, validations, and intercomparisons. *Journal of Climate*, 30:8179–8205, 5 2017. ISSN 0894-8755. doi: 10.1175/JCLI-D-16-0836.1. URL https://journals.ametsoc.org/view/journals/clim/30/20/jcli-d-16-0836.1.xml. 22

S. Ineson and A. A. Scaife. The role of the stratosphere in the european climate response to el nĩo. *Nature Geoscience*, 2:32–36, 5 2009. ISSN 17520894. doi: 10.1038/ngeo381. 3

J. C. Jimenez, J. A. Marengo, L. M. Alves, J. C. Sulca, K. Takahashi, S. Ferrett, and M. Collins. The role of enso flavours and tna on recent droughts over amazon forests and the northeast brazil region. *International Journal of Climatology*, page joc.6453, 5 2019. ISSN 0899-8418. doi: 10.1002/joc.6453. URL https://onlinelibrary.wiley.com/doi/abs/10.1002/joc.6453. 4

B. Jiménez-Esteve and D. I. V. Domeisen. The tropospheric pathway of the enso–north atlantic teleconnection. *Journal of Climate*, 31:4563 – 4584, 2018. doi: https://doi.org/10.1175/JCLI-D-17-0716.1. URL https://journals.ametsoc.org/view/journals/clim/31/11/jcli-d-17-0716.1.xml. 14

E. K. Jin, J. L. Kinter, B. Wang, C.-K. Park, I.-S. Kang, B. P. Kirtman, J.-S. Kug, A. Kumar, J.-J. Luo, J. Schemm, J. Shukla, and T. Yamagata. Current status of enso prediction skill in coupled ocean–atmosphere models. *Climate Dynamics*, 31:647–664, 2008. ISSN 1432-0894. doi: 10.1007/s00382-008-0397-3. URL https://doi.org/10.1007/s00382-008-0397-3. 15

F.-F. Jin. Tropical ocean-atmosphere interaction, the pacific cold tongue, and the el nixf1;o-southern oscillation. *Science*, 274:76–78, 1996. doi: 10.1126/science.274.5284.76. URL https://www.science.org/doi/abs/10.1126/science.274.5284.76. 15, 16

F.-F. Jin. An equatorial ocean recharge paradigm for enso. part i: Conceptual model. *Journal of the Atmospheric Sciences*, 54:811–829, 5 1997a. ISSN 0022-4928. doi: 10.1175/1520-0469(1997)054. URL https://journals.ametsoc.org/view/journals/atsc/54/7/1520-0469_1997_054_0811_aeorpf_2.0.co_2.xml. 15, 16, 17

F.-F. Jin. An equatorial ocean recharge paradigm for enso. part i: Conceptual model. *Journal of the Atmospheric Sciences*, 54:811 – 829, 1997b. doi: https://doi.org/10.1175/1520-0469(1997)054<0811:AEORPF>2.0.CO;2. URL https://journals.ametsoc.org/view/journals/atsc/54/7/1520-0469_1997_054_0811_aeorpf_2.0.co_2.xml. 16

REFERENCES

F.-F. Jin and S.-I. An. Thermocline and zonal advective feedbacks within the equatorial ocean recharge oscillator model for enso. *Geophysical Research Letters*, 26:2989–2992, 5 1999. ISSN 00948276. doi: 10.1029/1999GL002297. URL http://doi.wiley.com/10.1029/1999GL002297. 20

F. F. Jin, S. T. Kim, and L. Bejarano. A coupled-stability index for enso. *Geophysical Research Letters*, 33, 5 2006. ISSN 00948276. doi: 10.1029/2006GL027221. URL https://agupubs.onlinelibrary.wiley.com/doi/full/10.1029/2006GL027221https://agupubs.onlinelibrary.wiley.com/doi/abs/10.1029/2006GL027221https://agupubs.onlinelibrary.wiley.com/doi/10.1029/2006GL027221. 18, 20

F.-F. Jin, H.-C. Chen, S. Zhao, M. Hayashi, C. Karamperidou, M. F. Stuecker, R. Xie, and L. Geng. Simple enso models, 2020. URL https://agupubs.onlinelibrary.wiley.com/doi/abs/10.1002/9781119548164.ch6. 16

N. C. Johnson and S.-P. Xie. Changes in the sea surface temperature threshold for tropical convection. *Nature Geoscience*, 3:842–845, 2010. ISSN 1752-0908. doi: 10.1038/ngeo1008. URL https://doi.org/10.1038/ngeo1008. 32, 33

N. C. Johnson, A. T. Wittenberg, A. J. Rosati, T. L. Delworth, and W. Cooke. Future changes in boreal winter enso teleconnections in a large ensemble of high-resolution climate simulations. *Frontiers in Climate*, 4, 2022. ISSN 2624-9553. doi: 10.3389/fclim.2022.941055. URL https://www.frontiersin.org/articles/10.3389/fclim.2022.941055. 4, 35

E. Kalnay, M. Kanamitsu, R. Kistler, W. Collins, D. Deaven, L. Gandin, M. Iredell, S. Saha, G. White, J. Woollen, Y. Zhu, M. Chelliah, W. Ebisuzaki, W. Higgins, J. Janowiak, K. C. Mo, C. Ropelewski, J. Wang, A. Leetmaa, R. Reynolds, R. Jenne, and D. Joseph. The ncep/ncar 40-year reanalysis project. *Bulletin of the American Meteorological Society*, 77:437–472, 1996. doi: https://doi.org/10.1175/1520-0477(1996)077<0437:TNYRP>2.0.CO;2. URL https://journals.ametsoc.org/view/journals/bams/77/3/1520-0477_1996_077_0437_tnyrp_2_0_co_2.xml. 13

N. S. Keenlyside, H. Ding, and M. Latif. Potential of equatorial atlantic variability to enhance el niño prediction. *Geophysical Research Letters*, 40:2278–2283, 2013. doi: https://doi.org/10.1002/grl.50362. URL https://agupubs.onlinelibrary.wiley.com/doi/abs/10.1002/grl.50362. 24

S. T. Kim and F. F. Jin. An enso stability analysis. part ii: Results from the twentieth and twenty-first century simulations of the cmip3 models. *Climate Dynamics*, 36:1609–1627, 5 2011. ISSN 09307575. doi: 10.1007/s00382-010-0872-5. URL https://link.springer.com/article/10.1007/s00382-010-0872-5. 20

S. T. Kim, W. Cai, F. F. Jin, and J. Y. Yu. Enso stability in coupled climate models and its association with mean state. *Climate Dynamics*, 42:3313–3321, 5 2014. ISSN 14320894. doi: 10.1007/s00382-013-1833-6. URL http://www-pcmdi.llnl.gov/ipcc/model_. 20

J. R. Knight, C. K. Folland, and A. A. Scaife. Climate impacts of the atlantic multidecadal oscillation. *Geophysical Research Letters*, 33:L17706, 9 2006. ISSN 0094-8276. doi: 10.1029/2006GL026242. URL http://doi.wiley.com/10.1029/2006GL026242. 25

Y. Kosaka and S.-P. Xie. Recent global-warming hiatus tied to equatorial pacific surface cooling. *Nature*, 501:403–407, 2013. ISSN 1476-4687. doi: 10.1038/nature12534. URL https://doi.org/10.1038/nature12534. 25

J.-S. Kug and I.-S. Kang. Interactive feedback between enso and the indian ocean. *Journal of Climate*, 19:1784 – 1801, 2006. doi: https://doi.org/10.1175/JCLI3660.1. URL https://journals.ametsoc.org/view/journals/clim/19/9/jcli3660.1.xml. 3, 24

K. K. Kumar, B. Rajagopalan, and M. A. Cane. On the weakening relationship between the indian monsoon and enso. *Science*, 284:2156–2159, 1999. doi: 10.1126/science.284.5423.2156. URL https://www.science.org/doi/abs/10.1126/science.284.5423.2156. 3, 14

A. W.-C. Lai, M. Herzog, and H.-F. Graf. Enso forecasts near the spring predictability barrier and possible reasons for the recently reduced predictability. *Journal of Climate*, 31:815 – 838, 2018. doi: https://doi.org/10.1175/JCLI-D-17-0180.1. URL https://journals.ametsoc.org/view/journals/clim/31/2/jcli-d-17-0180.1.xml. 15

J.-Y. Lee, J. Marotzke, G. Bala, L. Cao, S. Corti, J. P. Dunne, F. Engelbrecht, E. Fischer, J. C. Fyfe, C. Jones, et al. Future global climate: scenario-based projections and near-term information. 2021. 29, 35

S. Lee, M. L'Heureux, A. T. Wittenberg, R. Seager, P. A. O'Gorman, and N. C. Johnson. On the future zonal contrasts of equatorial pacific climate: Perspectives from observations, simulations, and theories. *npj Climate and Atmospheric Science*, 5:82, 2022. ISSN 2397-3722. doi: 10.1038/s41612-022-00301-2. URL https://doi.org/10.1038/s41612-022-00301-2. 31

S.-K. Lee, C. Wang, and B. E. Mapes. A simple atmospheric model of the local and teleconnection responses to tropical heating anomalies. *Journal of Climate*, 22:272 – 284, 2009. doi: https://doi.org/10.1175/2008JCLI2303.1. URL https://journals.ametsoc.org/view/journals/clim/22/2/2008jcli2303.1.xml. 12

A. F. Z. Levine, M. J. McPhaden, and D. M. W. Frierson. The impact of the amo on multidecadal enso variability. *Geophysical Research Letters*, 44:3877–3886, 5 2017. ISSN 19448007. doi: 10.1002/2017GL072524. URL http://doi.wiley.com/10.1002/2017GL072524. 4, 20, 28

Z. Liu, S. Vavrus, F. He, N. Wen, and Y. Zhong. Rethinking tropical ocean response to global warming: The enhanced equatorial warming. *Journal of Climate*, 18:4684 – 4700, 2005. doi: https://doi.org/10.1175/JCLI3579.1. URL https://journals.ametsoc.org/view/journals/clim/18/22/jcli3579.1.xml. 30

J. Lloyd, E. Guilyardi, H. Weller, and J. Slingo. The role of atmosphere feedbacks during enso in the cmip3 models. *Atmospheric Science Letters*, 10:170–176, 7

2009. ISSN 1530261X. doi: 10.1002/asl.227. URL http://doi.wiley.com/10.1002/asl.227. 20

J. Lloyd, E. Guilyardi, and H. Weller. The role of atmosphere feedbacks during enso in the cmip3 models. part iii: The shortwave flux feedback. *Journal of Climate*, 25:4275 – 4293, 2012. doi: https://doi.org/10.1175/JCLI-D-11-00178.1. URL https://journals.ametsoc.org/view/journals/clim/25/12/jcli-d-11-00178.1.xml. 20

K. Lu, J. He, B. Fosu, and M. Rugenstein. Mechanisms of fast walker circulation responses to co2 forcing. *Geophysical Research Letters*, 48:e2021GL095708, 2021. doi: https://doi.org/10.1029/2021GL095708. URL https://agupubs.onlinelibrary.wiley.com/doi/abs/10.1029/2021GL095708. e2021GL095708 2021GL095708. 31

J. López-Parages, B. Rodríguez-Fonseca, D. Dommenget, and C. Frauen. Enso influence on the north atlantic european climate: a non-linear and non-stationary approach. *Climate Dynamics*, 47:2071–2084, 2016. ISSN 1432-0894. doi: 10.1007/s00382-015-2951-0. URL https://doi.org/10.1007/s00382-015-2951-0. 12

J. F. Lübbecke and M. J. Mcphaden. A comparative stability analysis of atlantic and pacific niño modes. *Journal of Climate*, 26:5965–5980, 8 2013. ISSN 08948755. doi: 10.1175/JCLI-D-12-00758.1. URL https://journals.ametsoc.org/view/journals/clim/26/16/jcli-d-12-00758.1.xml. 20

N. Maher, R. C. J. Wills, P. DiNezio, J. Klavans, S. Milinski, S. C. Sanchez, S. Stevenson, M. F. Stuecker, and X. Wu. The future of the el niño–southern oscillation: using large ensembles to illuminate time-varying responses and inter-model differences. *Earth System Dynamics*, 14:413–431, 2023. doi: 10.5194/esd-14-413-2023. URL https://esd.copernicus.org/articles/14/413/2023/. 4, 30, 31

M. Martin-Rey, B. Rodriguez-Fonseca, I. Polo, and F. Kucharski. On the atlantic-pacific niños connection: a multidecadal modulated mode. *Climate dynamics*, 43:3163–3178, 2014. 24, 28

V. Masson-Delmotte, P. Zhai, A. Pirani, S. L. Connors, C. Péan, S. Berger, N. Caud, Y. Chen, L. Goldfarb, M. I. Gomis, et al. Climate change 2021: the physical science basis. *Contribution of working group I to the sixth assessment report of the intergovernmental panel on climate change*, 2, 2021. 29

G. J. McCabe, M. A. Palecki, and J. L. Betancourt. Pacific and atlantic ocean influences on multidecadal drought frequency in the united states. *Proceedings of the National Academy of Sciences*, 101:4136–4141, 2004. doi: 10.1073/pnas.0306738101. URL https://www.pnas.org/doi/abs/10.1073/pnas.0306738101. 26

S. McGregor, A. Timmermann, M. F. Stuecker, M. H. England, M. Merrifield, F. F. Jin, and Y. Chikamoto. Recent walker circulation strengthening and pacific cooling amplified by atlantic warming. *Nature Climate Change*, 4:888–892, 5 2014. ISSN 17586798. doi: 10.1038/nclimate2330. 4, 25, 30

S. McGregor, C. Cassou, Y. Kosaka, and A. S. Phillips. Projected enso teleconnection changes in cmip6. *Geophysical Research Letters*, 49:e2021GL097511, 2022. doi: https://doi.org/10.1029/2021GL097511. URL https://agupubs.onlinelibrary.wiley.com/doi/abs/10.1029/2021GL097511. e2021GL097511 2021GL097511. 4, 30, 34, 35

M. J. McPhaden, A. J. Busalacchi, R. Cheney, J. R. Donguy, K. S. Gage, D. Halpern, M. Ji, P. Julian, G. Meyers, G. T. Mitchum, P. P. Niiler, J. Picaut, R. W. Reynolds, N. Smith, and K. Takeuchi. The tropical ocean-global atmosphere observing system: a decade of progress. *Journal of Geophysical Research: Oceans*, 103:14169–14240, 1998. ISSN 21699291. doi: 10.1029/97jc02906. 9

M. J. McPhaden, A. J. Busalacchi, and D. L. Anderson. A toga retrospective. *Oceanography*, 23:87–103, 9 2010. ISSN 10428275. doi: 10.5670/OCEANOG.2010.26. 9

C. S. Meinen and M. J. McPhaden. Observations of warm water volume changes in the equatorial pacific and their relationship to el niño and la niña. *Journal of Climate*, 13:3551 – 3559, 2000.

doi: https://doi.org/10.1175/1520-0442(2000)013<3551:OOWWVC>2.0.CO;2. URL https://journals.ametsoc.org/view/journals/clim/13/20/1520-0442_2000_013_3551_oowwvc_2.0.co_2.xml. 22

B. Mezzina, F. M. Palmeiro, J. García-Serrano, I. Bladé, L. Batté, and M. Benassi. Multi-model assessment of the late-winter stratospheric response to el niño and la niña. *Climate Dynamics*, 58:1987–2007, 2022. ISSN 1432-0894. doi: 10.1007/s00382-021-05836-3. URL https://doi.org/10.1007/s00382-021-05836-3. 12

K. C. Mo and R. W. Higgins. The pacific–south american modes and tropical convection during the southern hemisphere winter. *Monthly Weather Review*, 126: 1581 – 1596, 1998. doi: https://doi.org/10.1175/1520-0493(1998)126<1581:TPSAMA>2.0.CO;2. URL https://journals.ametsoc.org/view/journals/mwre/126/6/1520-0493_1998_126_1581_tpsama_2.0.co_2.xml. 12

E. Mohino, S. Janicot, and J. Bader. Sahel rainfall and decadal to multi-decadal sea surface temperature variability. *Climate Dynamics*, 37:419–440, 2011. ISSN 1432-0894. doi: 10.1007/s00382-010-0867-2. URL https://doi.org/10.1007/s00382-010-0867-2. 26

D. Mukhin, A. Gavrilov, A. Seleznev, and M. Buyanova. An atmospheric signal lowering the spring predictability barrier in statistical enso forecasts. *Geophysical Research Letters*, 48:e2020GL091287, 2021. doi: https://doi.org/10.1029/2020GL091287. URL https://agupubs.onlinelibrary.wiley.com/doi/abs/10.1029/2020GL091287. e2020GL091287 2020GL091287. 15

L. N. Murphy, K. Bellomo, M. Cane, and A. Clement. The role of historical forcings in simulating the observed atlantic multidecadal oscillation. *Geophysical Research Letters*, 44:2472–2480, 2017. doi: https://doi.org/10.1002/2016GL071337. URL https://agupubs.onlinelibrary.wiley.com/doi/abs/10.1002/2016GL071337. 27

G. Muñoz, L. Goddard, A. W. Robertson, Y. Kushnir, and W. Baethgen. Cross–time scale interactions and rainfall extreme events in southeastern south america for the austral summer. part i: Potential predictors. *Journal of Climate*, 28:7894 – 7913, 2015. doi: https://doi.org/10.1175/JCLI-D-14-00693.1. URL https://journals.ametsoc.org/view/journals/clim/28/19/jcli-d-14-00693.1.xml. 3

W. A. Müller and E. Roeckner. Enso impact on midlatitude circulation patterns in future climate change projections. *Geophysical Research Letters*, 33, 3 2006. ISSN 1944-8007. doi: 10.1029/2005GL025032. URL https://onlinelibrary.wiley.com/doi/full/10.1029/2005GL025032https://onlinelibrary.wiley.com/doi/abs/10.1029/2005GL025032https://agupubs.onlinelibrary.wiley.com/doi/10.1029/2005GL025032. 4, 12

S. E. Nicholson and J. Kim. The relationship of the el nin˜onin˜nin˜o-southern oscillation to african rainfall. *INTERNATIONAL JOURNAL OF CLIMATOLOGY*, 17:117–135, 1997. doi: 10.1002/(SICI)1097-0088(199702)17:2<117::AID-JOC84>3.0.CO;2-O. URL https://rmets.onlinelibrary.wiley.com/doi/10.1002/. 14

Y. M. Okumura, M. Ohba, C. Deser, and H. Ueda. A proposed mechanism for the asymmetric duration of el niño and la niña. *Journal of Climate*, 24:3822 – 3829, 2011. doi: https://doi.org/10.1175/2011JCLI3999.1. URL https://journals.ametsoc.org/view/journals/clim/24/15/2011jcli3999.1.xml. 24

C. H. O'Reilly, M. Patterson, J. Robson, P. A. Monerie, D. Hodson, and Y. Ruprich-Robert. Challenges with interpreting the impact of atlantic multidecadal variability using sst-restoring experiments. *npj Climate and Atmospheric Science*, 6:14, 2023. ISSN 2397-3722. doi: 10.1038/s41612-023-00335-0. URL https://doi.org/10.1038/s41612-023-00335-0. 28

P. I. Palmer, C. M. Wainwright, B. Dong, R. I. Maidment, K. G. Wheeler, N. Gedney, J. E. Hickman, N. Madani, S. S. Folwell, G. Abdo, R. P. Allan, E. C. L. Black, L. Feng, M. Gudoshava, K. Haines, C. Huntingford,

M. Kilavi, M. F. Lunt, A. Shaaban, and A. G. Turner. Drivers and impacts of eastern african rainfall variability. *Nature Reviews Earth Environment*, 4:254–270, 2023. ISSN 2662-138X. doi: 10.1038/s43017-023-00397-x. URL https://doi.org/10.1038/s43017-023-00397-x. 14

S. J. Perry, S. McGregor, A. S. Gupta, and M. H. England. Future changes to el niño–southern oscillation temperature and precipitation teleconnections. *Geophysical Research Letters*, 44:10, 608–610, 616, 2017. doi: https://doi.org/10.1002/2017GL074509. URL https://agupubs.onlinelibrary.wiley.com/doi/abs/10.1002/2017GL074509. 4, 35

J. Picaut, F. Masia, and Y. du Penhoat. An advective-reflective conceptual model for the oscillatory nature of the enso. *Science*, 277:663–666, 1997. doi: 10.1126/science.277.5326.663. URL https://www.science.org/doi/abs/10.1126/science.277.5326.663. 15

I. Polo, M. Martin-Rey, B. Rodriguez-Fonseca, F. Kucharski, and C. R. Mechoso. Processes in the pacific la niña onset triggered by the atlantic niño. *Climate Dynamics*, 44:115–131, 5 2014. ISSN 14320894. doi: 10.1007/s00382-014-2354-7. URL https://link.springer.com/article/10.1007/s00382-014-2354-7. 24

S. B. Power and F. P. D. Delage. El niño–southern oscillation and associated climatic conditions around the world during the latter half of the twenty-first century. *Journal of Climate*, 31:6189 – 6207, 2018. doi: https://doi.org/10.1175/JCLI-D-18-0138.1. URL https://journals.ametsoc.org/view/journals/clim/31/15/jcli-d-18-0138.1.xml. 33

S. Qasmi, E. Sanchez-Gomez, Y. Ruprich-Robert, J. Boé, and C. Cassou. Modulation of the occurrence of heatwaves over the euro-mediterranean region by the intensity of the atlantic multidecadal variability. *Journal of Climate*, 34:1099–1114, 2 2021. ISSN 0894-8755. doi: 10.1175/JCLI-D-19-0982.1. URL https://journals.ametsoc.org/view/journals/clim/34/3/JCLI-D-19-0982.1.xml. 26

REFERENCES

E. M. Rasmusson and J. M. Wallace. Meteorological aspects of the el nixf1;o/southern oscillation. *Science*, 222:1195–1202, 1983. doi: 10.1126/science.222.4629.1195. URL https://www.science.org/doi/abs/10.1126/science.222.4629.1195. 5

J. V. Ratnam, S. K. Behera, Y. Masumoto, and T. Yamagata. Remote effects of el niño and modoki events on the austral summer precipitation of southern africa. *Journal of Climate*, 27:3802 – 3815, 2014. doi: https://doi.org/10.1175/JCLI-D-13-00431.1. URL https://journals.ametsoc.org/view/journals/clim/27/10/jcli-d-13-00431.1.xml. 14

B. Rodríguez-Fonseca, I. Polo, J. García-Serrano, T. Losada, E. Mohino, C. R. Mechoso, and F. Kucharski. Are atlantic niños enhancing pacific enso events in recent decades? *Geophysical Research Letters*, 36, 2009. doi: https://doi.org/10.1029/2009GL040048. URL https://agupubs.onlinelibrary.wiley.com/doi/abs/10.1029/2009GL040048. 3, 24

Y. Ruprich-Robert, R. Msadek, F. Castruccio, S. Yeager, T. Delworth, and G. Danabasoglu. Assessing the climate impacts of the observed atlantic multidecadal variability using the gfdl cm2.1 and ncar cesm1 global coupled models. *Journal of Climate*, 30:2785 – 2810, 2017. doi: https://doi.org/10.1175/JCLI-D-16-0127.1. URL https://journals.ametsoc.org/view/journals/clim/30/8/jcli-d-16-0127.1.xml. 26, 27

Y. Ruprich-Robert, E. Moreno-Chamarro, X. Levine, A. Bellucci, C. Cassou, F. Castruccio, P. Davini, R. Eade, G. Gastineau, L. Hermanson, D. Hodson, K. Lohmann, J. Lopez-Parages, P.-A. Monerie, D. Nicolì, S. Qasmi, C. D. Roberts, E. Sanchez-Gomez, G. Danabasoglu, N. Dunstone, M. Martin-Rey, R. Msadek, J. Robson, D. Smith, and E. Tourigny. Impacts of atlantic multidecadal variability on the tropical pacific: a multi-model study. *npj Climate and Atmospheric Science*, 4:33, 12 2021. ISSN 2397-3722. doi: 10.1038/s41612-021-00188-5. URL http://www.nature.com/articles/s41612-021-00188-5. 3, 28

N. H. Saji, B. N. Goswami, P. N. Vinayachandran, and T. Yamagata. A dipole mode in the tropical indian ocean. *Nature*, 401:360–363, 5 1999. ISSN 00280836. doi: 10.1038/43854. 24

A. Santoso, W. Cai, M. Collins, M. McPhaden, F. F. Jin, E. Guilyardi, G. Vecchi, D. Dommenget, and G. Wang. Enso extremes and diversity. dynamics, teleconnections, and impacts. *Bulletin of the American Meteorological Society*, 96:1969–1972, 11 2015. ISSN 11. doi: 10.1175/BAMS-D-15-00141.1. URL https://repository.library.noaa.gov/view/noaa/13185. 21

A. Santoso, M. J. Mcphaden, and W. Cai. The defining characteristics of enso extremes and the strong 2015/2016 el niño. *Reviews of Geophysics*, 55:1079–1129, 12 2017. ISSN 19449208. doi: 10.1002/2017RG000560. 21

T. M. Smith, R. W. Reynolds, T. C. Peterson, and J. Lawrimore. Improvements to noaa's historical merged land–ocean surface temperature analysis (1880–2006). *Journal of Climate*, 21:2283–2296, 5 2008. ISSN 0894-8755. doi: 10.1175/2007JCLI2100.1. URL https://journals.ametsoc.org/view/journals/clim/21/10/2007jcli2100.1.xml. 27

A. H. Sobel, J. Nilsson, and L. M. Polvani. The weak temperature gradient approximation and balanced tropical moisture waves. *Journal of the Atmospheric Sciences*, 58:3650 – 3665, 2001. doi: https://doi.org/10.1175/1520-0469(2001)058<3650:TWTGAA>2.0.CO;2. URL https://journals.ametsoc.org/view/journals/atsc/58/23/1520-0469_2001_058_3650_twtgaa_2.0.co_2.xml. 33

M. J. Suarez and P. S. Schopf. A delayed action oscillator for enso. *Journal of Atmospheric Sciences*, 45:3283 – 3287, 1988. doi: https://doi.org/10.1175/1520-0469(1988)045<3283:ADAOFE>2.0.CO;2. URL https://journals.ametsoc.org/view/journals/atsc/45/21/1520-0469_1988_045_3283_adaofe_2_0_co_2.xml. 15

R. T. Sutton and B. Dong. Atlantic ocean influence on a shift in european climate in the 1990s. *Nature Geoscience*, 5:788–792, 2012. ISSN 1752-0908. doi: 10.1038/ngeo1595. URL https://doi.org/10.1038/ngeo1595. 26

R. T. Sutton and D. L. R. Hodson. Climate response to basin-scale warming and cooling of the north atlantic ocean. *Journal of Climate*, 20:891 – 907, 2007. doi: https://doi.org/10.1175/JCLI4038.1. URL https://journals.ametsoc.org/view/journals/clim/20/5/jcli4038.1.xml. 26

R. T. Sutton, S. P. Jewson, and D. P. Rowell. The elements of climate variability in the tropical atlantic region. *Journal of Climate*, 13:3261 – 3284, 2000. doi: https://doi.org/10.1175/1520-0442(2000)013<3261:TEOCVI>2.0.CO;2. URL https://journals.ametsoc.org/view/journals/clim/13/18/1520-0442_2000_013_3261_teocvi_2.0.co_2.xml. 24

A. S. Taschetto and M. H. England. El niño modoki impacts on australian rainfall. *Journal of Climate*, 22:3167 – 3174, 2009. doi: https://doi.org/10.1175/2008JCLI2589.1. URL https://journals.ametsoc.org/view/journals/clim/22/11/2008jcli2589.1.xml. 21

A. S. Taschetto, C. C. Ummenhofer, M. F. Stuecker, D. Dommenget, K. Ashok, R. R. Rodrigues, and S.-W. Yeh. Enso atmospheric teleconnections. *El Niño Southern Oscillation in a Changing Climate*, pages 309–335, 2020. doi: https://doi.org/10.1002/9781119548164.ch14. URL https://agupubs.onlinelibrary.wiley.com/doi/abs/10.1002/9781119548164.ch14. 13, 23, 34

M. Ting, Y. Kushnir, R. Seager, and C. Li. Forced and internal twentieth-century sst trends in the north atlantic. *Journal of Climate*, 22:1469–1481, 5 2009. ISSN 08948755. doi: 10.1175/2008JCLI2561.1. 27

P. Trascasa-Castro, A. C. Maycock, Y. Y. S. Yiu, and J. K. Fletcher. On the linearity of the stratospheric and euro-atlantic sector response to enso. *Journal of Climate*, 32:6607–6626, 10 2019. ISSN 0894-8755. doi: 10.1175/JCLI-D-18-0746.1. URL https://journals.ametsoc.org/view/journals/clim/32/19/jcli-d-18-0746.1.xml. 12

K. E. Trenberth, G. W. Branstator, D. Karoly, A. Kumar, N.-C. Lau, and C. Ropelewski. Progress during toga in understanding and modeling global teleconnections associated with tropical sea surface temperatures. *Journal of Geo-*

physical Research: Oceans, 103:14291–14324, 5 1998. ISSN 2169-9291. doi: 10.1029/97jc01444. 12

G. A. Vecchi and B. J. Soden. Global warming and the weakening of the tropical circulation. *Journal of Climate*, 20:4316 – 4340, 2007. doi: https://doi.org/10.1175/JCLI4258.1. URL https://journals.ametsoc.org/view/journals/clim/20/17/jcli4258.1.xml. 4

G. A. Vecchi, B. J. Soden, A. T. Wittenberg, I. M. Held, A. Leetmaa, and M. J. Harrison. Weakening of tropical pacific atmospheric circulation due to anthropogenic forcing. 2006. doi: 10.1038/nature04744. 30

D. J. Vimont and J. P. Kossin. The atlantic meridional mode and hurricane activity. *Geophysical Research Letters*, 34, 2007. doi: https://doi.org/10.1029/2007GL029683. URL https://agupubs.onlinelibrary.wiley.com/doi/abs/10.1029/2007GL029683. 26

C. Wang, S. Dong, A. T. Evan, G. R. Foltz, and S.-K. Lee. Multidecadal covariability of north atlantic sea surface temperature, african dust, sahel rainfall, and atlantic hurricanes. *Journal of Climate*, 25:5404 – 5415, 2012. doi: https://doi.org/10.1175/JCLI-D-11-00413.1. URL https://journals.ametsoc.org/view/journals/clim/25/15/jcli-d-11-00413.1.xml. 26

W. Wang and M. J. McPhaden. The surface-layer heat balance in the equatorial pacific ocean. part ii: Interannual variability. *Journal of Physical Oceanography*, 30:2989 – 3008, 2000. doi: https://doi.org/10.1175/1520-0485(2001)031<2989:TSLHBI>2.0.CO;2. URL https://journals.ametsoc.org/view/journals/phoc/30/11/1520-0485_2001_031_2989_tslhbi_2.0.co_2.xml. 20

M. Watanabe and H. Tatebe. Reconciling roles of sulphate aerosol forcing and internal variability in atlantic multidecadal climate changes. *Climate Dynamics*, 53:4651–4665, 2019. ISSN 1432-0894. doi: 10.1007/s00382-019-04811-3. URL https://doi.org/10.1007/s00382-019-04811-3. 27

C. Wengel, S.-S. Lee, M. F. Stuecker, A. Timmermann, J.-E. Chu, and F. Schloesser. Future high-resolution el niño/southern oscillation dynamics. *Nature Climate Change*, 2021. doi: 10.1038/s41558-021-01132-4. URL https://doi.org/10.1038/s41558-021-01132-4. 29

K. Wyrtki. Water displacements in the pacific and the genesis of el nino cycles. *Journal of Geophysical Research: Oceans*, 90:7129–7132, 1985. doi: https://doi.org/10.1029/JC090iC04p07129. URL https://agupubs.onlinelibrary.wiley.com/doi/abs/10.1029/JC090iC04p07129. 7, 22

S.-P. Xie, H. Annamalai, F. A. Schott, and J. P. McCreary. Structure and mechanisms of south indian ocean climate variability. *Journal of Climate*, 15:864 – 878, 2002. doi: https://doi.org/10.1175/1520-0442(2002)015<0864:SAMOSI>2.0.CO;2. URL https://journals.ametsoc.org/view/journals/clim/15/8/1520-0442_2002_015_0864_samosi_2.0.co_2.xml. 24

S.-P. Xie, C. Deser, G. A. Vecchi, J. Ma, H. Teng, and A. T. Wittenberg. Global warming pattern formation: Sea surface temperature and rainfall. *Journal of Climate*, 23:966 – 986, 2010. doi: https://doi.org/10.1175/2009JCLI3329.1. URL https://journals.ametsoc.org/view/journals/clim/23/4/2009jcli3329.1.xml. 30

S. G. Yeager and J. I. Robson. Recent progress in understanding and predicting atlantic decadal climate variability. *Current Climate Change Reports*, 3:112–127, 2017. ISSN 2198-6061. doi: 10.1007/s40641-017-0064-z. URL https://doi.org/10.1007/s40641-017-0064-z. 26

S.-W. Yeh, W. Cai, S.-K. Min, M. J. McPhaden, D. Dommenget, B. Dewitte, M. Collins, K. Ashok, S.-I. An, B.-Y. Yim, and J.-S. Kug. Enso atmospheric teleconnections and their response to greenhouse gas forcing. *Reviews of Geophysics*, 56:185–206, 2018. doi: https://doi.org/10.1002/2017RG000568. URL https://agupubs.onlinelibrary.wiley.com/doi/abs/10.1002/2017RG000568. 12

J. Ying, M. Collins, W. Cai, A. Timmermann, P. Huang, D. Chen, and K. Stein. Emergence of climate change in the tropical pacific. *Nature Climate Change*,

12:356–364, 2022. ISSN 1758-6798. doi: 10.1038/s41558-022-01301-z. URL https://doi.org/10.1038/s41558-022-01301-z. 4, 31, 33

K.-S. Yun, J.-Y. Lee, A. Timmermann, K. Stein, M. F. Stuecker, J. C. Fyfe, and E.-S. Chung. Increasing enso–rainfall variability due to changes in future tropical temperature–rainfall relationship. *Communications Earth Environment*, 2:43, 2021. ISSN 2662-4435. doi: 10.1038/s43247-021-00108-8. URL https://doi.org/10.1038/s43247-021-00108-8. 29, 34

R. Zhang and T. L. Delworth. Impact of atlantic multidecadal oscillations on india/sahel rainfall and atlantic hurricanes. *Geophysical Research Letters*, 33, 2006. doi: https://doi.org/10.1029/2006GL026267. URL https://agupubs.onlinelibrary.wiley.com/doi/abs/10.1029/2006GL026267. 26

W. Zhang, Z. Wang, M. F. Stuecker, A. G. Turner, F. F. Jin, and X. Geng. Impact of enso longitudinal position on teleconnections to the nao. *Climate Dynamics*, 52, 2019. ISSN 14320894. doi: 10.1007/s00382-018-4135-1. 25, 26

W. Zhang, F. Jiang, M. F. Stuecker, F.-F. Jin, and A. Timmermann. Spurious north tropical atlantic precursors to el niño. *Nature Communications 2021 12:1*, 12:1–8, 5 2021. ISSN 2041-1723. doi: 10.1038/s41467-021-23411-6. URL https://www.nature.com/articles/s41467-021-23411-6. 21

Chapter 2

Warm phase of the Atlantic Multidecadal Variability damps ENSO through weakened thermocline feedback

Authors: **Paloma Trascasa-Castro, Yohan Ruprich-Robert, Frederic Castruccio and Amanda C. Maycock.**

Necesito el mar porque me enseña,
no sé si aprendo música o conciencia
no sé si es ola sola o ser profundo
o sólo ronca voz o deslumbrante
suposición de peces y navíos.
El hecho es que hasta cuando estoy dormido,
de algún modo magnético circulo
en la universidad del oleaje.

El mar[1], by Pablo Neruda.

[1]Translation: I need the sea because it teaches me. I don't know if I learn music or awareness, if it's a single wave or its vast existence, or only its harsh voice or its shining suggestion of fishes and ships. The fact is that until I fall asleep, in some magnetic way I move in the university of the waves

Abstract

Interactions between ocean basins affect El Niño–Southern Oscillation (ENSO), altering its impacts on society. Here, we explore the effect of Atlantic Multidecadal Variability (AMV) on ENSO behavior using idealized experiments performed with the NCAR-CESM1 model. Comparing warm (AMV+) to cold (AMV-) AMV conditions, we find that ENSO sea surface temperature (SST) anomalies are reduced by 10% and ENSO precipitation anomalies are shifted to the west during El Niño and east during La Niña. Using the Bjerknes stability index, we attribute the reduction in ENSO variability to a weakened thermocline feedback in boreal autumn. In AMV+, the Walker circulation and trade winds strengthen over the tropical Pacific, increasing the background zonal SST gradient. The background changes shift ENSO anomalies westwards, with wind stress anomalies more confined to the west. We suggest the changes in ENSO-wind stress decrease the strength of the thermocline feedback in the east, eventually reducing ENSO growth rate.

Plain Language Summary

El Niño–Southern Oscillation (ENSO) is the dominant mode of year-to-year climate variability in the tropics and affects regional climates around the world. Understanding the drivers of ENSO behavior is important for its prediction. One influential factor is communication between ocean basins, such as the North Atlantic interaction with the tropical Pacific. In our work, we use idealized simulations that represent the positive and negative phases of the Atlantic Multidecadal Variability (AMV) to understand how sea surface temperature changes in the North Atlantic affect the dynamics of ENSO in the tropical Pacific. We find that both El Niño and La Niña events are weaker when the North Atlantic is warmer than usual, and vice versa. During the warm phase of the AMV (AMV+), the trade winds associated with the Walker circulation are localized in the west Pacific, directly impacting sea surface temperature patterns associated with ENSO events. Reduced wind stress in the eastern equatorial Pacific means that the

upper ocean heat content is less perturbed in the AMV+ simulation, eventually feeding back to ENSO-related sea surface temperatures.

2.1. Introduction

El Niño–Southern Oscillation (ENSO) is the dominant mode of interannual climate variability in the tropics. The spatiotemporal characteristics of ENSO exhibit variations (Dieppois et al., 2021; Wittenberg, 2009) driven by chaotic atmosphere–ocean dynamics (Fedorov et al., 2003; Zhang et al., 2021) and sources of variability from outside the tropical Pacific (Meehl et al., 2001). Given the global reach of ENSO and its impacts (Diaz et al., 2001), understanding and predicting changes in ENSO is a major challenge for the scientific community.

In the last decade, it has become evident that climate variability and changes in other ocean basins can affect the tropical Pacific and ENSO (Cai et al., 2019). One example is the impact of Atlantic Multidecadal Variability (AMV) on the mean climate in the tropical Pacific (e.g., (Ruprich-Robert et al., 2017)). However, the extent to which AMV affects ENSO remains unclear (Dong and Sutton, 2007; Hu and Fedorov, 2018; Levine et al., 2017; Yu et al., 2015). On interannual time scales, sea surface temperature (SST) anomalies in the tropical North Atlantic alter tropical Pacific SSTs via subtropical teleconnections (Ham and Kug, 2015; Wang et al., 2017). Warm SST anomalies in the equatorial Atlantic are known to influence ENSO variability by strengthening the Walker circulation (Polo et al., 2014; Rodríguez-Fonseca et al., 2009). The intensified descending branch in the equatorial east Pacific reinforces the trade winds and supports the development of a La Niña event in the following winter.

Levine et al. (2017) found that the AMV alters both the seasonal and annual ENSO stability by changing the mean seasonal cycle in the tropical Pacific. In the relatively short observational record, they found evidence for reduced ENSO growth rate in boreal autumn and winter when the North Atlantic is anomalously warm, but their model experiments did not reproduce this and instead

showed the opposite behavior. Zanchettin et al. (2016) identified a delayed response to the AMV in the tropical Pacific and suggested this could contribute to multidecadal ENSO variability. Both Zanchettin et al. (2016) and Levine et al. (2017) highlight that changes in thermocline dynamics are key to understanding the modulation of ENSO by the AMV. Despite this common finding, owing to the short observational record and different results from model studies, there remains uncertainty around the impact of the AMV on ENSO. This study aims to advance understanding of the processes by which the AMV affects ENSO characteristics using idealized simulations performed with the NCAR-CESM1 climate model. The paper explores changes in the atmospheric and oceanic processes that are responsible for ENSO growth and decay using the Bjerknes stability index (hereafter BJ index). With this comprehensive approach, we are able to identify specific mechanisms involved in changes in ENSO under different AMV states.

2.2. Data and Methods

2.2.1. Climate Model Simulations

Simulations were performed with the NCAR-CESM1(CAM5) model (hereafter CESM1; (Kay et al., 2015)). All components of CESM1 have 1° horizontal resolution. The atmospheric component CAM5.2 has 30 hybrid vertical levels. The ocean component POP2 has 60 vertical levels and a meridional mesh refinement down to 0.25° near the equator. CESM1 simulates ENSO in good agreement with observations (Figure 2.6 in Supporting Information); (DiNezio et al., 2017; Wu et al., 2021; Zhang et al., 2017)).

To assess the impacts of the AMV on ENSO behavior, idealized experiments were performed in which warm (AMV+) and cold (AMV-) SST anomalies equivalent in amplitude but opposite in sign are imposed in the North Atlantic through surface relaxation (Figure 2.5 in Supporting Information; (Castruccio et al., 2019; Ruprich-Robert et al., 2017)). The imposed SST anomalies do not vary in time nor account for AMV seasonality. The simulations follow the protocol of the Decadal Climate Prediction Project Phase C Idealized AMV experiment (Boer

et al., 2016), with the minor exception that the observed AMV pattern was computed from the ERSSTv3b (Smith et al., 2008) data set instead of ERSSTv4 (Huang and Xie, 2015).

Three ocean initial states are obtained from a preindustrial control simulation; the corresponding atmospheric conditions are perturbed at round-off level in the potential temperature field to obtain 10 different atmospheric initial conditions (Castruccio et al., 2019). This produces 30 ensemble members each integrated for 10 years, giving a total of 300 years for each AMV phase. The first 11 months of the simulation are discarded and the analysis presents results from the remaining period.

2.2.2. Analysis Methods

2.2.2.1. ENSO definition

El Niño and La Niña events occur when SST anomalies in the Niño3.4 region (5°N–5°S, 170°W–120°W, cf. Figure 2.1a) exceed ±0.5 K during boreal winter (from December to February, hereafter DJF) relative to the climatology of each simulation. This identifies 77 and 79 El Niños in the AMV+ and AMV- simulations, respectively. For La Niña, there are 91 events in AMV+ and 103 in AMV-.

To estimate the AMV modulation of ENSO impacts, we first estimate El Niño anomalies with respect to each AMV experiment mean state and then subtract the AMV- El Niño composite from AMV+ the El Niño composite:

$$(ElNiño_{AMV+} - \mu_{AMV+}) - (ElNiño_{AMV-} - \mu_{AMV-}) \tag{2.1}$$

where μ_{AMV+} and μ_{AMV-} are time averaged SSTs in the AMV+ and AMV- simulations, respectively. The AMV modulation of La Niña impacts is calculated following the same approach.

2.2.2.2. The Bjerknes Stability Index

To examine the processes underpinning any changes in ENSO characteristics due to the AMV, we use the BJ index introduced by Jin et al. (2006), which is proportional to ENSO growth rate. This is based on the recharge oscillator model (Jin, 1997a) and captures the main atmosphere and ocean processes responsible for ENSO growth and decay (Kim and Jin, 2011b). The BJ index has been widely used to compare ENSO behavior between different climate models (Kim and Jin, 2011a,b), time periods (Lübbecke McPhaden, 2013), and background states (Ferrett and Collins, 2019; Levine et al., 2017). The BJ index is defined as:

$$\begin{aligned} 2\mathrm{BJ}= &- \left[a_1 \frac{\langle \Delta\bar{u} \rangle_E}{L_x} + a_2 \frac{\langle \Delta\bar{v} \rangle_E}{L_y}\right]_{CD} - [\alpha_s]_{TD} + \left[\mu_a \beta_u \langle -\frac{\delta\bar{T}}{\delta x} \rangle_E\right]_{ZA} + \\ &\left[\mu_a \beta_w \langle -\frac{\delta\bar{T}}{\delta z} \rangle_E\right]_{EK} + \left[\mu_a \beta_h \langle -\frac{\bar{w}}{H_1} \rangle_E a_h\right]_{TC} \end{aligned} \tag{2.2}$$

The ENSO growth rate is estimated as the sum of, from left to right, the current damping (CD), thermodynamic (TD), zonal advective (ZA), Ekman (EK), and thermocline (TC) feedbacks. Following previous studies (An and Kim, 2017; Guilyardi et al., 2009; Jin et al., 2006; Kim and Jin, 2011a,b; Lübbecke and Mcphaden, 2013), the BJ index terms are calculated using linear regression between variables across all years in the simulations. A full description of the equation is given in Section 2.6.

The BJ index assumes linearity between variables and may therefore fail to represent processes that are nonlinear by nature, such as the dependence of shortwave fluxes on SSTs (see Figure 2.8 in 2.6; (Graham et al., 2014; Lloyd et al., 2012). However, as discussed below, we find that for the feedbacks that are responsible for the AMV modulation of ENSO, the linear approximation is reasonable to first order (Figure 2.9 in 2.6). Despite certain simplifying assumptions used in the BJ index, it has been widely used and shown to be insightful for understanding

ENSO behavior.

The relative contributions of the individual terms in the feedbacks in Equation 2 to the modulation of ENSO growth rate are calculated using a delta method where for a given term the difference between AMV+ and AMV- is multiplied by the AMV- value of all the other terms. The delta method applied to the thermocline feedback is as follows:

$$\begin{aligned}
\Delta\mu_a &= (\mu_{AMV+} - \mu_{AMV-}) \times \beta_{hAMV-} \times \frac{\bar{w}}{H_{1AMV-}} \times a_{hAMV-} \\
\Delta\beta_h &= \mu_{AMV-} \times (\beta_{hAMV+} - \beta_{hAMV-}) \times \frac{\bar{w}}{H_{1AMV-}} \times a_{hAMV-} \\
\Delta\frac{\bar{w}}{H_1} &= \mu_{AMV-} \times \beta_{hAMV-} \times \left(\frac{\bar{w}}{H_{1AMV+}} - \frac{\bar{w}}{H_{1AMV-}}\right) \times a_{hAMV-} \\
\Delta a_h &= \mu_{AMV-} \times \beta_{hAMV-} \times \frac{\bar{w}}{H_{1AMV-}} \times (a_{hAMV+} - a_{hAMV+})
\end{aligned} \tag{2.3}$$

Finally, to test whether the difference in ENSO impacts and feedbacks between AMV+ and AMV- is statistically significant at the 95% confidence level, we perform a nonparametric bootstrap test with replacement, subsampling 70% of years on each iteration repeated 10^4 times and where we assume that all years are independent from each other.

2.3. Results

2.3.1. AMV Modulation of Pacific Mean State and ENSO Variability

In boreal winter (DJF), warm AMV conditions drive tropical Pacific cooling of 0.23 K in the Niño3.4 region, with a minimum of 0.35 K near the dateline (Figure 2.1a). This response is consistent with modeling studies (Dong and Sutton, 2007; Ruprich-Robert et al., 2017; Zanchettin et al., 2016), although CESM1 simulates a stronger tropical Pacific response than some other climate models for similar imposed AMV anomalies (Ruprich-Robert et al., 2021). The mean precipitation response to AMV+ (Figure 2.1b) shows that the Intertropical Convergence Zone

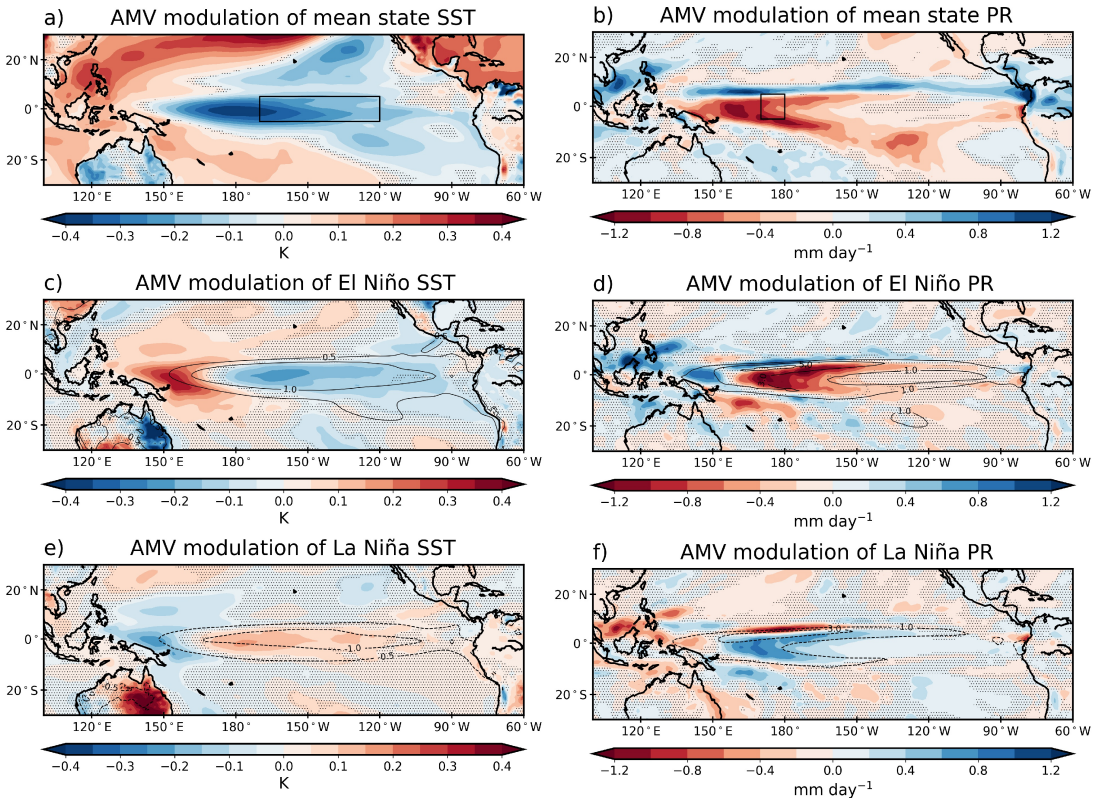

Figure 2.1: Anomalies for boreal winter (December–February; DJF). (top) Tropical Pacific mean state changes between Atlantic Multidecadal Variability (AMV)+ and AMV- in (a) sea surface temperature (SST) and (b) precipitation and 850 hPa winds. (middle) AMV modulation of El Niño (c) SST and (d) precipitation (shading); composite El Niño anomalies from AMV overlaid in contours. (bottom) As in middle, but for La Niña. Black boxes in (a) and (b) denote the Niño3.4 region and the region used for the precipitation index, respectively. Note inverted color bars in the left and right columns. Stippling means not significance at the 95% confidence level.

(ITCZ) is shifted north in boreal winter, and the South Pacific Convergence Zone (SPCZ) is weakened. These changes in the tropical Pacific mean state are a signature of a strengthened Walker circulation (Lübbecke and McPhaden, 2014), a key mechanism in the tropical Pacific response to warm SSTs in the tropical Atlantic at any time scale (Ham and Kug, 2015; Kosaka and Xie, 2013; Meehl et al., 2011; Ruprich-Robert et al., 2017).

In DJF, AMV+ damps ENSO variability, reducing the magnitude of SST and precipitation anomalies in both El Niño and La Niña phases (Figures 2.1c and 2.1e). El Niño events in AMV+ have, on average, cooler SSTs in the central and eastern equatorial Pacific (hereafter EP), and relatively warmer SSTs in the west Pacific, as compared to AMV-. The Niño3.4 SST difference between AMV+ and AMV- is 0.17 K (13%). The modulation of La Niña SSTs by the AMV has a similar pattern with opposite sign and a slightly smaller amplitude: the La Niña composite Niño3.4 SST is 0.09 K (9%) warmer in AMV+. Hence, in CESM1 AMV modulates the amplitude of ENSO SST anomalies by around 10% in the Niño3.4 region.

The AMV modulation of ENSO SSTs is accompanied by modulation of precipitation anomalies in the equatorial Pacific. During AMV+, the area of maximum anomalous precipitation associated with El Niño shifts from the central to the western Pacific, with a reduction in precipitation anomaly of up to 1.15 mm day^{-1} around the equator and between 170°E and 180° (Figure 2.1d) and an increase in precipitation anomalies over the warm pool and the Maritime continent. This represents a statistically significant decrease in the central Pacific precipitation anomaly under El Niño by 40% (see box in Figure 2.1b) as compared to AMV-. AMV modulates the precipitation response to La Niña in a similar way (Figure 2.1f). In this case, during AMV+, the precipitation anomaly decreases in the western equatorial Pacific and increases over the central Pacific by 0.65 mm day^{-1} (45%). Hence, in CESM1 the modulation by AMV of ENSO precipitation is proportionately larger than for SSTs. This can be explained by the nonlinear relationship between precipitation and SST in the Niño3.4 region. To test this nonlinearity, a simple regression model was built considering only El Niño events.

This model shows that around 90% of the El Niño precipitation modulation by AMV can be explained by the SST modulation (not shown). Hence, the modulation by AMV of ENSO SST signal is of leading importance for the modulation of ENSO atmospheric response.

The decrease in ENSO variability simulated by CESM1 in AMV+ is consistent with observations (Levine et al., 2017; Lübbecke and McPhaden, 2014; Zanchettin et al., 2016). Our results are also consistent with the modeling study of Dong and Sutton (2007), but opposite to the ones of Levine et al. (2017). To further understand the modulation of ENSO by AMV, we next investigate the physical processes driving this modulation using the BJ index (cf. Section 2.2.2.2).

2.3.2. AMV Modulation of ENSO Feedbacks

CESM1 simulates a realistic seasonal cycle of ENSO growth rate in the reference AMV- simulation (Figure 2.2a), with a minimum of -2.4 year^{-1} in spring and a maximum of 1.7 year^{-1} in autumn (cf., solid black line). Maximum values of the BJ index in October–December coincide with the development and growth of ENSO events, whereas minimum values are reached in March–May, when ENSO decays. On average over the year, the ENSO growth rate simulated by CESM1 is -0.22 year^{-1}, which is very close to reanalysis-based estimates of -0.24 year^{-1} (Kim et al., 2014).

The annual growth rate depends on the balance between positive and negative feedbacks. The negative sign of the annual mean BJ index is dominated by the damping of SST anomalies by the thermodynamic feedback, peaking in early spring, which is composed of the sum of the surface heat fluxes. The thermocline feedback peaking in late fall is the main process that intensifies ENSO anomalies Jin et al. (2020). Consistent with the damped ENSO variability seen in Figure 2.1, AMV+ leads to a more negative annual mean ENSO growth rate by 0.07 year^{-1} (Figure 2.2b), which represents a 30% decrease in magnitude compared to AMV-. The main contributions to the decreased annual ENSO growth rate in AMV+ are a weakened thermocline feedback (0.08 year^{-1}) and a stronger current

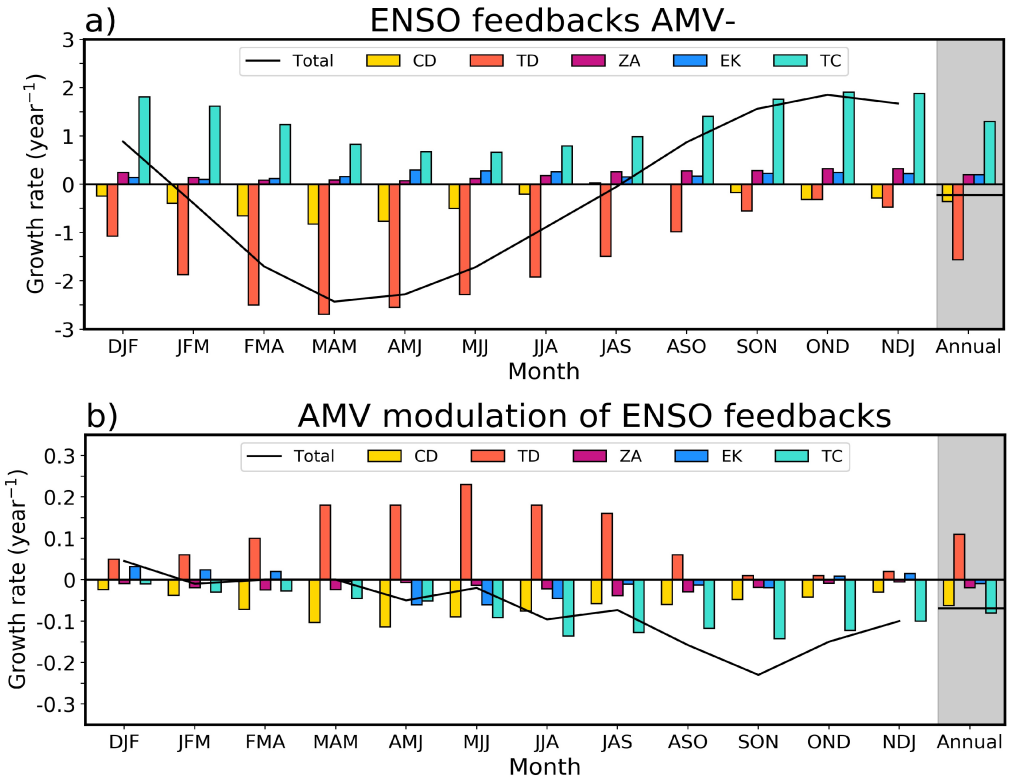

Figure 2.2: Annual cycle ENSO feedbacks expressed as growth rate (year^{-1}) in (a) the AMV- simulation, and (b) the difference between AMV+ and AMV-. Monthly values are smoothed with a 3-month running mean. Feedbacks are: current damping (CD, yellow), thermodynamic (TD, orange), zonal advective (ZA, magenta), Ekman (EK, dark blue), and thermocline (TC, light blue). The solid line denotes the total Bjerknes stability (BJ) index.

damping feedback (0.06 year^{-1}; Figure 2.2b). These changes are partly offset by a weakened (i.e., reduced damping) thermodynamic feedback by 0.1 year^{-1}. There are negligible changes in the Ekman feedback and zonal advective feedback due to AMV (see also Figure 2.7 in 2.6) and these will not be discussed further.

The AMV modulation of the thermodynamic feedback is strongest in boreal summer, contributing to an increase in growth rate of up to 0.23 year^{-1} in May–July. Of the two terms contributing to a reduced ENSO growth rate, the modulation of the current damping peaks in April–June. The modulation of the thermocline feedback by AMV dominates from boreal summer through early winter (JJA to NDJ) and therefore has a particular influence during the ENSO growth season. This suggests that the thermocline feedback is an important driver of the changes in ENSO behavior between AMV+ and AMV-.

Investigation of the contributions of individual terms in Equation 2 to the overall modulation of the BJ index feedbacks (Figure 2.7 in 2.6) reveals that the modulation of most terms is not strongly statistically significant. The main exception which is relevant to understanding the dampening of ENSO by AMV+ is the thermocline feedback, which is dominated by a statistically significant decrease in the magnitude of the regression between equatorial Pacific wind stress anomalies and the thermocline slope (β_h in Equation 2, orange bar Figure 2.3a). This leads to a reduction in ENSO growth rate by 0.1 year^{-1}. The finding that the AMV modulates ENSO through modifying how the thermocline slope responds to equatorial Pacific wind stress anomalies is in agreement with Zanchettin et al. (2016). We discuss in the following section how the AMV impacts on the equatorial Pacific mean state alter this relationship.

2.4. Discussion

A mean tropical Pacific cooling in response to a tropical Atlantic warming is well documented in the literature (Figure 2.4a). Warm tropical Atlantic SST anomalies intensify deep convection and lead to upper tropospheric mass divergence over the tropical Atlantic, which modifies the entire Walker circulation

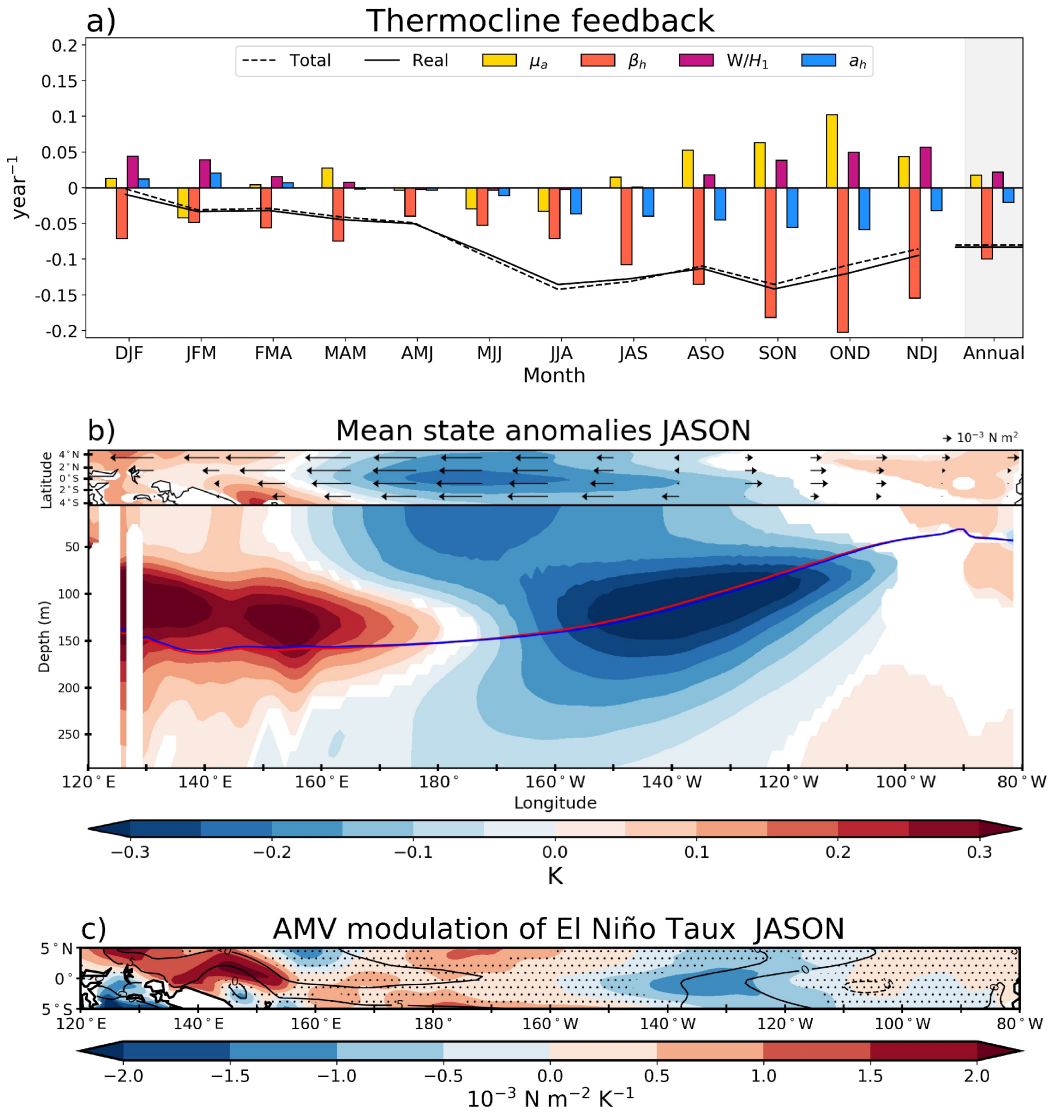

Figure 2.3: (a) AMV modulation of the thermocline feedback and contributions from individual terms. (b) Three-dimensional mean state ocean temperature differences (AMV+ minus AMV-) in the equatorial Pacific in JASON. White areas cover non-significant anomalies at the 95% confidence level. (top) Arrows are zonal wind stress anomalies; (bottom) red and blue lines show depth of 20°C isotherm in the AMV+ and AMV states, respectively. (c) AMV modulation of equatorial wind stress in the JASON season prior to El Niño events. Anomalies are normalized by the mean Niño3.4 SST amplitude in AMV+ and AMV, respectively. Black contours show wind stress anomalies in the AMV simulation. Dotted areas show nonsignificant anomalies at the 95% confidence level.

(Dong and Sutton, 2007; Ham and Kug, 2015; Martin-Rey et al., 2014; McGregor et al., 2014; Polo et al., 2014; Rodríguez-Fonseca et al., 2009; Ruprich-Robert et al., 2017, 2021; Zanchettin et al., 2016). This is associated with an intensification of the trade winds, which deepens the thermocline in the west Pacific and steepens the thermocline slope (Figure 2.3b); (Kucharski et al., 2014; Meehl et al., 2021; Polo et al., 2014).

Differences in the mean state between AMV+ and AMV- damp ENSO in CESM1 mainly by a weakened thermocline feedback. The weaker thermocline slope sensitivity to equatorial Pacific wind stress (i.e., smaller β_h) can be explained by a decrease in ocean stratification associated with a deepening of the thermocline (Jin and An, 1999; Zebiak and Cane, 1987) and/or a change in the wind stress forcing pattern (Choi et al., 2011; Kang and Kug, 2002; Wang and An, 2002).

Dong and Sutton (2007) found that intensified trade winds during AMV+ led to a deepened thermocline in the western and central tropical Pacific. They argue that this deepening reduces the development of subsurface temperature anomalies in response to wind stress (Zebiak and Cane, 1987), which eventually weakens ENSO. We also find the thermocline deepens by 0.6 m on average in the western tropical Pacific from late summer to early winter in AMV+ (Figure 2.3b). Conversely, the thermocline shallows by 0.7 m over the central and eastern equatorial Pacific, which following this logic would increase its sensitivity to wind stress anomalies. The climatological thermocline in this region is shallower than over the western Pacific and therefore potentially more responsive to wind anomalies (Castaño-Tierno et al., 2018). The shallowing of the thermocline in the central and eastern equatorial Pacific would therefore lead to an increase in β_h. Thus, we conclude that this mechanism cannot explain the ENSO response in our simulations.

Regarding the second mechanism, we find the pattern of wind stress anomalies associated with ENSO is modulated by AMV (Figure 2.3c). During AMV+, equatorial wind stress anomalies are stronger over the western Pacific but extend

less to the east (between 150°W and 120°W), where the thermocline is shallower and therefore more sensitive to wind stress (Castaño-Tierno et al., 2018). We suggest this weakening of ENSO-wind stress anomalies in the region where the thermocline is more sensitive to wind forcing can explain the β_h decrease in AMV+. This conclusion aligns with previous studies that also find a reduction in ENSO variance associated with a steeper thermocline mean state in the equatorial Pacific (Fedorov and Philander, 2000; Hu and Fedorov, 2018; Lübbecke and McPhaden, 2014).

Following Lübbecke and McPhaden (2014), we argue that the decrease of the ENSO-wind forcing over the eastern Pacific in AMV+ is linked to a strengthening of the climatological zonal SST gradient (Figure 2.3b). Associated with the stronger zonal SST gradient in the tropical Pacific, the warmest SSTs are shifted westward compared to AMV-. The response of deep convection to SST anomalies in the tropics is a function of the climatological SST, with stronger precipitation responses over climatologically warm SSTs (Graham and Barnett, 1987), so the ENSO precipitation and associated wind convergence anomalies are also expected to shift westward in AMV+.

With a similar experimental design but a different model, Levine et al. (2017) found that AMV+ increases ENSO growth rate and amplitude, in contrast to the modulation apparent in observations and found in our simulations. They suggest this discrepancy comes from a too sensitive thermocline feedback to SST anomalies in the eastern tropical Pacific in their model (Kim and Jin, 2011b). Nevertheless, this difference in behavior of models calls for a multimodel analysis, which will be conducted in a future study using the AMV idealized experiments performed within the Component C of the Decadal Climate Prediction Project (Boer et al., 2016).

2.5. Conclusions

We have used idealized ensemble simulations with the CESM1 model where North Atlantic SSTs are restored toward observed warm (AMV+) and cold (AMV-

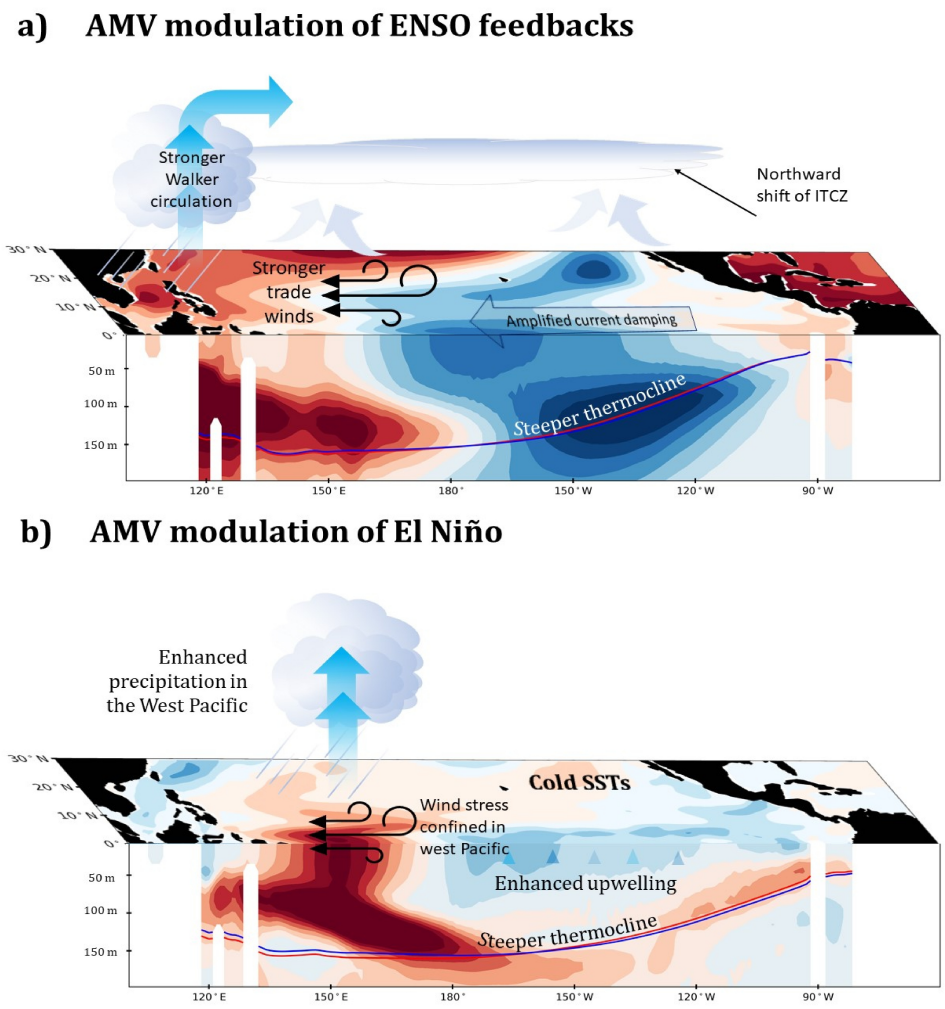

Figure 2.4: Schematic overlay of (a) the mean state changes due to AMV in the equatorial Pacific in JASON and (b) the climate response to El Niño modulated by the AMV in DJF. Shading shows ocean temperature anomalies. Red and blue lines in both panels show the 20°C isotherm in the AMV+ and AMV- experiments, respectively.

) AMV states to investigate its impact on ENSO variability. Comparing AMV+ to AMV-, we find that warm North Atlantic conditions reduce the amplitude of SST anomalies associated with ENSO by around 10% in both El Niño and La Niña phases. ENSO precipitation anomalies decrease by a larger proportion of up to 45%. During AMV+, the trade wind slackening associated with El Niño are more confined to the west and are accompanied by a westward shift of the maximum SST and deep convection anomalies (Figure 2.4b).

Using the BJ index as a proxy for ENSO growth rate, we find that the decrease of ENSO variance under AMV+ conditions comes mainly from a decrease in the thermocline feedback in AMV+ and, to a smaller extent, by a decrease of the current damping feedback. We hypothesize that the decrease of the thermocline feedback in AMV+ results from the strengthened trade winds localized over the western equatorial Pacific, and associated steepening of the background thermocline, which increase the east-west mean SST gradient in the equatorial Pacific. In the equatorial east Pacific, climatological zonal ocean currents are weaker during boreal autumn in AMV+ compared to AMV-, as is the zonal SST gradient. During El Niño events, this increased zonal SST gradient prevents the convection and westerlies anomalies from propagating through the east where the thermocline is shallower and therefore more responsive to wind stress anomalies. It results in a weakening of the wind–thermocline relationship, which eventually reduces ENSO growth rate.

Our results show a substantial modulation of ENSO by AMV in the CESM1 model. The AMV modulation of ENSO growth rate is opposite to the projected changes under global warming (Collins et al., 2010). Decadal climate variability may therefore mask or amplify the signature of anthropogenic climate change and must be accounted for in future ENSO predictions. Changes to ENSO SST and precipitation variability are likely to have extratropical implications. Further work will explore the role of the AMV in the modulation of ENSO extratropical impacts and their variability.

2.6. Supporting information

This section provides additional graphic information to support our results, including the sea surface temperature (SST) anomaly pattern associated with the positive phase of the Atlantic Multidecadal Variability (AMV) and El Niño Southern Oscillation (ENSO), a decomposition of the AMV modulation of ENSO feedbacks in its individual terms and an illustration of the linearity of the SW and β_h terms. Additionally, this document contains detailed instructions to calculate the Bjerknes Stability index.

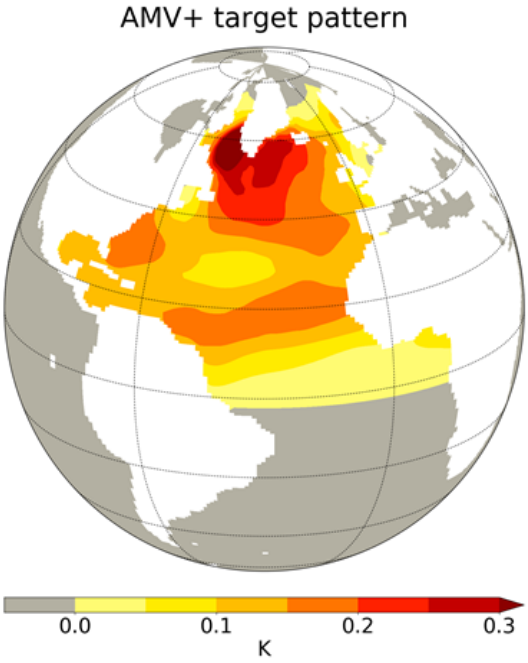

Figure 2.5: Target AMV+ sea surface temperature (SST) pattern. The AMV- is equivalent in amplitude but with opposite sign SST anomalies.

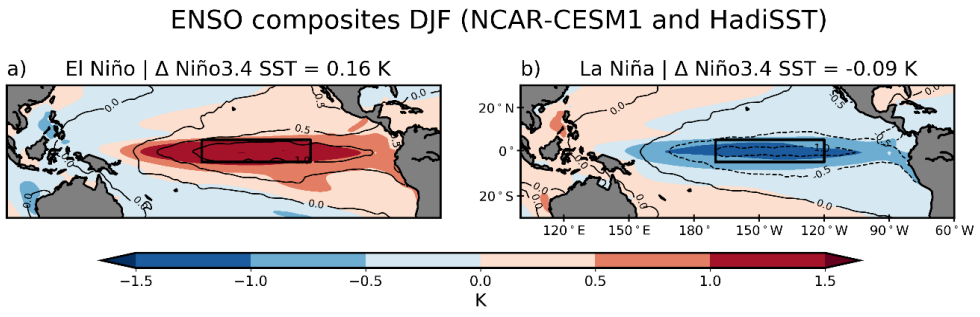

Figure 2.6: El Niño (a) and La Niña (b) SST anomaly composite in NCAR-CESM1 (filled contours) and observations (HadiSST, black contours). The differences in Niño3.4 SST anomalies between the model and observations is 0.16 K for El Niño and -0.09 for La Niña. The black rectangle denotes the Niño3.4 region (5°N-5°S, 170°E-120°E)

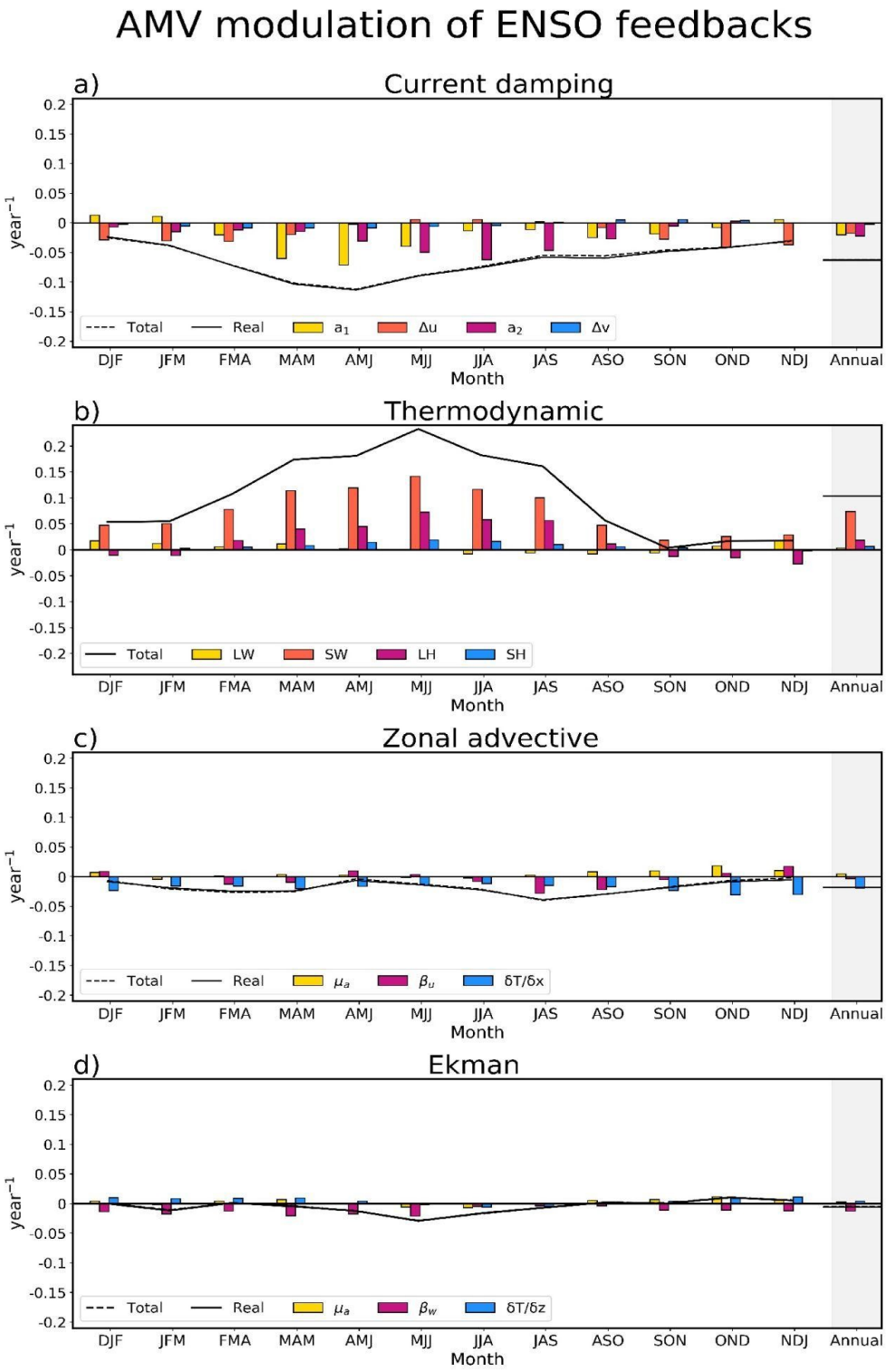

Figure 2.7: Figure AMV modulation of the ENSO feedbacks, decomposed onto their independent terms to homogenize their units. Monthly values are smoothed with a 3-month running mean.

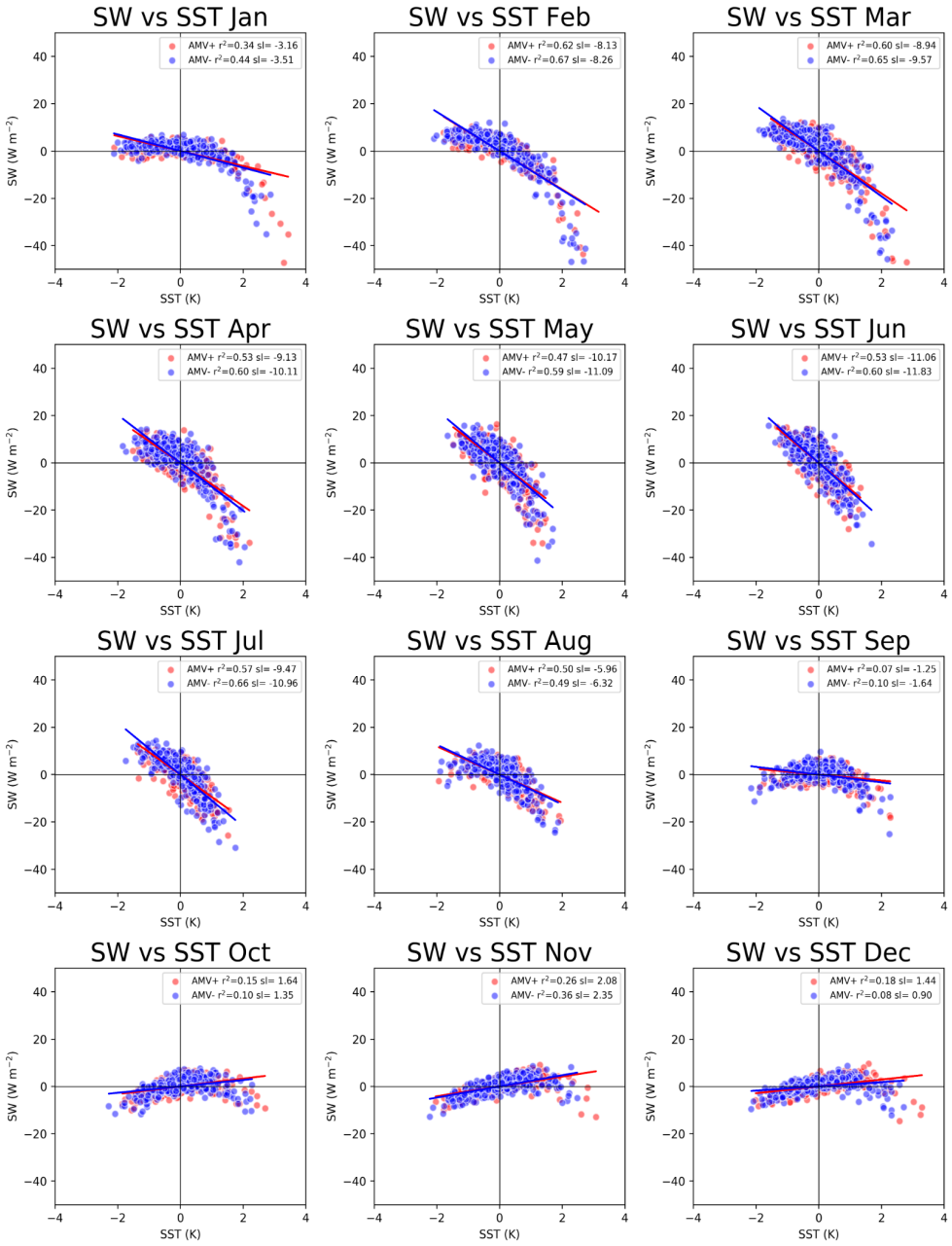

Figure 2.8: Scatterplot of monthly east Pacific shortwave radiation anomalies vs. east Pacific sea surface temperature anomalies in the AMV+ (red) and AMV- (blue) experiments. The legend shows the regression slope (W m^{-2} K^{-1}) and r^2 value.

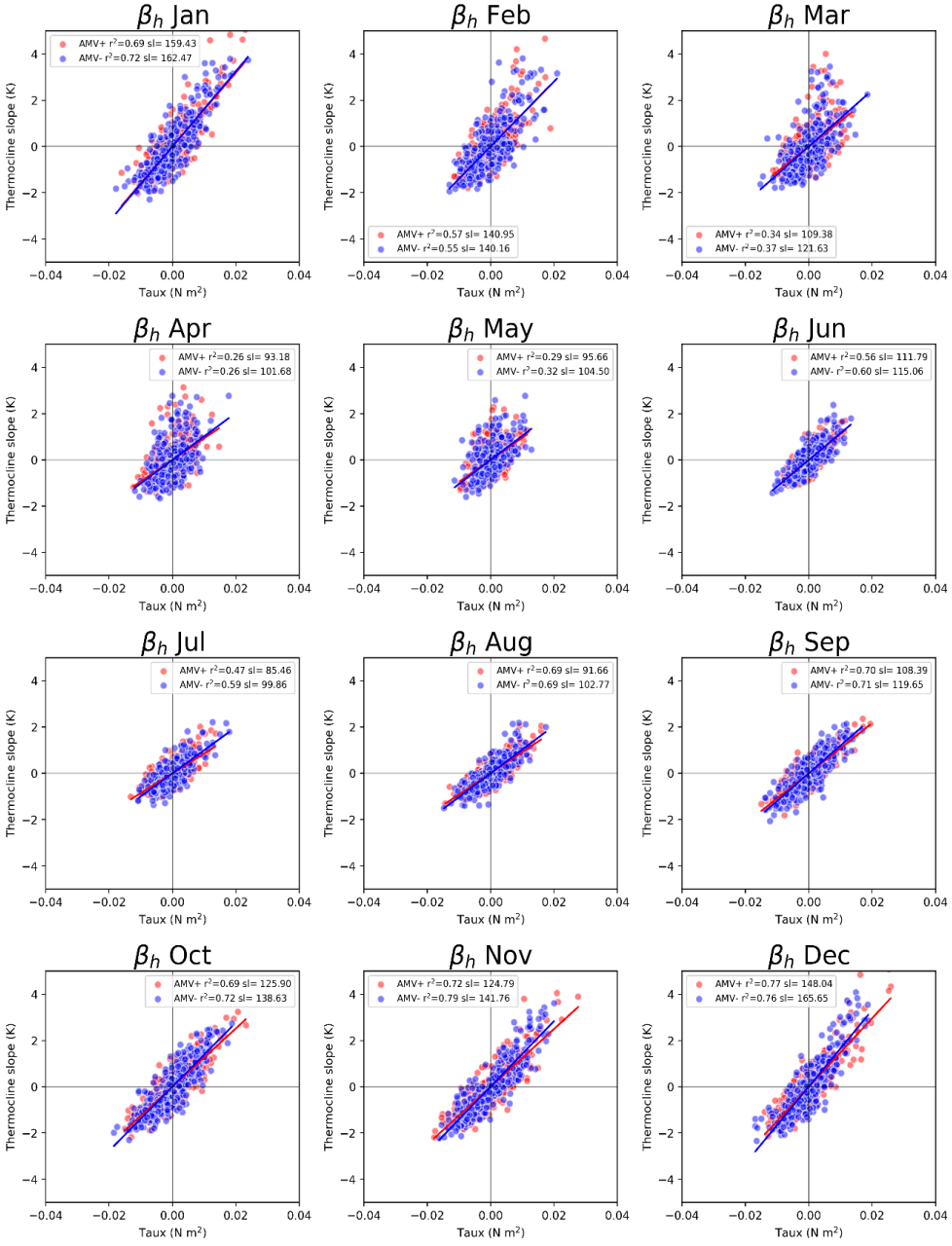

Figure 2.9: Scatterplot of monthly east Pacific thermocline slope anomalies vs. equatorial Pacific wind stress anomalies in the AMV+ (red) and AMV- (blue) experiments. The legend shows the regression slope (K^{-1} (N m^2) and r^2 value.

2.6.1. Methodology to calculate the BJ index

$$2\text{BJ}=\text{-}\left[a_1\frac{\langle\Delta\bar{u}\rangle_E}{L_x}+a_2\frac{\langle\Delta\bar{v}\rangle_E}{L_y}\right]_{CD}-[\alpha_s]_{TD}+\left[\mu_a\beta_u\langle-\frac{\delta\bar{T}}{\delta x}\rangle_E\right]_{ZA}+\left[\mu_a\beta_w\langle-\frac{\delta\bar{T}}{\delta z}\rangle_E\right]_{EK}+\left[\mu_a\beta_h\langle-\frac{\bar{w}}{H_1}\rangle_E a_h\right]_{TC} \tag{2.4}$$

The Bjerknes Stability Index (hereafter BJ index) is based on the recharge oscillator model ((Jin, 1997b)) and was introduced by Jin et al. (2006) with the aim of quantifying the different atmosphere and ocean mechanisms involved in ENSO growth rate.

The ENSO growth rate is estimate as the sum of, from left to right, the current damping (CD), thermodynamic (TD), zonal advective (ZA), Ekman (EK), and thermocline (TC) feedbacks. Following previous studies (An and Kim, 2017; Guilyardi et al., 2009; Jin et al., 2006; Kim and Jin, 2011a,b; Kim et al., 2014; Lübbecke and McPhaden, 2014) the BJ index terms are calculated using linear regression between variables across all years in the simulations.

The boundary between the eastern and western Pacific is defined by regressing ocean heat content anomalies onto the timeseries of the first empirical orthogonal function (EOF) of anomalous SSTs. For the CESM1 model, the nodal line crosses the equator at 170°E, hence our eastern Pacific domain extends from 170°E to 80°W and from 5°N to 5°S. The equatorial Pacific domain has the same latitudinal boundaries that the EP region, but reaches 120°E on its western boundary.

2.6.1.1. Current damping

a_1

Linear regression of the SST difference between the western boundary of the eastern Pacific domain (i.e., averaged SST between 5ºS-5ºN at 170°E) and the

eastern boundary of the domain (i.e., averaged SST between 5ºS-5ºN at 80°W) onto the mean SST of the eastern Pacific domain (i.e., averaged SST over 170°E-80°W/5°N-5°S).

$\langle \Delta \bar{u} \rangle_E$

Difference of the climatological surface ocean zonal current between the western boundary of the East Pacific domain (5ºS-5ºN at 170°E) and the eastern boundary (5ºS5ºN at 80°W). Units are m year^{-1}.

L_x and L_y

L_x is the longitudinal extent of the Eastern Pacific domain, in this case = 14,513,590 m. L_y is the latitudinal extent = 2,480,797 m.

a_2

Linear regression of SSTs in the northern boundary of the Eastern Pacific box (5°N) minus SSTs in the southern boundary of the box (5°S) onto mean SSTs in the EP box (170°E80°W, 5°N-5°S). First of all, average SSTs between 170°E and 80°W, then extract SST values at the north and south locations and subtract N-S. Use absolute values, not anomalies. Units are K K^{-1}.

$\langle \Delta \bar{v} \rangle_E$

Climatological surface meridional ocean current difference between the northern boundary of the East Pacific box (5°N) minus southern boundary (5°S). Units are m year^{-1}.

2.6.1.2. Thermodynamic

Negative feedback. Longwave, shortwave, latent and sensible heat flux and SST anomalies are averaged over our East Pacific region. Then flux anomalies

are regressed onto SST anomalies.

Units are in W m^{-2} K^{-1}, multiply by 0.14 to convert to $year^{-1}$ (Divide by the heat capacity of the water (4180 J kg^{-1} K^{-1}), the density of seawater (1029 kg m^{-3}) and the mixed layer depth (50 m), then multiply by 31,536,000 to convert from $second^{-1}$ to $year^{-1}$).

2.6.1.3. Zonal advective

μ_a

Equatorial Pacific (120°E - 80°W, 5°N - 5°S) wind stress anomalies regressed onto East Pacific (170°E - 80°W, 5°N - 5°S) SST anomalies. Units are 10^{-3}N m^{-2} K^{-1}. Area averaged before regression.

β_u

Regression of EP (170°E - 80°W, 5°N - 5°S) ocean surface zonal current anomalies (10^{-2} m s^{-1}) against equatorial Pacific (120°E - 80°W, 5°N - 5°S) (10^{-3}N m^{-2}). Units are in seconds, multiply by 31,536,000 to get units of $year^{-1}$. Area averaged before regression.

$\langle -\frac{\delta \bar{T}}{\delta x} \rangle_E$

Mean zonal SST gradient over EP (170°E - 80°W, 5°N - 5°S). Use climatological SSTs, not anomalies.

2.6.1.4. Ekman

See zonal advective feedback for the definition of μ_a.

β_w

Regression of EP (170°E - 80°W) upwelling ocean current anomalies (10^{-2} m

s^{-1}): Average values from 0-50m against equatorial Pacific (120°E and 80°W) surface wind stress anomalies (10^{-3}N m^{-2}).

$\langle -\frac{\delta \bar{T}}{\delta z} \rangle_E$

Mean vertical temperature gradient over EP (average 170°E - 80°W, 5°N - 5°S) from 0 to 50m depth. Use climatological SSTs, not anomalies.

2.6.1.5. Thermocline

See zonal advective feedback for the definition of μ_a.

β_h

Regression of thermocline slope anomalies =difference between EP (170°E - 80°W) and WP (120°E - 170°E) ocean temperatures averaged from the surface to 300m against equatorial Pacific (120°E - 80°W) surface wind stress anomalies.

$\langle -\frac{\bar{w}}{H_1} \rangle_E$

Climatological upwelling values over the East Pacific (170°E - 80°W) divided by 50 m. Negative w set to 0 instead of masking.

a_h

Upper ocean heat content (temperatures averaged from 0 to 300m) anomalies in the East Pacific regressed onto temperature anomalies at 50m depth, accounting only for upwelling.

References

S.-I. An and J.-W. Kim. Role of nonlinear ocean dynamic response to wind on the asymmetrical transition of el niño and la niña. *Geophysical Research Letters*, 44:393–400, 5 2017. ISSN 00948276. doi: 10.1002/2016GL071971. URL http://doi.wiley.com/10.1002/2016GL071971. 67, 84

G. J. Boer, D. M. Smith, C. Cassou, F. Doblas-Reyes, G. Danabasoglu, B. Kirtman, Y. Kushnir, M. Kimoto, G. A. Meehl, R. Msadek, W. A. Mueller, K. E. Taylor, F. Zwiers, M. Rixen, Y. Ruprich-Robert, and R. Eade. The decadal climate prediction project (dcpp) contribution to cmip6. *Geoscientific Model Development*, 9:3751–3777, 2016. doi: 10.5194/gmd-9-3751-2016. URL https://gmd.copernicus.org/articles/9/3751/2016/. 65, 76

W. Cai, L. Wu, M. Lengaigne, T. Li, S. McGregor, J.-S. Kug, J.-Y. Yu, M. F. Stuecker, A. Santoso, X. Li, Y.-G. Ham, Y. Chikamoto, B. Ng, M. J. McPhaden, Y. Du, D. Dommenget, F. Jia, J. B. Kajtar, N. Keenlyside, X. Lin, J.-J. Luo, M. Martín-Rey, Y. Ruprich-Robert, G. Wang, S.-P. Xie, Y. Yang, S. M. Kang, J.-Y. Choi, B. Gan, G.-I. Kim, C.-E. Kim, S. Kim, J.-H. Kim, and P. Chang. Pantropical climate interactions. *Science*, 363:eaav4236, 2019. doi: 10.1126/science.aav4236. URL https://www.science.org/doi/abs/10.1126/science.aav4236. 64

A. Castaño-Tierno, E. Mohino, B. Rodríguez-Fonseca, and T. Losada. Revisiting the cmip5 thermocline in the equatorial pacific and atlantic oceans. *Geophysical Research Letters*, 45:12, 912–963, 971, 5 2018. ISSN 1944-8007. doi: 10.1029/2018GL079847. URL https://onlinelibrary.wiley.com/doi/full/10.1029/2018GL079847https://onlinelibrary.wiley.com/doi/abs/10.1029/2018GL079847https://agupubs.onlinelibrary.wiley.com/doi/10.1029/2018GL079847. 75, 76

F. S. Castruccio, Y. Ruprich-Robert, S. G. Yeager, G. Danabasoglu, R. Msadek, and T. L. Delworth. Modulation of arctic sea ice loss by atmospheric teleconnections from atlantic multidecadal variability. *Journal of Climate*, 32:1419–1441, 3 2019. ISSN 0894-8755. doi: 10.1175/

JCLI-D-18-0307.1. URL https://journals.ametsoc.org/view/journals/clim/32/5/jcli-d-18-0307.1.xml. 65, 66

J. Choi, S. I. An, J. S. Kug, and S. W. Yeh. The role of mean state on changes in el niño's flavor. *Climate Dynamics*, 37:1205–1215, 5 2011. ISSN 09307575. doi: 10.1007/S00382-010-0912-1/FIGURES/10. URL https://link.springer.com/article/10.1007/s00382-010-0912-1. 75

M. Collins, S.-I. An, W. Cai, A. Ganachaud, E. Guilyardi, F.-F. Jin, M. Jochum, M. Lengaigne, S. Power, A. Timmermann, G. Vecchi, and A. Wittenberg. The impact of global warming on the tropical pacific ocean and el niño. *Nature Geoscience*, 3:391–397, 2010. ISSN 1752-0908. doi: 10.1038/ngeo868. URL https://doi.org/10.1038/ngeo868. 78

H. F. Diaz, M. P. Hoerling, and J. K. Eischeid. Enso variability, teleconnections and climate change. *International Journal of Climatology*, 21:1845–1862, 12 2001. ISSN 08998418. doi: 10.1002/JOC.631. 64

B. Dieppois, A. Capotondi, B. Pohl, K. P. Chun, A. Monerie, and J. Eden. Robust decadal variations in enso diversity, and its impact on future scenarios 2, 5 2021. URL https://www.researchsquare.comhttps://www.researchsquare.com/article/rs-387048/v1. 64

P. N. DiNezio, C. Deser, Y. Okumura, and A. Karspeck. Predictability of 2-year la niña events in a coupled general circulation model. *Climate Dynamics*, 49:4237–4261, 2017. ISSN 1432-0894. doi: 10.1007/s00382-017-3575-3. URL https://doi.org/10.1007/s00382-017-3575-3. 65

B. Dong and R. T. Sutton. Enhancement of enso variability by a weakened atlantic thermohaline circulation in a coupled gcm. *Journal of Climate*, 20: 4920 – 4939, 2007. doi: https://doi.org/10.1175/JCLI4284.1. URL https://journals.ametsoc.org/view/journals/clim/20/19/jcli4284.1.xml. 64, 68, 71, 75

A. V. Fedorov and S. G. Philander. A stability analysis of tropical ocean-atmosphere interactions: Bridging measurements and theory for el niño, 2000. 76

A. V. Fedorov, S. L. Harper, S. G. Philander, B. Winter, and A. Wittenberg. How predictable is el niño? *Bulletin of the American Meteorological Society*, 84:911–920, 5 2003. ISSN 0003-0007. doi: 10.1175/BAMS-84-7-911. URL https://journals.ametsoc.org/view/journals/bams/84/7/bams-84-7-911.xml. 64

S. Ferrett and M. Collins. Enso feedbacks and their relationships with the mean state in a flux adjusted ensemble. *Climate Dynamics*, 52:7189–7208, 5 2019. ISSN 14320894. doi: 10.1007/s00382-016-3270-9. URL https://doi.org/10.1007/s00382-016-3270-9. 67

F. S. Graham, J. N. Brown, C. Langlais, S. J. Marsland, A. T. Wittenberg, and N. J. Holbrook. Effectiveness of the bjerknes stability index in representing ocean dynamics. *Climate Dynamics*, 43:2399–2414, 2014. ISSN 1432-0894. doi: 10.1007/s00382-014-2062-3. URL https://doi.org/10.1007/s00382-014-2062-3. 67

N. E. Graham and T. P. Barnett. Sea surface temperature, surface wind divergence, and convection over tropical oceans. *Science*, 238:657–659, 5 1987. ISSN 00368075. doi: 10.1126/SCIENCE.238.4827.657. URL https://www.science.org/doi/10.1126/science.238.4827.657. 76

E. Guilyardi, P. Braconnot, F. F. Jin, S. T. Kim, M. Kolasinski, T. Li, and I. Musat. Atmosphere feedbacks during enso in a coupled gcm with a modified atmospheric convection scheme. *Journal of Climate*, 22:5698–5718, 5 2009. ISSN 08948755. doi: 10.1175/2009JCLI2815.1. URL http://journals.ametsoc.org/jcli/article-pdf/22/21/5698/3952066/2009jcli2815_1.pdf. 67, 84

Y.-G. Ham and J.-S. Kug. Role of north tropical atlantic sst on the enso simulated using cmip3 and cmip5 models. *Climate Dynamics*, 45:3103–3117, 2015. ISSN 1432-0894. doi: 10.1007/s00382-015-2527-z. URL https://doi.org/10.1007/s00382-015-2527-z. 64, 70, 75

S. Hu and A. V. Fedorov. Cross-equatorial winds control el niño diversity and change. *Nature Climate Change*, 8:798–802, 9 2018. ISSN

17586798. doi: 10.1038/s41558-018-0248-0. URL https://doi.org/10.1038/s41558-018-0248-0. 64, 76

P. Huang and S.-P. Xie. Mechanisms of change in enso-induced tropical pacific rainfall variability in a warming climate. *Nature Geoscience*, 8:922–926, 2015. ISSN 1752-0908. doi: 10.1038/ngeo2571. URL https://doi.org/10.1038/ngeo2571. 66

F.-F. Jin. An equatorial ocean recharge paradigm for enso. part i: Conceptual model. *Journal of the Atmospheric Sciences*, 54: 811–829, 5 1997a. ISSN 0022-4928. doi: 10.1175/1520-0469(1997)054. URL https://journals.ametsoc.org/view/journals/atsc/54/7/1520-0469_1997_054_0811_aeorpf_2.0.co_2.xml. 67

F.-F. Jin. An equatorial ocean recharge paradigm for enso. part i: Conceptual model. *Journal of the Atmospheric Sciences*, 54:811 – 829, 1997b. doi: https://doi.org/10.1175/1520-0469(1997)054<0811:AEORPF>2.0.CO;2. URL https://journals.ametsoc.org/view/journals/atsc/54/7/1520-0469_1997_054_0811_aeorpf_2.0.co_2.xml. 84

F.-F. Jin and S.-I. An. Thermocline and zonal advective feedbacks within the equatorial ocean recharge oscillator model for enso. *Geophysical Research Letters*, 26:2989–2992, 5 1999. ISSN 00948276. doi: 10.1029/1999GL002297. URL http://doi.wiley.com/10.1029/1999GL002297. 75

F. F. Jin, S. T. Kim, and L. Bejarano. A coupled-stability index for enso. *Geophysical Research Letters*, 33, 5 2006. ISSN 00948276. doi: 10.1029/2006GL027221. URL https://agupubs.onlinelibrary.wiley.com/doi/full/10.1029/2006GL027221https://agupubs.onlinelibrary.wiley.com/doi/abs/10.1029/2006GL027221https://agupubs.onlinelibrary.wiley.com/doi/10.1029/2006GL027221. 67, 84

F.-F. Jin, H.-C. Chen, S. Zhao, M. Hayashi, C. Karamperidou, M. F. Stuecker, R. Xie, and L. Geng. Simple enso models, 2020. URL https://agupubs.onlinelibrary.wiley.com/doi/abs/10.1002/9781119548164.ch6. 71

I. S. Kang and J. S. Kug. El niño and la niña sea surface temperature anomalies: Asymmetry characteristics associated with their wind stress anomalies. *Journal of Geophysical Research: Atmospheres*, 107:ACL 1–1, 5 2002. ISSN 2156-2202. doi: 10.1029/2001JD000393. URL https://onlinelibrary.wiley.com/doi/full/10.1029/2001JD000393https://onlinelibrary.wiley.com/doi/abs/10.1029/2001JD000393https://agupubs.onlinelibrary.wiley.com/doi/10.1029/2001JD000393. 75

J. E. Kay, C. Deser, A. Phillips, A. Mai, C. Hannay, G. Strand, J. M. Arblaster, S. C. Bates, G. Danabasoglu, J. Edwards, M. Holland, P. Kushner, J. F. Lamarque, D. Lawrence, K. Lindsay, A. Middleton, E. Munoz, R. Neale, K. Oleson, L. Polvani, and M. Vertenstein. The community earth system model (cesm) large ensemble project: A community resource for studying climate change in the presence of internal climate variability. *Bulletin of the American Meteorological Society*, 96:1333–1349, 5 2015. ISSN 0003-0007. doi: 10.1175/BAMS-D-13-00255.1. URL https://journals.ametsoc.org/view/journals/bams/96/8/bams-d-13-00255.1.xml. 65

S. T. Kim and F. F. Jin. An enso stability analysis. part ii: Results from the twentieth and twenty-first century simulations of the cmip3 models. *Climate Dynamics*, 36:1609–1627, 5 2011a. ISSN 09307575. doi: 10.1007/s00382-010-0872-5. URL https://link.springer.com/article/10.1007/s00382-010-0872-5. 67, 84

S. T. Kim and F. F. Jin. An enso stability analysis. part ii: Results from the twentieth and twenty-first century simulations of the cmip3 models. *Climate Dynamics*, 36:1609–1627, 4 2011b. ISSN 09307575. doi: 10.1007/s00382-010-0872-5. URL https://link.springer.com/article/10.1007/s00382-010-0872-5. 67, 76, 84

S. T. Kim, W. Cai, F. F. Jin, and J. Y. Yu. Enso stability in coupled climate models and its association with mean state. *Climate Dynamics*, 42:3313–3321, 5 2014. ISSN 14320894. doi: 10.1007/s00382-013-1833-6. URL http://www-pcmdi.llnl.gov/ipcc/model_. 71, 84

Y. Kosaka and S.-P. Xie. Recent global-warming hiatus tied to equatorial pacific surface cooling. *Nature*, 501:403–407, 2013. ISSN 1476-4687. doi: 10.1038/nature12534. URL https://doi.org/10.1038/nature12534. 70

F. Kucharski, F. S. Syed, A. Burhan, I. Farah, and A. Gohar. Tropical atlantic influence on pacific variability and mean state in the twentieth century in observations and cmip5. *Climate Dynamics*, 44:881–896, 5 2014. ISSN 14320894. doi: 10.1007/s00382-014-2228-z. 75

A. F. Z. Levine, M. J. McPhaden, and D. M. W. Frierson. The impact of the amo on multidecadal enso variability. *Geophysical Research Letters*, 44:3877–3886, 5 2017. ISSN 19448007. doi: 10.1002/2017GL072524. URL http://doi.wiley.com/10.1002/2017GL072524. 64, 65, 67, 71, 76

J. Lloyd, E. Guilyardi, and H. Weller. The role of atmosphere feedbacks during enso in the cmip3 models. part iii: The shortwave flux feedback. *Journal of Climate*, 25:4275 – 4293, 2012. doi: https://doi.org/10.1175/JCLI-D-11-00178.1. URL https://journals.ametsoc.org/view/journals/clim/25/12/jcli-d-11-00178.1.xml. 67

J. F. Lübbecke and M. J. Mcphaden. A comparative stability analysis of atlantic and pacific niño modes. *Journal of Climate*, 26:5965–5980, 8 2013. ISSN 08948755. doi: 10.1175/JCLI-D-12-00758.1. URL https://journals.ametsoc.org/view/journals/clim/26/16/jcli-d-12-00758.1.xml. 67

J. F. Lübbecke and M. J. McPhaden. Assessing the twenty-first-century shift in enso variability in terms of the bjerknes stability index. *Journal of Climate*, 27:2577 – 2587, 2014. doi: https://doi.org/10.1175/JCLI-D-13-00438.1. URL https://journals.ametsoc.org/view/journals/clim/27/7/jcli-d-13-00438.1.xml. 70, 71, 76, 84

M. Martin-Rey, B. Rodriguez-Fonseca, I. Polo, and F. Kucharski. On the atlantic-pacific niños connection: a multidecadal modulated mode. *Climate dynamics*, 43:3163–3178, 2014. 75

S. McGregor, A. Timmermann, M. F. Stuecker, M. H. England, M. Merrifield, F. F. Jin, and Y. Chikamoto. Recent walker circulation strengthening and pacific cooling amplified by atlantic warming. *Nature Climate Change*, 4:888–892, 5 2014. ISSN 17586798. doi: 10.1038/nclimate2330. 75

G. A. Meehl, P. R. Gent, J. M. Arblaster, B. L. Otto-Bliesner, E. C. Brady, and A. Craig. Factors that affect the amplitude of el nino in global coupled climate models. *Climate Dynamics*, 17:515–526, 2001. ISSN 1432-0894. doi: 10.1007/PL00007929. URL https://doi.org/10.1007/PL00007929. 64

G. A. Meehl, J. M. Arblaster, J. T. Fasullo, A. Hu, and K. E. Trenberth. Model-based evidence of deep-ocean heat uptake during surface-temperature hiatus periods. *Nature Climate Change*, 1:360–364, 2011. ISSN 1758-6798. doi: 10.1038/nclimate1229. URL https://doi.org/10.1038/nclimate1229. 70

G. A. Meehl, A. Hu, F. Castruccio, M. H. England, S. C. Bates, G. Danabasoglu, S. McGregor, J. M. Arblaster, S.-P. Xie, and N. Rosenbloom. Atlantic and pacific tropics connected by mutually interactive decadal-timescale processes. *Nature Geoscience*, 14:36–42, 2021. ISSN 1752-0908. doi: 10.1038/s41561-020-00669-x. URL https://doi.org/10.1038/s41561-020-00669-x. 75

I. Polo, M. Martin-Rey, B. Rodriguez-Fonseca, F. Kucharski, and C. R. Mechoso. Processes in the pacific la niña onset triggered by the atlantic niño. *Climate Dynamics*, 44:115–131, 5 2014. ISSN 14320894. doi: 10.1007/s00382-014-2354-7. URL https://link.springer.com/article/10.1007/s00382-014-2354-7. 64, 75

B. Rodríguez-Fonseca, I. Polo, J. García-Serrano, T. Losada, E. Mohino, C. R. Mechoso, and F. Kucharski. Are atlantic niños enhancing pacific enso events in recent decades? *Geophysical Research Letters*, 36, 2009. doi: https://doi.org/10.1029/2009GL040048. URL https://agupubs.onlinelibrary.wiley.com/doi/abs/10.1029/2009GL040048. 64, 75

Y. Ruprich-Robert, R. Msadek, F. Castruccio, S. Yeager, T. Delworth, and G. Danabasoglu. Assessing the climate impacts of the observed atlantic multidecadal variability using the gfdl cm2.1 and ncar cesm1 global coupled models. *Journal of Climate*, 30:2785 – 2810, 2017. doi: https://doi.org/10.1175/JCLI-D-16-0127.1. URL https://journals.ametsoc.org/view/journals/clim/30/8/jcli-d-16-0127.1.xml. 64, 65, 68, 70, 75

Y. Ruprich-Robert, E. Moreno-Chamarro, X. Levine, A. Bellucci, C. Cassou, F. Castruccio, P. Davini, R. Eade, G. Gastineau, L. Hermanson, D. Hodson, K. Lohmann, J. Lopez-Parages, P.-A. Monerie, D. Nicolì, S. Qasmi, C. D. Roberts, E. Sanchez-Gomez, G. Danabasoglu, N. Dunstone, M. Martin-Rey, R. Msadek, J. Robson, D. Smith, and E. Tourigny. Impacts of atlantic multidecadal variability on the tropical pacific: a multi-model study. *npj Climate and Atmospheric Science*, 4:33, 12 2021. ISSN 2397-3722. doi: 10.1038/s41612-021-00188-5. URL http://www.nature.com/articles/s41612-021-00188-5. 68, 75

T. M. Smith, R. W. Reynolds, T. C. Peterson, and J. Lawrimore. Improvements to noaa's historical merged land–ocean surface temperature analysis (1880–2006). *Journal of Climate*, 21:2283–2296, 5 2008. ISSN 0894-8755. doi: 10.1175/2007JCLI2100.1. URL https://journals.ametsoc.org/view/journals/clim/21/10/2007jcli2100.1.xml. 66

B. Wang and S. I. An. A mechanism for decadal changes of enso behavior: roles of background wind changes. *Climate Dynamics 2002 18:6*, 18:475–486, 2002. ISSN 1432-0894. doi: 10.1007/S00382-001-0189-5. URL https://link.springer.com/article/10.1007/s00382-001-0189-5. 75

G. Wang, W. Cai, B. Gan, L. Wu, A. Santoso, X. Lin, Z. Chen, and M. J. McPhaden. Continued increase of extreme el niño frequency long after 1.5°c warming stabilization. *Nature Climate Change*, 7:568–572, 2017. ISSN 1758-6798. doi: 10.1038/nclimate3351. URL https://doi.org/10.1038/nclimate3351. 64

A. T. Wittenberg. Are historical records sufficient to constrain enso simulations? *Geophysical Research Letters*, 36, 2009. doi: https://doi.org/10.1029/2009GL038710. URL https://agupubs.onlinelibrary.wiley.com/doi/abs/10.1029/2009GL038710. 64

X. Wu, Y. M. Okumura, and P. N. Dinezio. Predictability of el niño duration based on the onset timing. *Journal of Climate*, 34:1351–1366, 5 2021. ISSN 08948755. doi: 10.1175/JCLI-D-19-0963.1. URL https://doi.org/10.1175/JCLI-D-19-. 65

J. Y. Yu, P. K. Kao, H. Paek, H. H. Hsu, C. W. Hung, M. M. Lu, and S. I. An. Linking emergence of the central pacific el niño to the atlantic multidecadal oscillation. *Journal of Climate*, 28:651–662, 5 2015. ISSN 08948755. doi: 10.1175/JCLI-D-14-00347.1. URL https://journals.ametsoc.org/view/journals/clim/28/2/jcli-d-14-00347.1.xml. 64

D. Zanchettin, O. Bothe, H. F. Graf, N. Omrani, A. Rubino, and J. H. Jungclaus. A decadally delayed response of the tropical pacific to atlantic multidecadal variability. *Geophysical Research Letters*, 43:784–792, 5 2016. ISSN 0094-8276. doi: 10.1002/2015GL067284. URL https://onlinelibrary.wiley.com/doi/abs/10.1002/2015GL067284. 65, 68, 71, 73, 75

S. E. Zebiak and M. A. Cane. A model el nintilde–southern oscillation. *Monthly Weather Review*, 115:2262–2278, 5 1987. ISSN 0027-0644. doi: 10.1175/1520-0493(1987)115<2262:ameno>2.0.co;2. URL https://journals.ametsoc.org/view/journals/mwre/115/10/1520-0493_1987_115_2262_ameno_2_0_co_2.xml. 75

T. Zhang, X. Shao, and S. Li. Impacts of atmospheric processes on enso asymmetry: A comparison between cesm1 and ccsm4. *Journal of Climate*, 30:9743–9762, 5 2017. ISSN 08948755. doi: 10.1175/JCLI-D-17-0360.1. URL www.ametsoc.org/PUBSReuseLicenses. 65

W. Zhang, F. Jiang, M. F. Stuecker, F.-F. Jin, and A. Timmermann. Spurious north tropical atlantic precursors to el niño. *Nature Communications 2021*

12:1, 12:1–8, 5 2021. ISSN 2041-1723. doi: 10.1038/s41467-021-23411-6. URL https://www.nature.com/articles/s41467-021-23411-6. 64

Chapter 3

Atlantic Multidecadal Variability modulates the climate impacts of El Niño-Southern Oscillation in Australia

Authors: **Paloma Trascasa-Castro, Amanda C. Maycock, Yohan Ruprich-Robert, Marco Turco and Paul W. Staten.**

I was just guessing
at numbers and figures
pulling the puzzles apart.
Questions of science,
science and progress
do not speak as loud as my heart.

The Scientist, by Coldplay.

Abstract

Atlantic Multidecadal Variability (AMV) modulates El Niño-Southern Oscillation (ENSO) dynamics. Here, we explore the effect of warm (AMV+) and cold (AMV-) AMV conditions on the austral summer teleconnection of ENSO to Australia using idealized simulations performed with the NCAR-CESM1 model. AMV+ strengthens the mean and extreme precipitation and temperature responses to El Niño in south-western Australia and weakens the mean precipitation and temperature impacts in north-eastern Australia. The modulation of La Niña impacts by AMV is asymmetric to El Niño, with a weakening of the mean and extreme precipitation and temperature responses in eastern Australia. Decomposing the total difference in ENSO response between AMV phases, we find that the signals are mainly explained by the direct AMV modulation of ENSO and its teleconnections rather than by changes in background climate induced by AMV. The exception is ENSO-driven fire impacts, where there is a significant increase in burned area in south-eastern Australia only when El Niño and AMV+ co-occur. However, modulation of ENSO between AMV+ and AMV- does offset 37% of the decrease in burned area extent during La Niña summers. The altered surface climate response to ENSO in Australia by AMV is attributed to variations in large-scale atmospheric circulation. Under AMV+, there is increased subsidence over western Australia during El Niño associated with a westward shift of the local Walker circulation. A weakening of the upwelling branch of the local Hadley circulation over north-eastern Australia is responsible for the weakening of La Niña impacts in AMV+, accompanied by a strengthening of subsidence in south central Australia due to a weakening of the local Hadley circulation, amplifying La Niña impacts over this region. The results suggest the potential for AMV to drive multidecadal variability in ENSO impacts over Australia.

3.1. Introduction

El Niño-Southern Oscillation (ENSO) is the dominant mode of interannual climate variability in the tropics. ENSO impacts remote ecosystems and populations through anomalous atmospheric circulation originating from changes in

deep convection in the equatorial Pacific. Anomalous upper-level divergence in the tropics during ENSO alters the Hadley (Trenberth et al., 1998) and Walker circulations, with the upward branch shifting to the central Pacific during El Niño and intensifying over the Maritime continent during La Niña (Walker, 1932).

Climate in Australia is strongly influenced by ENSO, especially the northern and eastern regions (Chung and Power, 2017). During El Niño, there is a precipitation deficit in austral spring and summer across Australia. Reduced cloud cover over south-east Australia increases downward shortwave radiation leading to an increase in surface temperature (Arblaster and Alexander, 2012). Higher daily temperatures combined with decreased precipitation under El Niño increases the likelihood of droughts and heatwaves (King et al., 2013). In contrast, during La Niña there is above normal precipitation in northern Australia in austral spring and summer due to the early onset of the monsoon (Drosdowsky and Wheeler, 2014). The increase in cloud cover during La Niña leads to cooler temperatures and a weakening of extreme heat episodes during austral summer (Perkins et al., 2015). Australia is one of the most susceptible regions to wildfires in the world (Archibald et al., 2013). While human activity is a dominant source of wildfires in Australia (Marcos et al., 2015), ENSO is an important driver of interannual variability (Abram et al., 2021), which may be superposed onto long-term climate trends (e.g., Dowdy et al. (2019)) and multidecadal variability (Canadell et al., 2021).

Recent studies show that decadal climate variability can modulate ENSO behaviour (Ham and Kug, 2015; Levine et al., 2017; Trascasa-Castro et al., 2021). For example, the Interdecadal Pacific Oscillation (IPO) alters the mean background state of the tropical Pacific and modulates ENSO-related impacts over Australia, including changes to seasonal mean impacts (Power et al., 1999), the frequency of extreme precipitation and its potential to lead to flooding events (King et al., 2013) and drought risk (Kiem and Franks, 2004). Multidecadal variations in ENSO characteristics may manifest in wildfire frequency and intensity, but the importance of this mechanism is not well quantified due to limited observational records (Liu et al., 2023).

Multidecadal variability in North Atlantic sea surface temperatures (SSTs) can also modulate tropical climate by altering large-scale overturning circulations (Liu et al., 2020; Meehl et al., 2021). Model studies show that the warm phase of Atlantic Multidecadal Variability (AMV+) can drive tropical Pacific cooling (Ruprich-Robert et al., 2017, 2021), although this signal might be overestimated in model simulations with prescribed SSTs in the tropical North Atlantic (O'Reilly et al., 2023). Trascasa-Castro et al. (2021) examined idealised experiments with imposed AMV anomalies and found that AMV+ damped the amplitude of ENSO by around 10% compared to AMV-. This raises the prospect that the remote impacts of ENSO could be modified by AMV. Past studies found a link between AMV+ and increased precipitation in north-western Australia (Lin and Li, 2012). However, there remain uncertainties in the modulation by AMV of ENSO impacts on Australian climate due to the relatively short observational record and the challenge of isolating causal factors in coupled simulations.

This study aims to understand the AMV modulation of ENSO-driven climate impacts in Australia using idealised coupled climate model simulations with imposed AMV conditions. Our results investigate changes in mean surface climate, extreme precipitation and temperature responses to ENSO, and burned area over south-eastern Australia. We further explore the physical mechanisms leading to AMV modulation of ENSO impacts over Australia by decomposing atmospheric circulation changes into contributions from local Hadley and Walker circulations. The paper is laid out as follows: Section 2 describes the simulations and analysis methods. Section 3 presents the results and Section 4 contains the discussion and conclusions of the study.

3.2. Data and methods

3.2.1. Climate model simulations

The relatively short observational record hinders the possibility of robustly attributing changes to ENSO variability and impacts to AMV, allowing to account

for just 1 full positive and negative AMV phases. To overcome this sampling issue, we use idealized experiments performed with the NCAR-CESM1 coupled climate model (Kay et al., 2015), in which time invariant anomalies corresponding to observed warm (AMV+) or cold (AMV-) AMV conditions are imposed in the North Atlantic (Fig. 3.8) for 10 years through SST restoring; the ocean-atmosphere being freely coupled outside of the constrained North Atlantic. The experiments comprise 30 ensemble members, giving a total of 300 years per ensemble/AMV phase (270 full boreal winter seasons). Those experiments were introduced in Ruprich-Robert et al. (2017) and used for several studies (Meehl et al., 2021; Ruprich-Robert et al., 2021; Trascasa-Castro et al., 2021). Further details about the ensemble initialisation is described in Castruccio et al. (2019). We stress that those experiments largely comply with the he Decadal Climate Prediction Project (DCPP; (Boer et al., 2016) of the Coupled Model Intercomparison Project Phase 6 (CMIP6; (Eyring et al., 2016)).

Zhang et al. (2017) evaluated the performance NCAR-CESM1 in simulating ENSO. The model overestimates SST anomalies associated with La Niña but simulates ENSO skewness relatively well. NCAR-CESM1 captures the sign of ENSO teleconnection to Australia in agreement with observations, although it overestimates the amplitude of precipitation and temperature anomalies (Fig. 3.9).

3.2.2. Composite analysis

We define the reference climatological state, μ, as the ensemble mean across both AMV+ and AMV- experiments. We define El Niño (La Niña) events in AMV+ or AMV- as austral summers (December-February) where the Niño3.4 index is at least 0.5 K warmer (colder) than in μ. Note this incorporates differences in mean state between AMV+ (μ^+) and AMV- (μ^-) into the identification of ENSO events. The μ^+ minus μ climatological DJF Niño3.4 anomaly is -0.23 K. This is larger than the direct modulation of ENSO amplitude between AMV+ and AMV-, which shows an average Nino3.4 anomaly of -0.17 K for El Niño and +0.09 K for La Niña (Trascasa-Castro et al., 2021). The μ^+ minus μ^- difference

means that El Niño (La Niña) events will be relatively less (more) frequent, in AMV+ than in AMV-. We adopt this definition because it more closely reflects how observations would be interpreted where interannual variability is superposed on multidecadal variability.

For a given variable, X, we define the mean ENSO impact as the average over all ENSO events in AMV phase η (either "+" or "-") minus the reference state μ, such that:

$$\overline{X^{\eta}} = \Sigma_{i=1}^{N} X_i^{\eta} - \mu \tag{3.1}$$

where X_i^{η} is the i^{th} El Niño or La Niña event. For each ENSO phase, we estimate the average climate impact independent of AMV, $\overline{X}$, as:

$$\overline{X} = \frac{\overline{X^{+}} + \overline{X^{-}}}{2} \tag{3.2}$$

We define the overall difference in ENSO climate response between AMV+ and AMV-, called hereafter "total modulation of ENSO impacts by AMV" $\Delta\overline{X}$, as:

$$\Delta\overline{X} = \overline{X^{+}} - \overline{X^{-}} \tag{3.3}$$

Conceptually, $\overline{X}$ can be understood as the sum of the change in mean state driven by AMV ($\Delta\mu$) and the "direct impacts of ENSO modulated by AMV" ($\overline{\Delta X_{ENSO}}$):

$$\Delta\overline{X} = \Delta\mu + \overline{\Delta X_{ENSO}} \tag{3.4}$$

where

$$\Delta\mu = \mu^{+} - \mu^{-} \tag{3.5}$$

and

$$\overline{\Delta X_{ENSO}} = \left(\overline{X^{+}} - \mu^{+}\right) - \left(\overline{X^{-}} - \mu^{-}\right) \tag{3.6}$$

We note that ΔX_{ENSO} encompasses the modulation of ENSO impacts due to both changes in ENSO teleconnections pathways (because of altered background circulation) and changes in ENSO characteristics (amplitude and/or spatial pattern).

We stress that our decomposition between mean state background changes and modulation of ENSO impacts is not exact (see Supplementary Information). In particular, we implicitly assume that there are no differences in the mean state AMV impact across ENSO phases and attribute those changes to direct ENSO impacts modulated by AMV.

We test for statistical significance by performing a nonparametric bootstrap test subsampling 70% of the 270 austral summer seasons with replacement on each iteration repeated 10^4 times. Differences are estimated to be significant at the 95% confidence level where the ensemble mean anomaly lies outside of 2.5-97.5$^{\text{th}}$ percentile range of the bootstrap samples.

3.2.3. Extreme climate response to ENSO

We analyse the following climate extreme indices (Donat et al., 2013):

- Warm days (TX90p): Number of days per summer season when daily maximum temperature exceeds the local 90$^{\text{th}}$ percentile.
- Warm nights (TN90p): Number of days per summer when daily minimum temperature exceeds the local 90$^{\text{th}}$ percentile.
- Wet days (R90p): Number of days when precipitation exceeds the local 90$^{\text{th}}$ percentile.
- Maximum number of consecutive dry days (CDD) per summer with daily precipitation less than 1 mm.

3.2.4. Empirical fire model

Burned area (BA) is a widely used metric of wildfire activity that integrates the total number of wildfires occurring over a season and their intensity (Andela et al., 2017). In Australia, the absence of a centralised national database has resulted in the aggregation of data from various fire management agencies in each state and territory (see Data Availability) to construct a comprehensive overview of the country's burned areas (Canadell et al., 2021). The data provided by these agencies are represented as polygons in vector files, obtained through diverse sources such as terrestrial mapping, aerial photography, GPS boundary plotting from ground assessments, and remote sensing. Extensive validation of this data has been conducted, and it has been previously utilized as a reference in numerous studies (e.g. (Bradstock, 2010; Murphy et al., 2013; Russell-Smith et al., 2007)). The datasets encompass various types of fires, including both prescribed fires and wildfires. Wildfires are commonly referred to as bushfires in the metadata of these data sources. The term "bushfire" is frequently used to describe vegetation fires in general. Within databases or public warning systems, "bushfires" are categorized as "unplanned fires" or "wildfires," contrasting with "planned fires," "hazard reduction burns," or "prescribed fire". We focus on changes in BA in the eastern Australian temperate forest region (Dinerstein

et al., 2017), which is highly populated, vulnerable to wildfires and has a 50-year fire data record. We aggregate all the wildfires whose centre of gravity falls in the study domain and which start in the fire season from September-February (Canadell et al., 2021). A fire year is defined by the year in which the fire season ends.

The Standardized Precipitation Evapotranspiration Index (SPEI) estimates the relationship between preconditioning meteorological conditions and the BA during the fire season, following Turco et al. (2018). SPEI accounts for total accumulated precipitation and potential evapotranspiration (PET). The Hargreaves method is used to estimate PET, including temperature and precipitation in its formulation (plus the latitudinal correction factor). We calculate the observed SPEI over 1971–2020 using monthly mean maximum near-surface temperature and precipitation from the Climate Research Unit dataset (CRUTS4.06, Harris et al. (2020)). Climate variables are spatially averaged over the southeast Australia domain for the analysis (Fig. 3.5a).

As in Turco et al. (2018), we express the SPEI-BA model as:

$$\log[BA(sc,m)] = \beta 1 + \beta 2 \times SPEI(sc,m) + \epsilon(sc) \tag{3.7}$$

Where sc is the timescale (varying from 1 to 12 months) used to compute the SPEI, m is the month for which the SPEI is computed (varying from September to February) and ϵ refers to noise caused by sources of BA variability other than the SPEI.

To find the highest fraction of variance explained, we calculate all the possible regression models by varying sc and m. The selected model explains 56% of the BA variability based on the $SPEI5_{Jan}$, i.e. the climate data aggregated from September to January. We apply the empirical observed relationship from

Eq. 3.7 to the NCAR-CESM1 AMV+ and AMV- output to determine effective changes in BA by AMV.

3.2.5. Atmospheric circulation decomposition into local Walker and Hadley components

To match anomalous ascent to changes in large-scale circulation and the relative importance of zonal and meridional overturning circulations, we perform a Helmholtz decomposition of the flow after Schwendike et al. (2014). Specifically, we first use spherical harmonics to isolate the divergent wind field from the full wind field. Then we use the kinematic method to calculate the component of ascent due to meridional (or zonal) overturning from the divergence of the meridional (or zonal) component of the divergent wind. This decomposition give us the local Hadley and Walker components of large-scale ascent.

Once the vertical motion of mass flux (m) is computed for both the zonal and meridional orthogonal directions obtained from the divergent parts of the wind, the zonal and meridional upward mass fluxes are estimated:

$$m_\lambda = -\omega_\lambda \frac{\cos\phi}{g} \text{ and}$$
$$m_\phi = -\omega_\phi \frac{\cos\phi}{g} \tag{3.8}$$

Where ω_λ and ω_ϕ represent the partitioned components of the vertical motion in the zonal and meridional directions, respectively, ϕ is the latitude, and g is the gravitational acceleration.

3.3. Results

3.3.1. AMV modulation of ENSO mean climate impacts over Australia

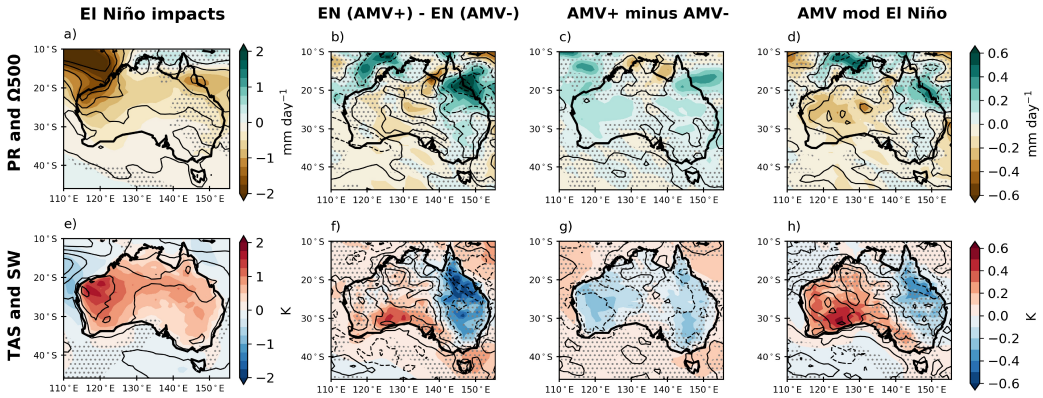

Figure 3.1: El Niño-related impacts over Australia in DJF. Top: precipitation (mm day^{-1}) in shading and vertical velocity at 500 hPa (Pa s^{-1}) with contours at ±0.02 Pa s^{-1} (a) and ±0.01 Pa s^{-1} (b, c and d). Bottom: near-surface temperature (K) in shading and net surface shortwave radiation with contours ±30 W m^{-2} (e) and ±10 W m^{-2} (f, g and h). Columns show: (a,e) Mean El Niño impacts (eq. 3.2); (b,f) the total El Niño modulation by AMV (eq. 3.3); (c,g) the mean background change due to AMV (eq. 3.5); and (d,h) the direct AMV modulation of El Niño impacts (eq. 3.6). Dotted areas denote absence of statistical significance in the precipitation (top) and near-surface temperature (bottom) at the 95% confidence level.

El Niño leads to a precipitation deficit and increased subsidence over Australia (Fig. 3.1a). Higher mean surface temperatures occur alongside increased net surface shortwave (SW) radiation (Fig. 3.1e). The strong spatial resemblance between anomalous surface SW radiation and mid-level vertical velocity (Fig. 3.1e) suggests anomalies in mean surface temperature are related to changes in large-scale atmospheric dynamics rather than local processes. During La Niña, the anomalies are of a similar amplitude but opposite sign (Figs. 3.2a, e).

The total El Niño modulation by AMV (Eq. 3.3) (Fig. 3.1b and f) shows a weaker precipitation decrease above 0.6 mm day^{-1} over north-east Australia, along with a damping of the local subsidence seen in the mean El Niño response

(compare contours between Figs. 3.1b and a). Alongside the weakening of El Niño-related precipitation, there is a weakening of mean near-surface warming of -0.6 K associated with reduced incoming SW radiation (Fig. 3.1 1f). In contrast, there is a slight strengthening of the El Niño impacts over south-central Australia under AMV+, with an increase in temperature of up to 0.4 K and a small but significant increase in precipitation deficit.

The total modulation of La Niña by AMV (Fig. 3.2b,e) displays a similar amplitude but opposite sign to that found for El Niño (Fig. 3.1b,e). However, the spatial locations of the anomalies differ, highlighting the asymmetry in the AMV modulation of ENSO impacts in Australia. In particular, the total modulation pattern in near-surface temperature during La Niña is shifted by 5° to the east compared to El Niño.

As explained in Section 3.2, the total modulation of ENSO impacts by AMV can be understood as the sum of the change in background climate between AMV phases (Eq. 3.5) and the direct modulation of ENSO characteristics and/or its teleconnections by AMV (Eq. 3.6). The mean state difference between AMV+ and AMV- is characterised by wetting and cooling over western and eastern Australia of up to 0.2 mm day^{-1} and 0.2 K, respectively (Fig. 3.1c,g). Therefore, the mean climate response to AMV+ tends to offset the total El Niño impacts over Australia compared to AMV-. This is consistent with the fact that, on average, in these experiments AMV+ drives tropical Pacific cooling, pushing the climate state towards a La Niña like background state ((Ruprich-Robert et al., 2017; Trascasa-Castro et al., 2021). Once the mean state changes are subtracted from the total modulation, we observe an east-west dipole pattern characterising the direct modulation of ENSO impacts by AMV (Figs. 3.1d,h; 3.2d,h), with a strengthening of the surface response to ENSO over southwestern Australia and a weakening of ENSO impacts over eastern Australia in austral summer.

Overall, the differences in the total modulation of ENSO impacts over Australia by AMV are primarily driven by the direct modulation of ENSO impacts by AMV and not mean state changes.

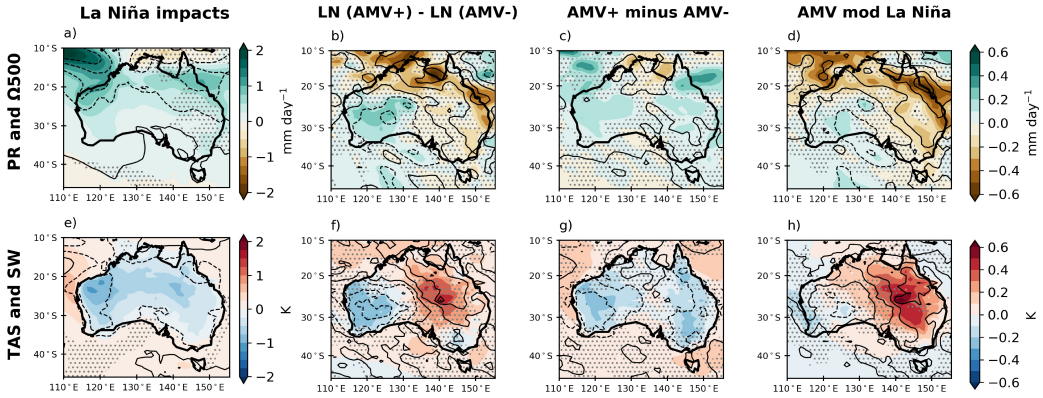

Figure 3.2: As in Figure 1 but for La Niña. Panels c and g are identical to Fig. 3.1 by construction.

3.3.2. AMV modulation of ENSO extremes over Australia

After showing that AMV modulates the summer mean ENSO-climate signals in Australia in NCAR-CESM1, primarily by modulating ENSO impacts, we now explore changes in daily precipitation and temperature extremes.

During El Niño, eastern Australia experiences a decrease in the number of summer wet days (Fig. 3.3a). There are up to 3 more warm days per summer in the north and north-west of Australia (Fig. 3.1e), and the period with CDD extends by one day. La Niña summers are characterised by anomalies that are equivalent in amplitude but opposite in sign to El Niño (Figs. 3.4 a and e).

The total modulation of El Niño-driven extremes by AMV shows a signal of 1 extra wet day per summer over eastern Australia associated with a decrease in CDD (Fig. 3.3b), and a decrease in R90p over the central part of Australia between 125°E-135°E, where there is also an increase of 1 extra warm day and night per summer (Fig. 3.3f). The total modulation of La Niña temperature extremes by AMV is stronger, with 2 more warm days and nights in eastern Australia (Fig. 3.4f). The magnitude of the total modulation of ENSO-driven changes in extremes by AMV is comparable to the mean ENSO signal in NCAR-CESM1, representing a substantial modification that may manifest on multi-decadal timescales.

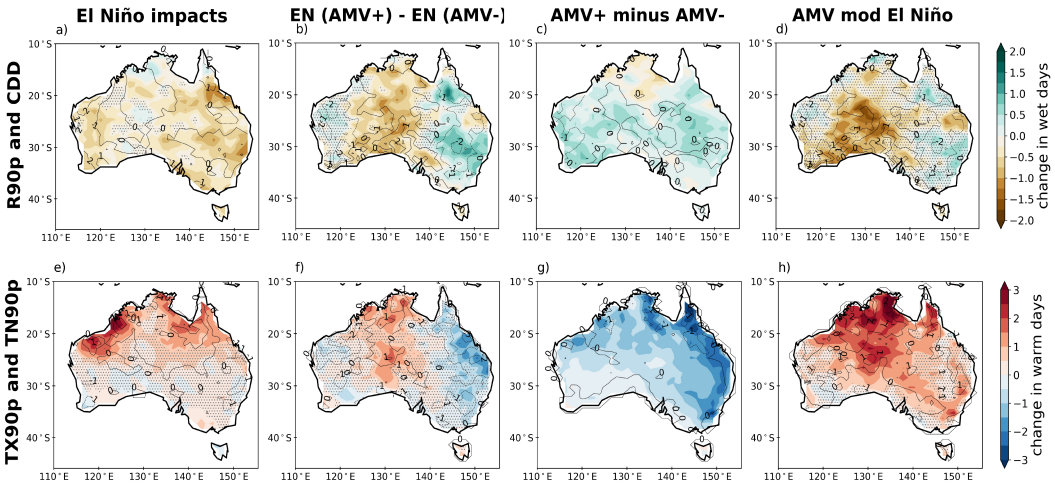

Figure 3.3: El Niño-related extremes over Australia in DJF. Top: change in no. wet days (R90p; shading) and consecutive dry days per summer (CDD; contours. Contour interval is 1 day). Bottom: change in no. warm days (TX90p; shading) and warm nights (TN90p; contours. Contour interval is 1 night). Columns show: (a,e) Mean El Niño impact (eq. 3.2); (b,f) the total El Niño modulation by AMV (eq. 3.3); (c,g) the mean change due to AMV (eq. 3.5); and (d,h) the direct AMV modulation of El Niño impacts (eq. 3.6). Stippled areas show non-significant anomalies in R90p (top) and TX90p (bottom) at the 95% confidence level.

The changes in precipitation extremes attributable to the mean climate response to AMV extend rather homogeneously across Australia (Fig. 3.3c); however, changes to temperature extremes are largest over northern and eastern regions (Fig. 3.3g). AMV modulation of the direct ENSO impacts on extreme precipitation and temperature (Figs. 3.3d, h and 3.4d, h) resemble the apparent differences in ENSO impacts shown in Figs. 3.3b, f and 3.4b, f, but with stronger relative amplitudes. In AMV+, the El Niño signal intensifies over central and southern Australia, evidenced by a decrease of 2 in R90p, and an increase in CDD. There is also an overall increase of up to 3 warm days and 2 warm nights per summer, peaking over the North of Australia. The AMV modulation of La Niña consists of a weakening of the mean La Niña response (Figs. 4.4a,e), with a significant decrease in R90p over eastern and Western Australia (Fig. 3.4d), and a larger increase of up to 3 warm and nights over eastern Australia (Fig. 3.4 h).

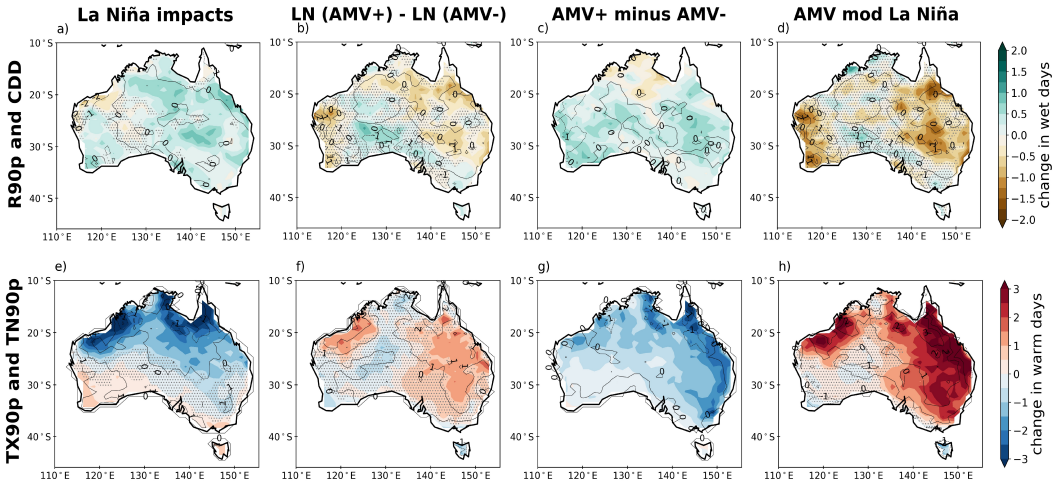

Figure 3.4: As in Fig. 3.3 but for La Niña. Panels c and g are identical to Fig. 3.3 by construction.

In comparison to the direct modulation of ENSO impacts by AMV (Figs. 3.1 and 3.2, right column), changes in extreme precipitation and temperature do not show a clear dipole with intensification over the west and weakening over the east (Figs. 3.3 and 3.4, right column). This reveals that the AMV modulation of ENSO extremes is not only asymmetric as ENSO mean impacts, but it is also nonlinear.

3.3.3. AMV modulation of ENSO-driven fire activity over Australia

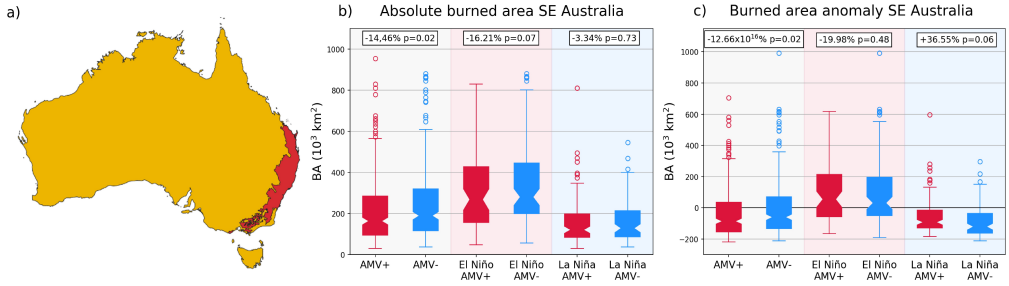

Figure 3.5: a) Focus area for the wildfire study (shaded in red). (b) Boxplots of absolute burned area (km^2) in SE Australia estimated using NCAR-CESM1 output with the empirical SPEI-BA relationship derived from observations using Eq 3.7 (c) Anomalies in burned area (km^2) with respect to the mean state of the matched AMV phase. Red (blue) boxplots show values in AMV+ (AMV-). Numbers on top show the % difference between El Niño (or La Niña) in AMV+ and AMV- and their associated p-value estimated with a two-sided Student's t-test.

Given the significant AMV modulation of the ENSO climate impacts over Australia in NCAR-CESM1, we make the further step to explore the implication for forest fires over south-eastern Australia (Fig. 3.5a) using the statistical model introduced in Section 3.2.4. The SPEI12 was chosen as an estimator of burned area, meaning that precipitation and temperature 12 months prior to the end of the fire season were considered. We considered other frequency of SPEI and found no significant changes in the AMV modulation of the ENSO-BA relationship in Australia. Figure 3.5b shows BA in each AMV phase (red AMV+, blue AMV-) and for El Niño (middle column) and La Niña (right column) events during each AMV phase. BA decreases significantly by 14.5% in AMV+ compared to AMV-. There is also a borderline significant (p-value < 0.07) decrease in BA of 16.2% during El Niño in AMV+ compared to AMV-. During La Niña, there are no statistically significant BA changes between AMV phases. The fact that ENSO and AMV signals are superimposed in Fig. 3.5b hinders the isolation of the proportion of ENSO-driven BA that is actually modulated by AMV.

To quantify the AMV modulation of direct ENSO impacts, we remove the mean

background AMV signal and show the results as anomalies relative to each AMV mean state (Fig. 3.5c). This shows that the AMV modulation of the direct El Niño-driven BA is not significant, but there is a significant offset of the decrease in BA during La Niña of around 37% (p-value < 0.06). As shown in Figs. 3.2d and 3.2h, the precipitation and temperature anomalies driven by La Niña in the south-east of Australia is damped by AMV+. Drier and warmer conditions induced by AMV+ increase the risk of fire weather during La Niña summers. During El Niño, the significant reduction in south-east Australia BA by AMV is due to the mean background climate effects rather than the modulation of the direct El Niño impacts by AMV.

3.3.4. AMV modulation of large-scale circulation leading to climate impacts

To understand the origins of the modulation of ENSO climate impacts discussed in Sections 3.2.1 and 3.2.2, we next examine the large-scale circulation response. In particular, we explore the physical origin of the modulation of the mid-tropospheric subsidence anomalies over Australia using the decomposition into local Hadley and Walker circulation components described in Section 3.2.5.

During El Niño, there is a shift in tropical convection from the warm pool towards the central equatorial Pacific resulting in negative 500 hPa pressure velocity anomalies and a weakening of the South Pacific Convergence Zone (SPCZ) (Fig. 3.6a). This response is mainly associated with changes in the local Hadley circulation (Fig. 3.6e), with the pressure velocity anomalies associated with the local Walker component (Fig. 3.6i) being roughly three times weaker. The total modulation by AMV of the local Hadley component response to El Niño (Fig. 3.6f) shows a weakening of the enhanced upward motion in the central equatorial Pacific, especially between 150-180°E. Between 15°S-15°N, this total modulation is explained by a general decrease of the El Niño impacts by the mean state change (Fig. 3.6h) and by a westward shift/extension of the canonical El Niño impacts by the AMV modulation of the El Niño impacts (Fig. 3.6h; see also Fig. 3.10), in agreement with Trascasa-Castro et al. (2021).

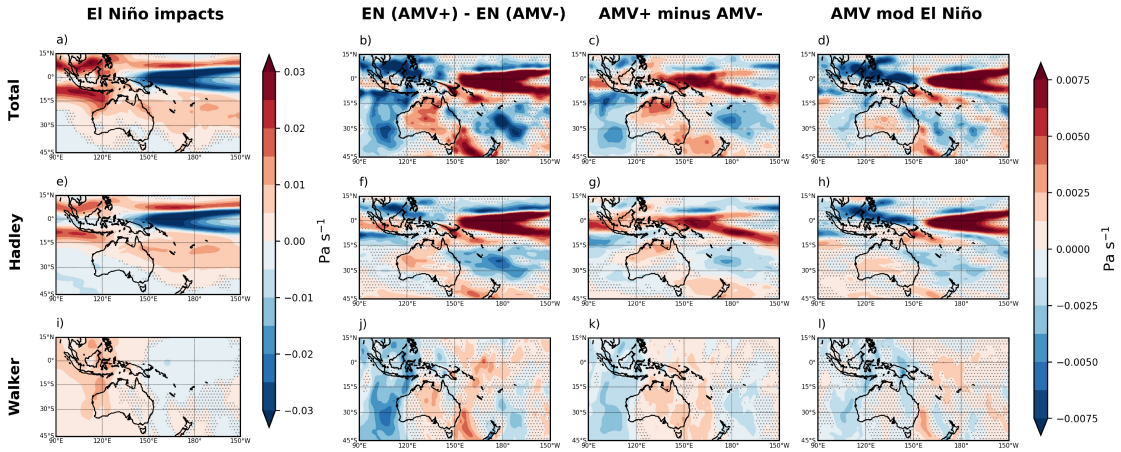

Figure 3.6: El Niño-related vertical velocity at 500 hPa (Pa s^{-1}) in DJF. Top row: total change, middle row: local Hadley component and bottom row: local Walker component. Columns show: (a,e,i) Mean El Niño impact (eq. 3.2); (b,f,j) the total El Niño modulation by AMV (eq. 3.3); (c,g,k) the mean change due to AMV (eq. 3.5); and (d,h,l) the direct AMV modulation of El Niño impacts (eq, 3.6. Negative values show ascent and positive values descent. Stippled areas show non-significant anomalies at the 95% confidence level.

Over Australia, the mean El Niño signal in pressure velocity comprises increased subsidence particularly over northern regions (Fig 3.6a). The total modulation of the vertical velocity response to El Niño by AMV (Fig. 3.6b) consists of intensified subsidence over central Australia with a similar contribution of the local Hadley and local Walker components. The changes in the Walker circulation can be explained mostly by the mean state AMV impact (Fig. 3.6k). Under warm AMV conditions (Figs. 3.6g and 3.7g), the deep convection associated with the ascending branch of the Hadley cell in the Pacific is shifted North during boreal winter, and the SPCZ loses strength. This is in broad agreement with observational and modelling studies linking AMV to changes in Hadley circulation pattern and strength (Liu et al., 2020; Žiga Zaplotnik et al., 2022).

Regarding the direct modulation of El Niño impacts, AMV+ enhances subsidence over central-western Australia and weakens ascent over Western Australia (Fig. 3.6d). This seems to be driven by a westward shift of the mean El Niño signature over Australia, which echoes the westward shift of the vertical velocity in the deep tropics (Fig. 3.10ac). The dipole structure of the vertical velocity

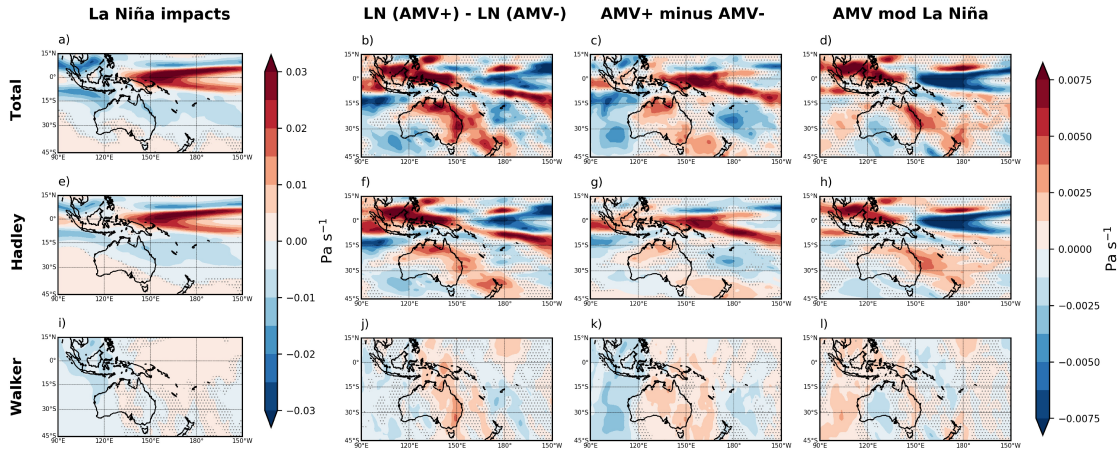

Figure 3.7: As in Fig. 3.6 but for La Niña. Panels c, g and k are identical to Fig. 3.6 by construction.

anomalies over Australia is reminiscent of the dipole anomalies already discussed for surface temperature and precipitation (Fig. 3.1a,e).

The mean La Niña signal is reduced upwelling in the equatorial Pacific (Fig. 3.7a), predominantly associated with the local Hadley circulation (Fig. 3.7e) with only a small role for local Walker circulation changes (Fig. 3.7i). Over eastern Australia, AMV+ weakens the total La Niña anomalies causing enhanced subsidence over the eastern coast (Fig. 3.7b), driven by both the direct AMV modulation of La Niña impacts (Fig. 3.7d) and the mean state AMV changes (Fig. 3.7c). This modulation is mainly caused by a weakening of the local Hadley circulation impacts (Fig. 3.7h vs Fig. 3.7e), with a minor contribution of the local Walker component (Fig. 3.7l). Over the western part of the country, AMV+ enhances the upward motion of air during La Niña summers (Fig. 3.7bd), driven by a strengthening of the zonal overturning circulation by modulating the direct La Niña impacts (Fig. 3.7l).

3.4. Discussion and conclusions

We analysed idealised model experiments to investigate how ENSO impacts on Australian climate are modulated by AMV. The large ensemble experiments

with 270 austral summers of perpetual AMV+/- conditions offer a large sample that allows a cleaner separation of the effects of AMV-ENSO interactions than can be achieved in the limited instrumental record. The total modulation of ENSO impacts by AMV (i.e. what one would observe in the real world) can be decomposed into a background state change due to AMV and a signal from modulation of the direct ENSO impacts by AMV, the latter implicitly includes effects from changes in ENSO characteristics and/or changes in teleconnections. This is an advance over some earlier studies where these components have not been explicitly separated (Maher et al., 2022), allowing contributing mechanisms from mean state changes and direct ENSO modulation to be distinguished. The study builds on the results of Trascasa-Castro et al. (2021) who showed a weakening of ENSO amplitude in the simulations by ∼10%.

An east-west dipole pattern, with warm AMV conditions strengthening (weakening) ENSO impacts over western (eastern) Australia, is found for changes in mean summer precipitation and temperature. Under El Niño (La Niña), the mean background state change due to AMV enhances (diminishes) the direct modulation of impacts by AMV in eastern Australia, with the opposite found in western Australia.

The reduction in wet days across most of Australia under El Niño is negated by the AMV modulation in eastern regions but is enhanced in the central and southern regions. Though the background state change by AMV leads to an increase in wet days across Australia, the direct modulation of El Niño impacts by AMV leads to a relatively stronger decrease in southern and central regions. In contrast, La Niña increases the frequency of wet days across most of Australia, with the total modulation by AMV muting this signal in eastern Australia making extreme wet days less likely in this region during AMV+. While the canonical El Niño response shows increases in warm days and nights confined to northern Australia, the direct modulation of ENSO impacts by AMV shows a reduction of warm days and nights in eastern Australia and increase in central Australia, and vice versa for La Niña. This east-west dipole resembles the pattern seen for seasonal mean precipitation and temperature modulation by AMV.

The east-west dipole across Australia seen in the total modulation of ENSO impacts by AMV on several climate indicators can be explained by changes in the equatorial Pacific atmospheric circulation. AMV drives background changes that project on a La Niña-like state (Ruprich-Robert et al., 2017; Trascasa-Castro et al., 2021), which are associated with changes in the Walker and Hadley circulations, mostly weakening the total El Niño teleconnections but strengthening the La Niña ones (Figs. 3.6cgk, 3.7cgk and 3.10). The AMV also modulates the ENSO characteristics, with weaker ENSO events and westward shifted El Niño events (i.e. more Central Pacific like) during AMV+ (Figs. 3.6dhl, 3.7dhl and 3.10), in agreement with the previous study of Trascasa-Castro et al. (2021). The east-west dipole across Australia seen in the total modulation of many ENSO impacts appears also explained by the combination of a La Niña-like background change and by a westward shift of ENSO teleconnections.

The results show no significant modulation of ENSO anomalies in burned area in south-east Australia by AMV, but during AMV- mean burned area is significantly higher than during AMV+. This finding contrasts with Liu et al. (2023), who explore the AMV modulation of the relationship between the autumn Niño3.4 index and the Fire Weather Index (FWI). They find a positive correlation between ENSO and Australian FWI in observations, with the relationship being stronger in AMV+ than in AMV-. Opposite to what our results show, they suggest that AMV+ reinforces the El Niño-driven hot and dry conditions over Australia given the warm and dry anomalies driven by AMV in austral spring. Therefore, uncertainty remains in the sign of the AMV modulation of ENSO-driven burned area variability in Australia and further work is needed to understand the sources of uncertainty and constrain the relationship.

The mechanisms proposed here could ultimately contribute to multidecadal variability in ENSO impacts, meaning that Australian climate may undergo periods of apparently more severe or muted climate variability on interannual timescales. Should such variability arise in observations, it would be superposed onto background climate trends driven by external forcings like greenhouse gases. Eastern

Australia has already experienced a rapid drying trend due to anthropogenic emissions of greenhouse gases (Abram et al., 2021). Hence, multidecadal variability may affect overall resilience and adaptation to climate extremes in a warming world, and hence internal variability should be considered within storylines for Australian climate change and stress testing against weather and climate extremes.

3.5. Data Availability Statement

The DCPP NCAR-CESM1 data are available through the CMIP6 archive on the Earth System Grid Federation.

State	Agency
New South Wales	Department of Planning, Industry and Environment
Queensland	Queensland Parks and Wildlife Service
Victoria	Department of Environment, Land, Water and Planning

3.6. Acknowledgements

P.T.-C. was supported by a PhD scholarship from the Natural Environment Research Council PANORAMA Doctoral Training Partnership (NE/S007458/1). Y.R.-R. received the support of a fellowship from "la Caixa" Foundation (ID 100010434) and from the European Union's Horizon 2020 research and innovation programme under the Marie Skłodowska-Curie grant agreement No 847648. The fellowship code is LCF/BQ/PR21/11840016. A.C.M. was supported by the European Union's Horizon 2020 research and innovation program under grant agreement no. 820829 (CONSTRAIN project) and The Leverhulme Trust (PLP-2018-278). M.T. acknowledges funding by the Spanish Ministry of Science, Innovation and Universities through the Ramón y Cajal Grant Reference RYC2019-027115-I and through the project ONFIRE, grant PID2021-123193OB-I00, funded by MCIN/AEI/ 10.13039/501100011033. Computing facilities were provided by the Barcelona Supercomputing Center and the University of Leeds. We thank Gokhan Danabasoglu and Fred Castruccio for providing the climate model output, and two anonymous reviewers for their constructive feedback, which helped to improve the readability and quality of this paper

3.7. Supporting information

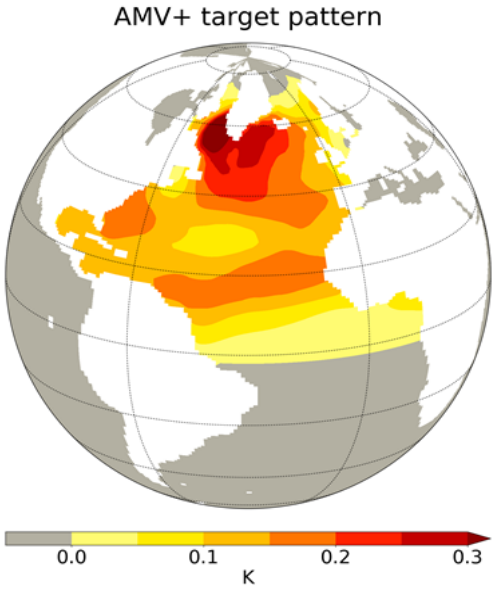

Figure 3.8: Target AMV+ sea surface temperature (SST) pattern. The AMV- is equivalent in amplitude but with opposite sign SST anomalies.

Model evaluation

ENSO surface temperature and precipitation response in Australia in DJF

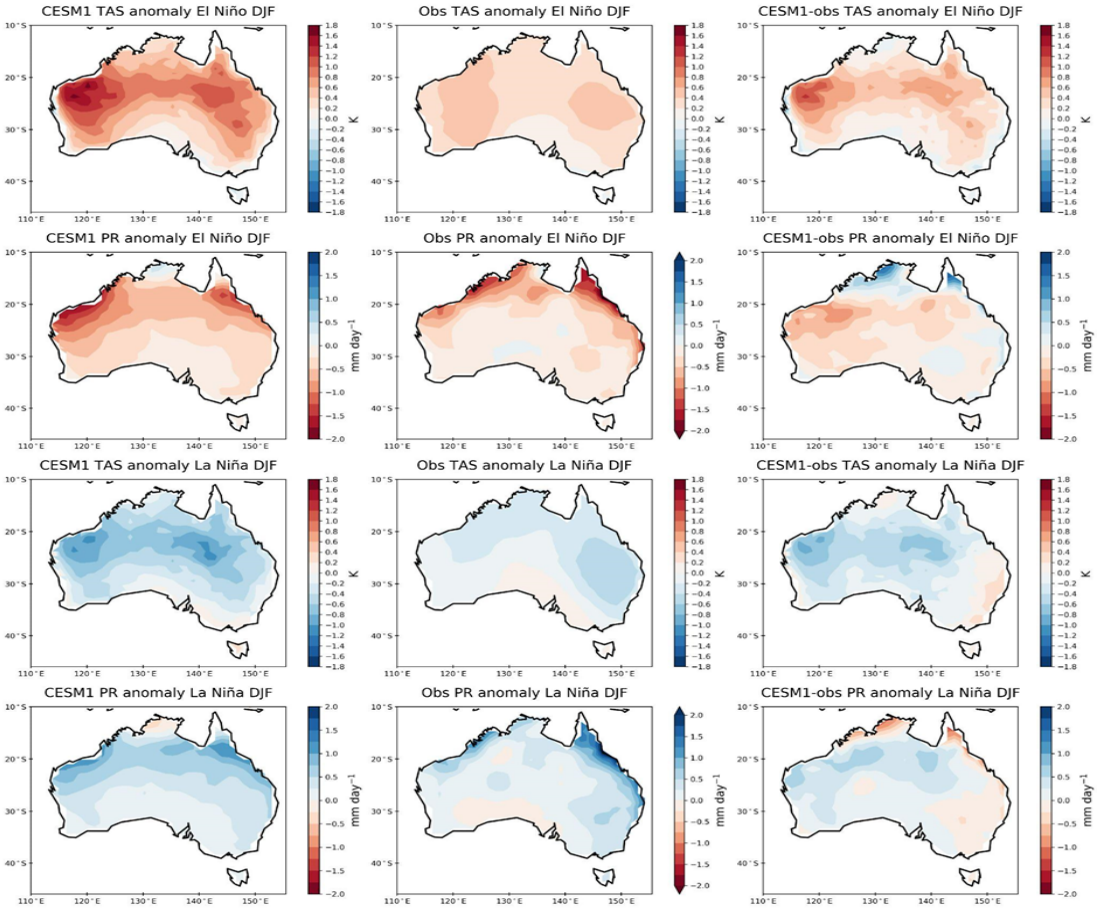

Figure 3.9: Precipitation and temperature anomalies during El Niño and La Niña. Comparison (third column) between NCAR-CESM1 (first column) and observations (CRU) from 1950 to 2019.

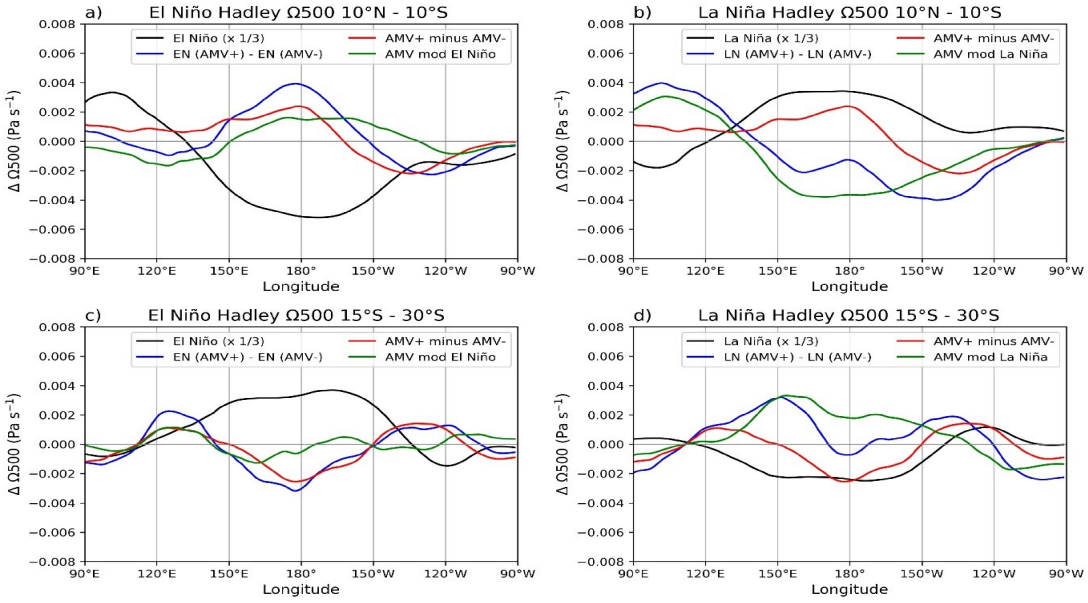

Figure 3.10: Hadley circulation anomalies during El Niño (left column) and La Niña (right column) averaged meridionally between 10°N-10°S (top) and 15°S-30°S (bottom). Colours the anomalies shown in figures 1, 2, 3, 4, 6 and 7, with ENSO impacts in black, the total AMV modulation of ENSO impacts in blue, the direct AMV impacts in red and the AMV modulation of ENSO in green.

Extended composite analysis method

We present here a more detailed decomposition of the modulation of a variable X by AMV and ENSO. We represent the sample k (k=1, 2, ..., K) of the ensemble η of a model variable X as the sum of its mean state μ, and of the superposition of AMV direct impacts α_k^η, ENSO direct impacts E_k^η and of direct impacts from any other modes of variability θ_k^η:

$$X_k^\eta = \mu + \alpha_k^\eta + E_k^\eta + \theta_k^\eta \tag{3.9}$$

Accounting for the fact that ENSO impacts E_k^η on X_k^η are a function of both the tropical Pacific SST anomalies and the atmospheric pathways of ENSO teleconnections, we assume that E_k^η can be expressed as:

$$E_k^\eta = \beta^\eta \varepsilon_k^{'\eta} \tag{3.10}$$

where E_k^η are SST anomalies with respect to the mean state in the tropical Pacific (e.g., the Niño3.4 index), $^\eta$ is the transfer function between the tropical Pacific SST anomalies and X_k^η. Combining eq. S1 and eq. S2:

$$X_k^\eta = \mu + \overline{\alpha_k^\eta} + \beta^\eta \varepsilon_k^{'\eta} + \theta_k^\eta \tag{3.11}$$

Averaging over the K samples of the ensemble η we obtain the ensemble mean $\overline{X^\eta}$ that we call μ^η:

$$\overline{X^\eta} = \mu^\eta = \mu + \overline{\alpha^\eta} + \overline{\beta^\eta \varepsilon'^\eta} + \overline{\theta^\eta}$$

(3.12)

The mean difference between AMV phases ($\Delta\overline{X} = \overline{X^+} - \overline{X^-}$) can therefore be written as:

$$\Delta\overline{X} = \Delta\mu = \Delta\overline{\alpha} + \Delta\overline{\beta\varepsilon'} + \Delta\overline{\theta}$$

(3.13)

This shows that mean difference between AMV phases $\Delta\mu$ (cf. Eq. 3.5) is due to the averaged direct impacts of AMV ($\Delta\overline{\alpha}$), but also to changes in the direct impact of ENSO ($\Delta\overline{\beta\varepsilon'}$) and any other modes of variability ($\Delta\overline{\theta}$) averaged over all their states within the AMV ensemble. Focusing on ENSO, those differences could arise from potential changes in its non-linear impacts on X and from the direct AMV impacts on tropical Pacific SST. In other words, this means that $\Delta\overline{\beta\varepsilon'}$ can be explained by either a mean shift of ε', a change in the variance of ε', or changes in β.

Focusing on the El Niño phase of ENSO, we write X as:

$$X^{\eta}_{EN,i} = \mu + \alpha^{\eta}_{EN,i} + \beta^{\eta}\varepsilon'^{\eta}_{EN,i} + \theta^{\eta}_{EN,i}$$

(3.14)

Where the subscripts "EN" and "i" indicate that we are focusing on the ith El Niño event of the AMV ensemble η (i=1, 2, ..., N; where N is the total number of El Niño events within a given AMV phase). When focusing on La Niña, we would replace the subscript "EN" for "LN". $X^{\eta}_{EN,i}$ can also be written as:

$$X^{\eta}_{EN,i} = \overline{X^{\eta}} + [\mathrm{X}^{\eta}_{EN}] + X^{\eta*}_{EN,i}$$

(3.15)

Where $\overline{X^{\eta}}$ is the ensemble mean introduced in eq. S4, $[X^{\eta}_{EN}]$ is the deviation from the ensemble mean of the average over all the El Niño events of the ensemble η, $X^{\eta*}_{EN,i}$ is the residual of the ith El Niño anomalies, specific to each El Niño event.

Similarly, $\alpha^{\eta}_{EN,i}$, $\beta\varepsilon'_{EN,i}$ and $\theta_{EN,i}$ can be decomposed into an ensemble mean component, an averaged deviation during El Niño events from this ensemble mean and a residual. Integrating this decomposition into eq. S7 and averaging over all the El Niño events, we obtain:

$$X^{\eta}_{EN,i} = \mu + \overline{\alpha^{\eta}} + \overline{\beta^{\eta}\varepsilon'^{\eta}} + \overline{\theta^{\eta}} + [\alpha^{\eta}_{EN}] + [\beta^{\eta}\varepsilon'^{\eta}_{EN}] + [\theta^{\eta}_{EN}]$$
$$X^{\eta}_{EN,i} = \mu^{\eta} + [\alpha^{\eta}_{EN}] + [\beta^{\eta}\varepsilon'^{\eta}_{EN}] + [\theta^{\eta}_{EN}]$$

(3.16)

Average changes in the El Niño impacts between AMV phases can therefore be written as:

$$\Delta\overline{X_{EN}} = \Delta\mu + \Delta([\alpha_{EN}] + [\beta\varepsilon'_{EN}] + [\theta_{EN}])$$

(3.17)

Eq. 3.17 shows that total modulation of El Niño impacts on X between AMV phases ($\Delta\overline{X_{EN}}$) can be understood as the sum of changes in the mean state between AMV phases ($\Delta\mu$) and of changes in the deviation from the ensemble mean of the averaged impacts on X during El Niño events of AMV ($\Delta[\alpha_{EN}]$), ENSO ($\Delta[\beta\varepsilon'_{EN}]$) and any other modes of variability (θ_{EN}]). Those last 3 terms are what we consider as the direct ENSO impacts modulated by AMV in the main text (cf. Eq. 3.6). Yet, eq. 3.17 reveals this is a permissive definition, since it also includes potential impacts of AMV and any other modes of variability on X that are specific to El Niño states. Attributing those changes to direct ENSO

impacts modulation or to AMV impacts specific to ENSO phases is arbitrary.

Finally, it is useful to note that the tropical Pacific SST anomalies ε' are partly driven by AMV impacts. Conceptually, we can separate those anomalies into a term controlled by the AMV impacts (α_ε) and a term representing the variability intrinsic to the tropical Pacific (γ_ε): $\varepsilon' = \alpha_\varepsilon + \gamma_\varepsilon$. This reveals that the term $[\beta\varepsilon'_{EN}]$ (but also the term $\Delta\overline{\beta\varepsilon'}$) includes indirect impacts of AMV on X through the AMV impacts on the tropical Pacific SST. Once more, attributing those impacts to the direct ENSO impacts rather than to AMV (indirect) impacts is arbitrary.

References

N. J. Abram, B. J. Henley, A. S. Gupta, T. J. R. Lippmann, H. Clarke, A. J. Dowdy, J. J. Sharples, R. H. Nolan, T. Zhang, M. J. Wooster, J. B. Wurtzel, K. J. Meissner, A. J. Pitman, A. M. Ukkola, B. P. Murphy, N. J. Tapper, and M. M. Boer. Connections of climate change and variability to large and extreme forest fires in southeast australia. *Communications Earth Environment*, 2: 8, 2021. ISSN 2662-4435. doi: 10.1038/s43247-020-00065-8. URL https://doi.org/10.1038/s43247-020-00065-8. 100, 119

N. Andela, D. C. Morton, L. Giglio, Y. Chen, G. R. van der Werf, P. S. Kasibhatla, R. S. DeFries, G. J. Collatz, S. Hantson, S. Kloster, D. Bachelet, M. Forrest, G. Lasslop, F. Li, S. Mangeon, J. R. Melton, C. Yue, and J. T. Randerson. A human-driven decline in global burned area. *Science*, 356:1356–1362, 2017. doi: 10.1126/science.aal4108. URL https://www.science.org/doi/abs/10.1126/science.aal4108. 105

J. M. Arblaster and L. V. Alexander. The impact of the el niño-southern oscillation on maximum temperature extremes. *Geophysical Research Letters*, 39, 2012. doi: https://doi.org/10.1029/2012GL053409. URL https://agupubs.onlinelibrary.wiley.com/doi/abs/10.1029/2012GL053409. 100

S. Archibald, C. E. R. Lehmann, J. L. Gómez-Dans, and R. A. Bradstock. Defining pyromes and global syndromes of fire regimes. *Proceedings of the National Academy of Sciences of the United States of America*, 110:6442–6447, 5 2013. ISSN 00278424. doi: 10.1073/PNAS.1211466110/SUPPL_FILE/PNAS.201211466SI.PDF. 100

G. J. Boer, D. M. Smith, C. Cassou, F. Doblas-Reyes, G. Danabasoglu, B. Kirtman, Y. Kushnir, M. Kimoto, G. A. Meehl, R. Msadek, W. A. Mueller, K. E. Taylor, F. Zwiers, M. Rixen, Y. Ruprich-Robert, and R. Eade. The decadal climate prediction project (dcpp) contribution to cmip6. *Geoscientific Model Development*, 9:3751–3777, 2016. doi: 10.5194/gmd-9-3751-2016. URL https://gmd.copernicus.org/articles/9/3751/2016/. 102

R. A. Bradstock. A biogeographic model of fire regimes in australia: current and future implications. *Global Ecology and Biogeography*, 19: 145–158, 2010. doi: https://doi.org/10.1111/j.1466-8238.2009.00512.x. URL https://onlinelibrary.wiley.com/doi/abs/10.1111/j.1466-8238.2009.00512.x. 105

J. G. Canadell, C. P. Meyer, G. D. Cook, A. Dowdy, P. R. Briggs, J. Knauer, A. Pepler, and V. Haverd. Multi-decadal increase of forest burned area in australia is linked to climate change. *Nature Communications 2021 12:1*, 12: 1–11, 5 2021. ISSN 2041-1723. doi: 10.1038/s41467-021-27225-4. URL https://www.nature.com/articles/s41467-021-27225-4. 100, 105, 106

F. S. Castruccio, Y. Ruprich-Robert, S. G. Yeager, G. Danabasoglu, R. Msadek, and T. L. Delworth. Modulation of arctic sea ice loss by atmospheric teleconnections from atlantic multidecadal variability. *Journal of Climate*, 32:1419–1441, 3 2019. ISSN 0894-8755. doi: 10.1175/JCLI-D-18-0307.1. URL https://journals.ametsoc.org/view/journals/clim/32/5/jcli-d-18-0307.1.xml. 102

C. T. Y. Chung and S. B. Power. The non-linear impact of el niño, la niña and the southern oscillation on seasonal and regional australian precipitation. *Journal of Southern Hemisphere Earth Systems Science*, 67:25–45, 2017. ISSN 22065865. doi: 10.22499/3.6701.003. 100

E. Dinerstein, D. Olson, A. Joshi, C. Vynne, N. D. Burgess, E. Wikramanayake, N. Hahn, S. Palminteri, P. Hedao, R. Noss, M. Hansen, H. Locke, E. C. Ellis, B. Jones, C. V. Barber, R. Hayes, C. Kormos, V. Martin, E. Crist, W. Sechrest, L. Price, J. E. M. Baillie, D. Weeden, K. Suckling, C. Davis, N. Sizer, R. Moore, D. Thau, T. Birch, P. Potapov, S. Turubanova, A. Tyukavina, N. de Souza, L. Pintea, J. C. Brito, O. A. Llewellyn, A. G. Miller, A. Patzelt, S. A. Ghazanfar, J. Timberlake, H. Klöser, Y. Shennan-Farpón, R. Kindt, J.-P. B. Lillesø, P. van Breugel, L. Graudal, M. Voge, K. F. Al-Shammari, and M. Saleem. An ecoregion-based approach to protecting half the terrestrial realm. *BioScience*, 67:534–545, 6 2017. ISSN 0006-3568. doi: 10.1093/biosci/bix014. URL https://doi.org/10.1093/biosci/bix014. 105

M. G. Donat, L. V. Alexander, H. Yang, I. Durre, R. Vose, R. J. H. Dunn, K. M. Willett, E. Aguilar, M. Brunet, J. Caesar, B. Hewitson, C. Jack, A. M. G. K. Tank, A. C. Kruger, J. Marengo, T. C. Peterson, M. Renom, C. O. Rojas, M. Rusticucci, J. Salinger, A. S. Elrayah, S. S. Sekele, A. K. Srivastava, B. Trewin, C. Villarroel, L. A. Vincent, P. Zhai, X. Zhang, and S. Kitching. Updated analyses of temperature and precipitation extreme indices since the beginning of the twentieth century: The hadex2 dataset. *Journal of Geophysical Research Atmospheres*, 118:2098–2118, 5 2013. ISSN 21698996. doi: 10.1002/jgrd.50150. 105

A. J. Dowdy, H. Ye, A. Pepler, M. Thatcher, S. L. Osbrough, J. P. Evans, G. D. Virgilio, and N. McCarthy. Future changes in extreme weather and pyroconvection risk factors for australian wildfires. *Scientific Reports 2019 9:1*, 9:1–11, 5 2019. ISSN 2045-2322. doi: 10.1038/s41598-019-46362-x. URL https://www.nature.com/articles/s41598-019-46362-x. 100

W. Drosdowsky and M. C. Wheeler. Predicting the onset of the north australian wet season with the poama dynamical prediction system. *Weather and Forecasting*, 29:150 – 161, 2014. doi: https://doi.org/10.1175/WAF-D-13-00091.1. URL https://journals.ametsoc.org/view/journals/wefo/29/1/waf-d-13-00091_1.xml. 100

V. Eyring, S. Bony, G. A. Meehl, C. A. Senior, B. Stevens, R. J. Stouffer, and K. E. Taylor. Overview of the coupled model intercomparison project phase 6 (cmip6) experimental design and organization. *Geoscientific Model Development*, 9:1937–1958, 2016. doi: 10.5194/gmd-9-1937-2016. URL https://gmd.copernicus.org/articles/9/1937/2016/. 102

Y.-G. Ham and J.-S. Kug. Role of north tropical atlantic sst on the enso simulated using cmip3 and cmip5 models. *Climate Dynamics*, 45:3103–3117, 2015. ISSN 1432-0894. doi: 10.1007/s00382-015-2527-z. URL https://doi.org/10.1007/s00382-015-2527-z. 100

I. Harris, T. J. Osborn, P. Jones, and D. Lister. Version 4 of the cru ts monthly high-resolution gridded multivariate climate dataset. *Scientific Data*, 7:109,

2020. ISSN 2052-4463. doi: 10.1038/s41597-020-0453-3. URL https://doi.org/10.1038/s41597-020-0453-3. 106

J. E. Kay, C. Deser, A. Phillips, A. Mai, C. Hannay, G. Strand, J. M. Arblaster, S. C. Bates, G. Danabasoglu, J. Edwards, M. Holland, P. Kushner, J. F. Lamarque, D. Lawrence, K. Lindsay, A. Middleton, E. Munoz, R. Neale, K. Oleson, L. Polvani, and M. Vertenstein. The community earth system model (cesm) large ensemble project: A community resource for studying climate change in the presence of internal climate variability. *Bulletin of the American Meteorological Society*, 96:1333–1349, 5 2015. ISSN 0003-0007. doi: 10.1175/BAMS-D-13-00255.1. URL https://journals.ametsoc.org/view/journals/bams/96/8/bams-d-13-00255.1.xml. 102

A. S. Kiem and S. W. Franks. Multi-decadal variability of drought risk, eastern australia. *Hydrological Processes*, 18:2039–2050, 2004. doi: https://doi.org/10.1002/hyp.1460. URL https://onlinelibrary.wiley.com/doi/abs/10.1002/hyp.1460. 100

A. D. King, L. V. Alexander, and M. G. Donat. Asymmetry in the response of eastern australia extreme rainfall to low-frequency pacific variability. *Geophysical Research Letters*, 40:2271–2277, 2013. doi: https://doi.org/10.1002/grl.50427. URL https://agupubs.onlinelibrary.wiley.com/doi/abs/10.1002/grl.50427. 100

A. F. Z. Levine, M. J. McPhaden, and D. M. W. Frierson. The impact of the amo on multidecadal enso variability. *Geophysical Research Letters*, 44:3877–3886, 5 2017. ISSN 19448007. doi: 10.1002/2017GL072524. URL http://doi.wiley.com/10.1002/2017GL072524. 100

Z. Lin and Y. Li. Remote influence of the tropical atlantic on the variability and trend in north west australia summer rainfall. *Journal of Climate*, 25:2408 – 2420, 2012. doi: https://doi.org/10.1175/JCLI-D-11-00020.1. URL https://journals.ametsoc.org/view/journals/clim/25/7/jcli-d-11-00020.1.xml. 101

G. Liu, J. Li, and T. Ying. Atlantic multi-decadal oscillation modulates the relationship between el niño-southern oscillation and fire weather in australia. *Atmospheric Chemistry and Physics Discussions*, 2023:1–17, 2023. doi: 10.5194/acp-2022-858. URL https://acp.copernicus.org/preprints/acp-2022-858/. 100, 118

Y. Liu, Z. Gong, C. Sun, J. Li, and L. Wang. Multidecadal seesaw in hadley circulation strength between the two hemispheres caused by the atlantic multidecadal variability. *Frontiers in Earth Science*, 8, 2020. ISSN 2296-6463. doi: 10.3389/feart.2020.580457. URL https://www.frontiersin.org/articles/10.3389/feart.2020.580457. 101, 115

N. Maher, J. E. Kay, and A. Capotondi. Modulation of enso teleconnections over north america by the pacific decadal oscillation. *Environmental Research Letters*, 17:114005, 10 2022. doi: 10.1088/1748-9326/ac9327. URL https://dx.doi.org/10.1088/1748-9326/ac9327. 117

R. Marcos, M. Turco, J. Bedia, M. C. Llasat, and A. Provenzale. Seasonal predictability of summer fires in a mediterranean environment, 2015. 100

G. A. Meehl, A. Hu, F. Castruccio, M. H. England, S. C. Bates, G. Danabasoglu, S. McGregor, J. M. Arblaster, S.-P. Xie, and N. Rosenbloom. Atlantic and pacific tropics connected by mutually interactive decadal-timescale processes. *Nature Geoscience*, 14:36–42, 2021. ISSN 1752-0908. doi: 10.1038/s41561-020-00669-x. URL https://doi.org/10.1038/s41561-020-00669-x. 101, 102

B. P. Murphy, R. A. Bradstock, M. M. Boer, J. Carter, G. J. Cary, M. A. Cochrane, R. J. Fensham, J. Russell-Smith, G. J. Williamson, and D. M. J. S. Bowman. Fire regimes of australia: a pyrogeographic model system. *Journal of Biogeography*, 40:1048–1058, 2013. doi: https://doi.org/10.1111/jbi.12065. URL https://onlinelibrary.wiley.com/doi/abs/10.1111/jbi.12065. 105

C. H. O'Reilly, M. Patterson, J. Robson, P. A. Monerie, D. Hodson, and Y. Ruprich-Robert. Challenges with interpreting the impact of atlantic multidecadal variability using sst-restoring experiments. *npj Climate and Atmospheric Science*, 6:14, 2023. ISSN 2397-3722. doi: 10.1038/s41612-023-00335-0. URL https://doi.org/10.1038/s41612-023-00335-0. 101

S. E. Perkins, D. Argüeso, and C. J. White. Relationships between climate variability, soil moisture, and australian heatwaves. *Journal of Geophysical Research: Atmospheres*, 120:8144–8164, 2015. doi: https://doi.org/10.1002/2015JD023592. URL https://agupubs.onlinelibrary.wiley.com/doi/abs/10.1002/2015JD023592. 100

S. Power, T. Casey, C. Folland, A. Colman, and V. Mehta. Inter-decadal modulation of the impact of enso on australia. *Climate Dynamics*, 15:319–324, 1999. ISSN 1432-0894. doi: 10.1007/s003820050284. URL https://doi.org/10.1007/s003820050284. 100

Y. Ruprich-Robert, R. Msadek, F. Castruccio, S. Yeager, T. Delworth, and G. Danabasoglu. Assessing the climate impacts of the observed atlantic multidecadal variability using the gfdl cm2.1 and ncar cesm1 global coupled models. *Journal of Climate*, 30:2785 – 2810, 2017. doi: https://doi.org/10.1175/JCLI-D-16-0127.1. URL https://journals.ametsoc.org/view/journals/clim/30/8/jcli-d-16-0127.1.xml. 101, 102, 109, 118

Y. Ruprich-Robert, E. Moreno-Chamarro, X. Levine, A. Bellucci, C. Cassou, F. Castruccio, P. Davini, R. Eade, G. Gastineau, L. Hermanson, D. Hodson, K. Lohmann, J. Lopez-Parages, P.-A. Monerie, D. Nicolì, S. Qasmi, C. D. Roberts, E. Sanchez-Gomez, G. Danabasoglu, N. Dunstone, M. Martin-Rey, R. Msadek, J. Robson, D. Smith, and E. Tourigny. Impacts of atlantic multidecadal variability on the tropical pacific: a multi-model study. *npj Climate and Atmospheric Science*, 4:33, 12 2021. ISSN 2397-3722. doi: 10.1038/s41612-021-00188-5. URL http://www.nature.com/articles/s41612-021-00188-5. 101, 102

J. Russell-Smith, C. P. Yates, P. J. Whitehead, R. Smith, R. Craig, G. E. Allan, R. Thackway, I. Frakes, S. Cridland, M. C. P. Meyer, and A. M. Gill. Bushfires down under: patterns and implications of contemporary australian landscape burning. *International Journal of Wildland Fire*, 16:361–377, 2007. URL https://doi.org/10.1071/WF07018. 105

J. Schwendike, P. Govekar, M. J. Reeder, R. Wardle, G. J. Berry, C. Jakob, J. Schwendike, P. Govekar, M. J. Reeder, R. Wardle, G. J. Berry, and C. Jakob. Local partitioning of the overturning circulation in the tropics and the connection to the hadley and walker circulations. *Journal of Geophysical Research: Atmospheres*, 119:1322–1339, 5 2014. ISSN 2169-8996. doi: 10.1002/2013JD020742. URL https://onlinelibrary.wiley.com/doi/full/10.1002/2013JD020742https://onlinelibrary.wiley.com/doi/abs/10.1002/2013JD020742https://agupubs.onlinelibrary.wiley.com/doi/10.1002/2013JD020742. 107

P. Trascasa-Castro, Y. Ruprich-Robert, F. Castruccio, and A. C. Maycock. Warm phase of amv damps enso through weakened thermocline feedback. *Geophysical Research Letters*, 48:e2021GL096149, 2021. doi: https://doi.org/10.1029/2021GL096149. URL https://agupubs.onlinelibrary.wiley.com/doi/abs/10.1029/2021GL096149. e2021GL096149 2021GL096149. 100, 101, 102, 109, 114, 117, 118

K. E. Trenberth, G. W. Branstator, D. Karoly, A. Kumar, N.-C. Lau, and C. Ropelewski. Progress during toga in understanding and modeling global teleconnections associated with tropical sea surface temperatures. *Journal of Geophysical Research: Oceans*, 103:14291–14324, 5 1998. ISSN 2169-9291. doi: 10.1029/97jc01444. 100

M. Turco, S. Jerez, F. J. Doblas-Reyes, A. Aghakouchak, M. C. Llasat, and A. Provenzale. Skilful forecasting of global fire activity using seasonal climate predictions. *Nature Communications*, 9, 2018. ISSN 20411723. doi: 10.1038/s41467-018-05250-0. URL http://dx.doi.org/10.1038/s41467-018-05250-0. 106

G. T. Walker. Mem. indian meterol. dept. 25, 275 (1924). gt walker, ew bliss. *Mem. R. Meteorol. Soc*, 4:53, 1932. 100

T. Zhang, X. Shao, and S. Li. Impacts of atmospheric processes on enso asymmetry: A comparison between cesm1 and ccsm4. *Journal of Climate*, 30: 9743–9762, 5 2017. ISSN 08948755. doi: 10.1175/JCLI-D-17-0360.1. URL www.ametsoc.org/PUBSReuseLicenses. 102

Žiga Zaplotnik, M. Pikovnik, and L. Boljka. Recent hadley circulation strengthening: A trend or multidecadal variability? *Journal of Climate*, 35:4157–4176, 5 2022. ISSN 0894-8755. doi: 10.1175/JCLI-D-21-0204.1. URL https://journals.ametsoc.org/view/journals/clim/35/13/JCLI-D-21-0204.1.xml. 115

Chapter 4

Future climate response to very strong El Niño events

Authors: **Paloma Trascasa-Castro, Yohan Ruprich-Robert and Amanda C. Maycock.**

Je mets
Ma désinvolture
Ma légèreté dans
Cette tragédie qu'est la vie.
Je mets
Toutes mes trouvailles
Mes idées en pagaille
Dans ce chantier qu'est la vie.

Je mets
Toute ma transcendance
Mon intelligence
Pour bien aimer cette folie.
Je mets
Toute mon éloquence
Toute ma poésie
Pour m'inventer un récit

La Succulente[1], 2 Systèmes Solaires, by Delphine Coutant.

[1]Translation: I put my poise, my causalness, in this tragedy that life is. I put all my findings, my chaotic ideas in this row that life is. I put all my transcendence, my intelligence, to love this madness. I put all my eloquence, all my poetry, to come up with a story.

Abstract

The future climate response to very strong El Niño events analogous to the 1982/83, 1997/98 and 2015/16 cases is investigated using pacemaker simulations with the EC-Earth3-CC model. Assuming that El Niño-SST anomalies will not change in a warmer climate, this chapter explores how changes in the background climate state between present-day and the end of the 21st century modulate the regional teleconnections of very strong El Niño events in boreal winter. In the future, the temperature response to very strong El Niño will intensify under the Shared Socioeconomic Pathway 2-4.5 (SSP2-4.5) scenario over North America, south of the Amazon and Congo basins, northern Africa and Australia. The teleconnection of El Niño to the North Atlantic sector is also expected to strengthen towards the future. In contrast, due to shifts in atmospheric circulation, El Niño events of large amplitudes will drive weaker anomalies over the La Plata Basin and southern Africa. Dry anomalies typically associated with very strong El Niño events over the Amazon basin will saturate and weaken towards the future. Analyses on regional daily temperature extremes reveal a strengthening of the regional response to very strong El Niño events in the future, with a further increase in cool days over eastern North America and an increase in frequency of summer heatwaves over Australia. On the contrary, the amount of heatwaves driven by very strong El Niño events in southern Africa will decrease in the future. Further work will identify regions where the background warming signal imposed by climate change will either exacerbate or damp the regional impacts occurring during very strong El Niño events in the future.

4.1. Introduction

El Niño-Southern Oscillation (ENSO) is the dominant mode of interannual climate variability across the globe. Every 2-7 years, anomalously warm sea surface temperature (SST) anomalies develop in the equatorial Pacific Ocean and trigger a global cascade of remote effects (Taschetto et al., 2020). The warm phase of ENSO, known as El Niño, leads to dry and hot conditions over Australia (Arblaster and Alexander, 2012), northern South America (Cai et al., 2020), southern

Africa (Ratnam et al., 2014) and the Indian Summer monsoon region (Mooley and Parthasarathy, 1983), as well as wet and cooler conditions over some parts of North America (Seager et al., 2005) and Eastern Africa (Goddard and Graham, 1999).

The strongest El Niño events since the late 19th century occurred in 1982/83, 1997/98, and 2015/16, when SST anomalies in the Niño3.4 region (SST averaged over 5^{o}S-5^{o}N , 170W^{o}-120^{o}W) reached 2.2^{o}C, 2.4^{o}C and 2.6^{o}C, respectively. These events led to widespread devastating impacts, including severe droughts in Southeast Asia, Northern and Southern Africa (Funk et al., 2018), the Amazon (Panisset et al., 2018), Mexico, Philippines and Australia (Duke et al., 2017); widespread fires in Indonesia (Page et al., 2002; Patra et al., 2017); storms in the US, flooding in Cuba, Peru, Bolivia and Ecuador (Glantz, 2001); large changes in the global carbon cycle (Quéré et al., 2018; Wang et al., 2018), and food insecurity (Anttila-Hughes et al., 2021; Funk et al., 2018).

Some of those devastating impacts appear to be particular to strong El Niño events. In fact, nonlinearity in the climate response exists within the same phases of ENSO (Santoso et al., 2017), with SST and precipitation anomalies extending further east in the equatorial Pacific during strong El Niño compared to moderate episodes (Cai et al., 2014; Santoso et al., 2013). Specifically in December-January-February (DJF), precipitation anomalies over the eastern equatorial Pacific during strong El Niño can reach 5 mm day^{-1} above those seen for moderate El Niño (Lengaigne and Vecchi, 2010). As a consequence, precipitation conditions in the equatorial Pacific are commonly used as a diagnostic to identify very strong El Niño events (Cai et al., 2017), and are the source for the nonlinear teleconnection response to different amplitudes of El Niño in the Indo-Pacific sector (Chung et al., 2014), Australian (Taschetto and England, 2009), North American (Wu et al., 2005) and North Atlantic-European (Trascasa-Castro et al., 2019) regions.

The global impacts of extreme El Niño events may change if there are ongoing increases in anthropogenic radiative forcing and, as a direct consequence, continued climate warming. Such changes could arise from two effects: 1) changes in

the frequency and/or characteristics of extreme El Niño; 2) changes in the processes that lead to teleconnections. Both 1 and 2 depend on the details of future changes in the background climate state and are therefore uncertain.

Regarding mechanism 1), in the tropical Pacific most climate models project a weakening of the Walker circulation and a reduction of the zonal SST gradient in the equatorial Pacific by the end of the 21st century. These changes in the mean state lead to an increase of ENSO variability under future scenarios of increased anthropogenic greenhouse gas forcing according to most CMIP6 models (Cai et al., 2022; Fredriksen et al., 2020), including an increase in the likelihood of extreme El Niño events (Cai et al., 2014; Heede and Fedorov, 2023).

Regarding mechanism 2, the Sixth Assessment Report (AR6) of the Intergovernmental Panel on Climate Change (IPCC) highlights a robust trend towards an increase in ENSO-driven precipitation variability in a warmer climate (Lee et al., 2021). Following the Clausius-Clapeyron relationship, a warmer atmosphere can hold approximately 7% more water vapour per degree of warming, hence the changes in tropical humidity driven by ENSO are expected to increase in the future (Hu et al., 2021). Ying et al. (2022) found that an anthropogenically forced signature in ENSO-related precipitation variability will emerge around 2040, decades before a robust change in ENSO SST can be detected in models. This means that we could expect changes in ENSO teleconnections to emerge before any changes in ENSO characteristics may be detectable from internal climate variability.

While several studies have examined ENSO teleconnections in a future climate, they have generally used freely evolving coupled climate models and therefore do not permit a separation of mechanisms 1 and 2 above (Cai et al., 2022; Fasullo et al., 2018; Maher et al., 2022; McGregor et al., 2022; Perry et al., 2020). McGregor et al. (2022) found significant changes in ENSO impacts over around one third of global land area in CMIP6 models, but it was unclear what factors cause this change. A small number of modelling studies have made the assumption

that ENSO characteristics will not change under greenhouse gas forcing and prescribed identical SST anomalies on top of different background climates, thereby isolating mechanism 2 (Drouard and Cassou, 2019; Zhou et al., 2014). These studies found an amplification of ENSO teleconnections in boreal winter in the North-Pacific and North Atlantic-European sectors under future climate conditions, but did not assess the global effects of a different mean climate state on ENSO impacts and did not specifically address extreme El Niño impacts.

Our study follows a similar approach by assuming that ENSO SST anomalies will not change in a warmer climate, and therefore focus on mechanism 2, but we specifically focus on very strong El Niños as these are the most impactful. We use the El Niño events of 1982/83, 1997/98 and 2015/16 as case studies for future strong El Niño analogues.

4.2. Methods

Pacemaker simulations are performed with the EC-Earth3-CC model (Döscher et al., 2022) to understand changes in the impacts of very strong El Niño events between present and future climates.

4.2.1. Model

EC-Earth3-CC is an Earth System model with an approximate atmosphere and ocean resolution of 1°. The atmospheric model is the European Center for Medium-range Weather Forecasts (ECMWF) Integrated Forecasting System (IFS) version 36r4, which is based on the ECMWF seasonal prediction system 4, and has a resolved stratosphere. NEMO3.6 and LIM3 are the ocean and sea ice components; biogeochemical processes in the ocean and over land are simulated by the PISCES and LPJ-GUESS models, respectively.

The EC-Earth3-CC model generally reproduces observed ENSO teleconnections. Supplementary Figure 4.10 compares the global ENSO precipitation and surface temperature teleconnections in the December-February (DJF) season in EC-

Earth3-CC with observations from the Global Precipitation Climatology Project (GPCP) v2.3 (Adler et al., 2018) and Berkeley Earth (Rohde and Hausfather, 2020) datasets. For the model-data comparison we use output of a tropical Pacemaker simulation run with the EC-Earth3-CC model, where historical SSTs are forced with observed SST anomalies in the tropical Pacific ocean. This ensures the ENSO events simulated in the model are comparable to those observed over the historical period. The model captures the sign and amplitude of ENSO-related precipitation anomalies over the tropical Pacific, but tends to overestimate the precipitation dipole response over the Indian Ocean (See Figure 4.10). Over the equatorial Atlantic, the model displays a weak zonal dipole consisting of dry conditions over the Amazon and western equatorial Atlantic and wet anomalies over the eastern Atlantic and the Gulf of Guinea, whereas observations show an overall negative precipitation anomaly that peaks off the east Brazilian coast. Regardless of these differences, the overall patterns of global response in temperature and precipitation are well captured by EC-Earth3-CC.

4.2.2. Experimental protocol

Six experiments are performed in which the model SSTs in the equatorial eastern Pacific are restored towards the observed SST anomalies from the 1982-1983, 1997-98 and 2015-16 strong El Niños superimposed on either the present day or future model climatological SST. Observed monthly SST anomalies are extracted from the Extended Reconstructed Sea Surface Temperature version 5 ERSSTv5 dataset (Huang et al., 2017) calculated relative to the period 1981-2010. Present day climatological values are estimated from the historical simulations of EC-Earth3-CC using the period 2005-2014. For the future, we use the Shared Socioeconomic Pathway (SSP) 2-4.5 scenario, a middle-of-the-road greenhouse gas emissions pathway where global mean surface temperature in EC-Earth3-CC increases by 2.8 K in 2100 relative to preindustrial times. The period 2085-2094 is used to define the future climatology. For each 10-year climatological period, we average over 10 initial condition ensemble members, meaning that the climatological states are calculated over 100 years.

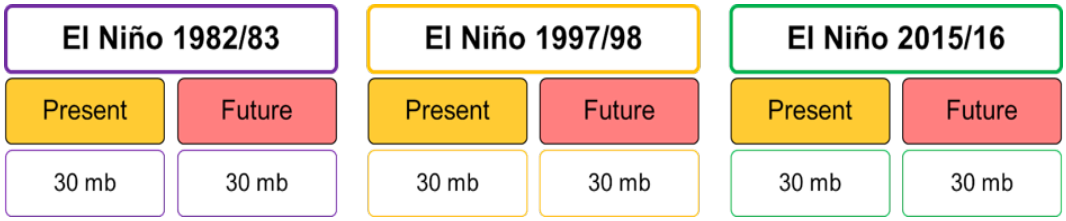

Figure 4.1: Schematic of the pacemaker experiments. "mb" means "member 2.

The observed ERSSTv5 SST anomalies for the 3 strong El Niño cases are interpolated to the model's ocean grid (ORCA1) and added to the present or future model climatology to produce the target restoring fields. For each experiment, a 30 member ensemble is generated by using 3 sets of initial conditions from each of the 10 historical or SSP2-4.5 simulations at 5 year intervals (for example for present-day we use 2005, 2010 and 2014). The SST target pattern is imposed through surface flux restoring with a restoring coefficient equal to -80 W m^{-2} K^{-1}. The restoring domain is 10°S - 10°N, 180° - 70°W, with a 10° buffer zone on each side except the eastern margin which coincides with the American continent (See black contours in Figs. 4.3a and b). All variables outside of the restoring region evolve freely. Each member is integrated for 2 years starting from January 1^{st} and the SST restoring is activated from the 1^{st} of May of the first year until the end of April of the second year. The result is a suite of 30-member ensemble simulations for 3 strong El Niño events in present and future climates (see Fig. 4.1. The analysis showed very similar changes in impacts for the 3 El Niño cases, so the analysis focuses on the "multi-event mean", hereafter MEM. We focus on the DJF season when the El Niño events peak and compare the anomalous response to strong El Niño in the future with that of the present. Anomalies from each period are calculated relative to their corresponding climatological values. Given the similarity in the projected impacts driven by our 3 strong El Niño pacemakers (1982/83, 1997/98 and 2015/16), we made a composite of all three events that we called "multi-event mean", hereafter MEM. The MEM accounts for 90 full winter seasons, 30 from each strong El Niño event and mean state.

4.2.3. Regional analyses of extreme indices

El Niño is known to drive weather extremes over North America (Glantz, 2001; Meehl and Teng, 2007), Australia and Southern Africa (Arblaster and Alexander, 2012), among other regions, so these are used as three regional case studies to examine the influence of future climate change on El Niño impacts.

In North America, we quantify the change in cool days per winter, which accounts for the number of days when maximum daily temperatures (Tmax) lay below the 10^{th} percentile (Donat et al., 2013). The 10^{th} percentile values of Tmax used to define cool days in the present and future climatologies over North America are shown in Figure 4.11. Secondly we explore changes in heatwave frequency in Australia and southern Africa as a response to very strong El Niño events in the future. We use the World Meteorological Organization definition of heatwaves, which is identified when daily Tmax goes over the averaged daily Tmax over a reference period + 5^{o}C for 5 consecutive days (Eqn. 4.1). The temperature of reference to define a heatwave is computed over the present-day climatology, and is also used to compute frequency of heatwaves in the future.

$$Heatwave = Tmax > \overline{Tmax} + 5^{\text{o}}C \tag{4.1}$$

Note that the thresholds to compute cool days and heat waves in the present and future are estimated relative to the present and future climatologies, respectively. The heatwave thresholds for Australia and southern Africa, as well as the climatological heatwave frequency are displayed in Figures 4.12 and 4.13.

To assess whether changes are statistically significant, we performed a two sided Student's t-test.

4.3. Results

4.3.1. Climate impacts of very strong El Niño events in the present

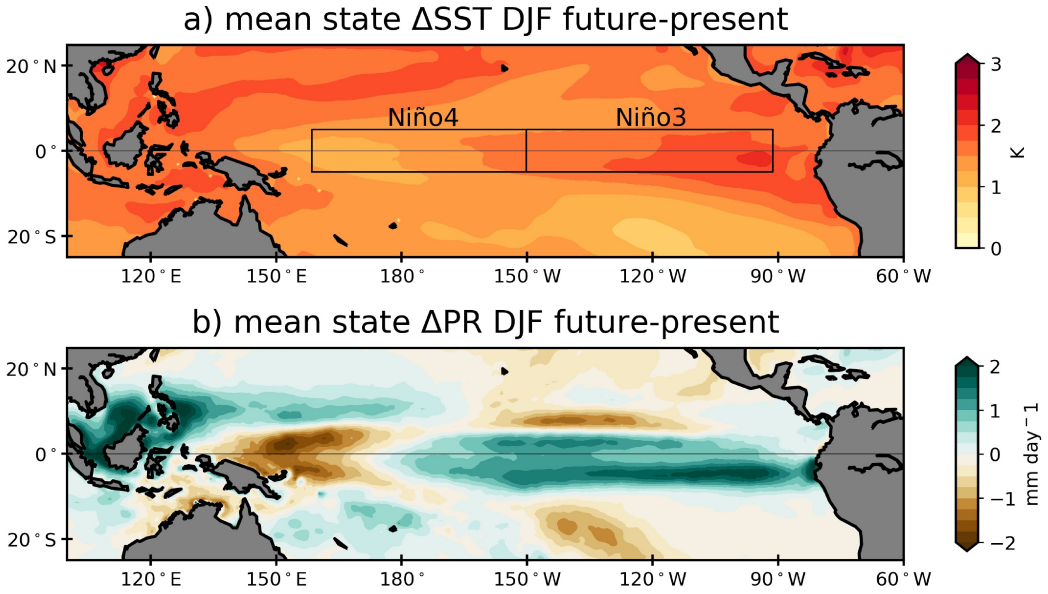

Figure 4.2: Mean state SST (a, K) and precipitation (b, mm day^{-1}) changes between present (2005-2014) and future (2085-2094) climatologies over the tropical Pacific Ocean.

We start by documenting the changes in mean climate between future and present day as simulated by EC-Earth3-CC (Fig. 4.2). The tropical Pacific warms overall by around 2.5 K (Fig. 4.2a), with the Niño4 (5°N-5°S, 160°E-150W) and Niño3 (5°N-5°S, 150°W-90°W) regions being 4.7% and 6.6% warmer, respectively in the future than in the present day. The zonal east-west SST gradient decreases by 19.5% by the end of the 21st century, similar to what is seen in many other CMIP6 models (Dhage and Widlansky, 2022). Along with those mean SST changes, there is a decrease in the strength of the Walker circulation, evidenced by a decrease in precipitation over the Warm Pool and an increase in precipitation over the Central and Eastern Pacific (Fig. 4.2b).

We focus now on the climate response to El Niño. Fig. 4.3a shows the MEM SST anomalies under present conditions. The experiment protocol produces the canonical eastern Pacific SST anomalies associated with strong El Niño events. The temporal evolution (Figure 4.3c) shows a lag in the Niño3.4 SST anomaly during the development stage with a later peak in January and a delayed decay phase. This reflects a delay of around 0.5 months in the El Niño growth and decay and an overestimate of the maximum Niño3.4 anomaly by around 0.5 K. These differences are manifested similarly in the Niño4 region (Figure 4.3c). Figures 4.4a,c show anomalous El Niño-driven precipitation and temperature impacts in DJF under the present day. In the tropical Pacific, strong El Niño events drive an eastward shift of the precipitation maximum, leading to precipitation anomalies of up to 15 mm day^{-1} over the central and eastern equatorial Pacific. Those positive anomalies contrasts with drier conditions localised off the equator, centred around 10^{o}N and around the South Pacific Convergence Zone.

Outside of the tropical Pacific, strong El Niño events in the EC-Earth3-CC model drive dry anomalies of up to 4 mm day^{-1} over the Amazon basin, although these anomalies might be overestimated relative to observations (Fig. 4.10), and around 1 mm day^{-1} over western Australia and Southern Africa. Looking at a composite of El Niño events in the historical period (Figure 4.10), we found that dry conditions driven by El Niño EC-Earth3-CC cover a wider area of Australia, and over Southern Africa these anomalies are slightly underestimated relative to observations, though we acknowledge there is large sampling uncertainty on the observed relationships due to only a few events having occurred.

There is a precipitation anomaly dipole over the North Atlantic, likely driven by a southward shift of the storm track and of the North Atlantic jet stream (Fig. 4.5a), characteristic of the link between El Niño and the negative phase of the North Atlantic Oscillation (NAO) (Brönnimann, 2007). Over the Congo basin and the horn of Africa, strong El Niño events lead to weak but significant positive precipitation anomalies. Precipitation also increases by 2.5 mm day^{-1} over the La Plata Basin during strong El Niño events, leading to wetter-than-usual summers in the North of Argentina, Uruguay and Paraguay.

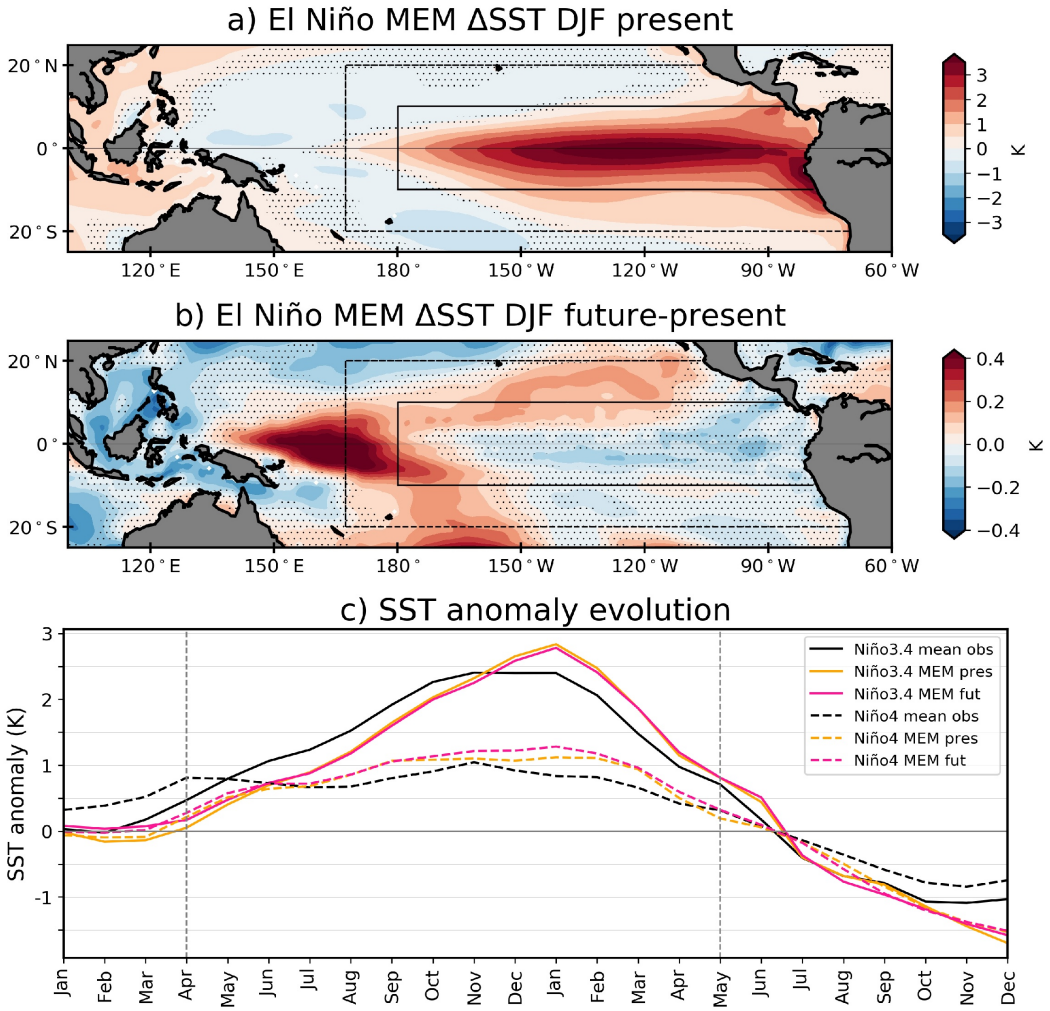

Figure 4.3: a) El Niño MEM SST anomalies (K) in the present conditions experiments, b)El Niño MEM SST differences between future and present conditions experiments, c) SST anomaly timeseries in the Niño3.4 (solid lines) and Niño4 (dashed lines) regions. Observations are shown in black, present-day anomalies in orange and future anomalies in pink.

Alongside changes in precipitation, strong El Niño events in the present day drive significant surface temperature impacts across the globe in DJF. Northern South America experiences warm anomalies reaching up to 4 K over the Amazon basin, as well as large parts of the African continent, with the exception of the region around Lake Victoria. It is worth mentioning that although the EC-Earth3-CC model appropriately captures the increase in precipitation driven by El Niño events in the Lake Victoria region relative to observations, it suggests that this increase in precipitation is accompanied by cooler temperatures, whereas observations show a modest but positive temperature anomaly (Figure 4.10). Western and eastern Australia experience hotter summers during very strong El Niño events, and southeast Asia also experience warm anomalies during very strong El Niño.

There are some regions, though, where El Niño leads to cold anomalies in DJF, such as the US and the La Plata basin in northern Argentina and Uruguay. The EC-Earth3-CC model captures the amplitude and spatial location of the average surface response to ENSO daily well over Australia, North America and Southern Africa relative to observations (Figure 4.10). We stress that the sample size of the observed ENSO composites shown in the supplement is larger for temperature (120 years) than for precipitation (40 years), probably affecting the robustness of the observed composites shown in Figure 4.10.

4.3.2. Global climate response to very strong El Niño events in the future

In the future experiments, the western Pacific El Niño SST anomalies are up to 0.4 K warmer than in the present-day experiment (Fig. 4.3b) and the SST anomalies in the central and eastern equatorial Pacific are slightly cooler than in the present (∼0.04 K on average over the Niño3.4 region, cf. Fig. 4.3c). The larger differences are outside of the restoring region. This indicates that the model is responding differently to the pacemaker restoring in the future because

of changes in the mean state. This reveals a limitation of our experimental design, in which the SST is not imposed but nudged towards a target by forcing the non-radiative surface fluxes, allowing the model to modify the emerging SST anomaly through oceanic feedbacks. Associated with the warmer SST anomalies in the western equatorial Pacific, the El Niño precipitation anomalies are also more positive in the future in this region by up to 2 mm day^{-1} (Figure 4.4b), while in the central Pacific the precipitation anomalies in the future decrease relative to present day by up to 2 mm day^{-1}. These changes do not match the projected change in El Niño-driven precipitation anomalies in the tropical Pacific suggested by the literature, consisting of an eastward shift of precipitation during El Niño under greenhouse gas forcing. In contrast, in our simulations, the ascending branch of the Walker Circulation is less shifted to the East in response to extreme El Niño in the future.

Outside the tropical Pacific, Southeast Asia sees an amplification of the dry response of very strong El Niño in the future. In southeast Australia, very strong El Niño events similar to the ones observed would lead to even drier conditions in the future, which taking into account the dry trend induced by climate change in this region (not shown), would make southeastern Australia even more vulnerable to the impacts of very strong El Niño events in the future.

In a limited number of regions, the precipitation response to very strong El Niño events is expected to weaken in the future. For instance, El Niño events typically drive dry anomalies over the Amazon basin (Fig. 4.4a), but this is expected to change in the future, where the drought induced by very strong El Niño would be significantly milder. Over the La Plata Basin, we observe a northward shift of precipitation anomalies (Fig. 4.4b). There is also some weakening of the dry conditions over south Africa.

In the future, the surface temperature response to very strong El Niño events in DJF is expected to increase in several regions. The same very strong El Niño events that we observed in the last decades would drive even hotter winters in the North of Africa and Northwest Himalayas, and even hotter summers in the South

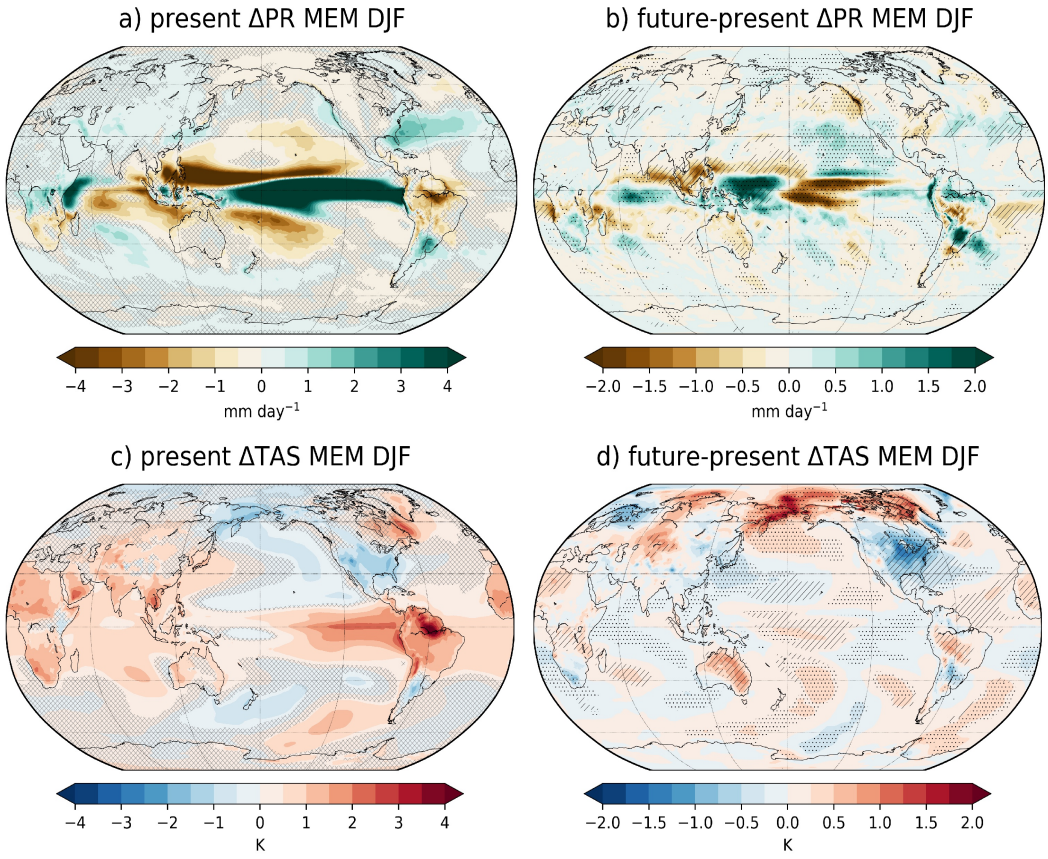

Figure 4.4: Global a,b) precipitation (mm day^{-1}) and c,d) temperature response to very strong El Niño events in a, c) present day and b,d) future - present in DJF. Hatching in subpanels a, c) show non statistical significance at the 95% confidence level (i.e. anomalies are not driven by El Niño), estimated with a double-sided t-test. In subpanels b and d, hatching (lines) show areas where there is an amplification of El Niño impacts (wet gets wetter or dry gets drier), and stippling (dots) denote regions where El Niño-driven impacts get muted in the future (wet gets dry or dry gets wet).

of the Amazon and Congo basins and Australia. Over the northeast of North America, cold anomalies driven by very strong El Niño would be stronger in the future. On the other hand, mean DJF El Niño-driven temperature anomalies in the future will weaken in other regions due to shifts in atmospheric circulation. For example cold anomalies over the northeast of Argentina, Paraguay and south Brazil extend more towards the North, following the northward shift of precipitation shown in Fig. 4.4b.

4.3.3. Tropospheric circulation response to strong El Niño and its changes under future conditions

To understand future changes in teleconnections of strong El Niños, we explore anomalies in geopotential height at 500 hPa (z500) and zonal wind at 200 hPa (u200) anomalies in DJF. During strong El Niño events in the present day (Fig. 4.5a), positive z500 anomalies of up to 40m arise in the tropics, triggering barotropic Rossby wave trains that project onto the Pacific North American (PNA) and Pacific South American (PSA1) patterns in the northern and southern hemispheres, respectively. The extratropical teleconnections of El Niño depend on the background flow, specifically on the upper troposphere zonal wind speed (Lee et al., 2009), which is stronger in the Northern hemisphere in DJF due to a stronger subtropical jet.

Outside of the Pacific sector, strong El Niño events are driving negative geopotential anomalies over the South-East of the USA, which extend eastward over the subtropical Atlantic ocean. Those negative anomalies contrast with positive anomalies spanning from the North East of Canada to the Norwegian Sea. Over The North Atlantic, those geopotential height anomalies project onto the negative phase of the NAO (NAO-), which is associated with a southward shift of the North Atlantic westerly jet stream (evident by the solid black contours), in agreement with the southward shift of precipitation anomalies shown in Fig. 4.4a. The simulations therefore suggest that the El Niño-negative NAO teleconnection will strengthen under future climate conditions (Fig. 4.5b).

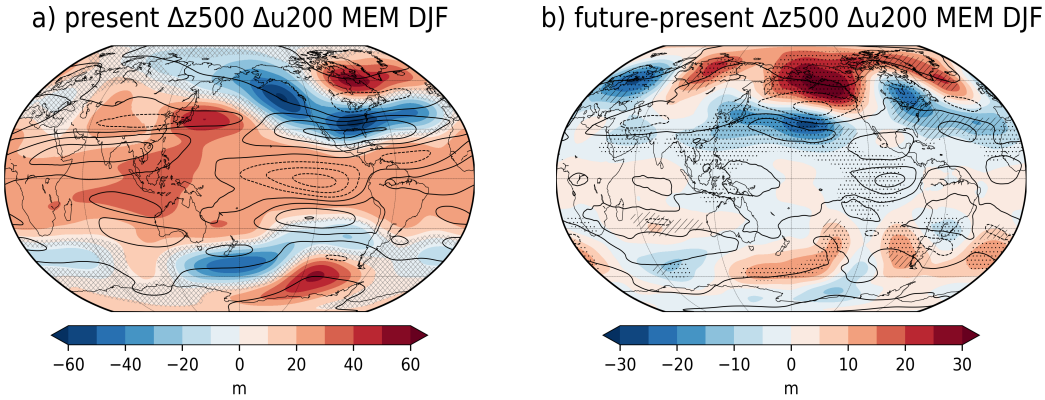

Figure 4.5: a) 500 hPa geopotential height (m, shading) and 200 hPa zonal wind (black contours) anomalies in the present MEM very strong El Niño experiments and b) their differences between future and present MEM El Niño experiments. Hatched areas in subpanel a) show areas where the MEM responses are not statistically significant at the 95% confidence level. In b), hatched areas show a significant amplification of MEM anomalies in the future, whereas stippling shows significant weakening of MEM anomalies.

Under future conditions, very strong El Niño events drive a weaker PNA response, especially around the Aleutian low region, where the differences of z500 between future and present project negatively on the present day impacts. In the Southern hemisphere, very strong El Niños trigger an anomalous wavetrain spanning the extratropics and subpolar regions and driving low pressure anomalies in southeastern South America.

4.3.4. Extreme temperature impacts

Fig. 4.3d suggests an intensification of strong El Niño-driven cold anomalies over North America in the future. Here we use daily temperature data to explore how those changes would translate in terms of cold extremes during the winter season. In particular, we use the cool day index, which is percentile-based (cf. Section 4.2.3), to understand changes to the distribution of cold anomalies driven by El Niño in the future by effectively removing any shift in the distribution of climatological cool days driven by greenhouse gas forcing.

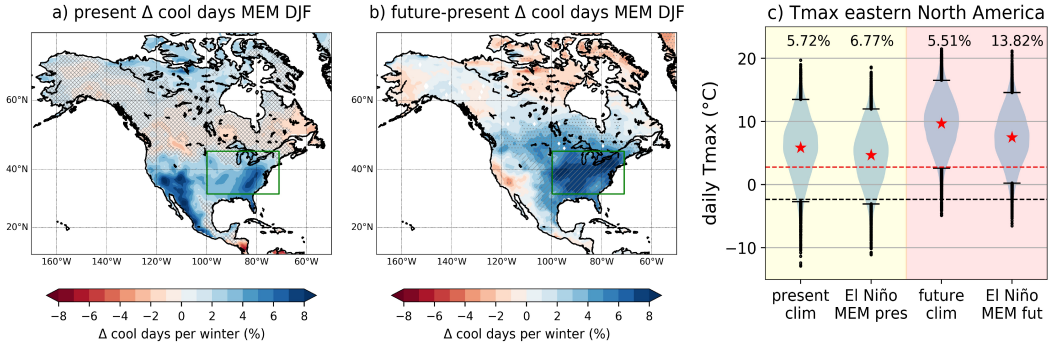

Figure 4.6: Anomalous cool days per winter (DJF) during very strong El Niño in North America in a) present conditions and b) future - present conditions. The hatching convention is the same as in Figs. 4.3 and 4.4. c) Violin plots of daily maximum temperature (Tmax) in the present conditions from the historical simulations, during very strong El Niño under present conditions, in the future conditions from the SSP2-4.5 simulations, and during very strong El Niño under future conditions, in the area over eastern North America delimited by the green rectangle in subpanels a and b. The black dashed line denotes the reference 10^{th} percentile from the present conditions and the red dashed line is the 10^{th} percentile from the future conditions. Numbers on top of the violin plots represent the percentage of days below the cool day threshold on each respective time period.

Very strong El Niño events in the present drive an increase of cool days in North America of up to 8% per winter, especially between 20°N-40°N over the southeast and southwest of the United States and the west of Mexico (Fig. 4.6a). Over the central-eastern US (cf. green box in Fig. 4.6a), there are on average 5.72% of cool days per winter in the present day conditions; very strong El Niño events increase this percentage to 6.77% (Fig. 4.6c). Under future conditions, the impacts of very strong El Niño events amplify over this central-eastern US region, with a further increase to 8% in cool days per winter compared to the averaged future conditions of 5.51% (Fig. 4.6c). The intensification of cold anomalies driven by El Niño under future conditions is striking given the shift of the distribution of maximum daily temperature towards hotter values due to global warming, as shown by the shift of the 10^{th} percentile between present and future climatologies from -2°C to 2°C, respectively.

We now explore how the warmer impacts of strong El Niño under future conditions over Australia (Fig. 4.4d) would translate in terms of summer heat waves.

Very strong El Niño events adds up to 1 additional heatwave per summer over the eastern and western margins of Australia, with the strongest increase at 22°S and 120°E in western Australia (Fig. 4.7a). As shown by the violin plots in Fig. 4.7c, the average frequency of heatwaves per summer in Australia is expected to increase from 0.69 in the present-day to 0.85 in the future, an increase in frequency of 19%. On average over Australia, very strong El Niño events increase the frequency of heatwaves by 22% compared to the climatology. In the future, the impacts of very strong El Niño will intensify in most of the country, with a significant increase in heatwave frequency by 1 per summer over central and northern Australia (Fig. 4.76b). Over the southwest of the country, there is a slight decrease in frequency due to future very strong El Niño events relative to their present analogues, but this weakening is not statistically significant. In the future, very strong El Niño events will increase the frequency of heatwaves by 29% relative to the averaged future conditions (third and fourth violin plots in Fig. 4.7c).

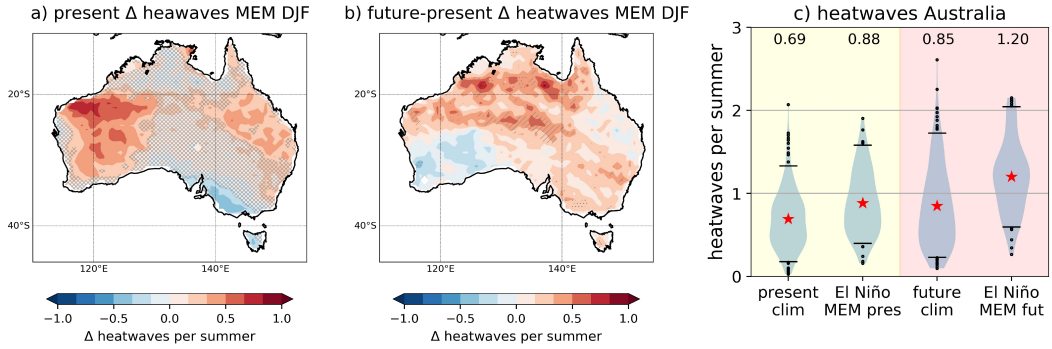

Figure 4.7: Anomalous heatwaves per summer (DJF) during very strong El Niño in Australia in a) present conditions and b) the difference between future and present conditions. The hatching convention is the same as in Figs. 4.3 and 4.4. c) Violin plots of heatwave frequency in the present conditions from the historical simulations, during very strong El Niño under present conditions, in the future conditions from the SSP2-4.5 simulations, and during very strong El Niño under future conditions. Violin plots show the averaged heatwave frequency over Australia in the present conditions, during very strong El Niño under present conditions, in the future conditions, and during very strong El Niño under future conditions.

According to EC-Earth3-CC, a smaller number of regions will see a weakening of the impacts of very strong El Niño events in the future. Fig. 4.4d shows that in

Southern Africa, very strong El Niño events drive cooler temperature anomalies in DJF compared to the same events under present conditions.

Fig. 4.8 shows changes in the frequency of heatwaves driven by very strong El Niño events between present and future conditions over southern Africa. The heatwave threshold as well as the average heatwave frequency in the present and future climatologies are shown in the supplementary figure 4.13. Under present conditions, Southern Africa experiences up to 2 additional heatwaves per summer during very strong El Niño events, relative to the averaged summer, with the strongest increase in the south of Namibia and north of South Africa.

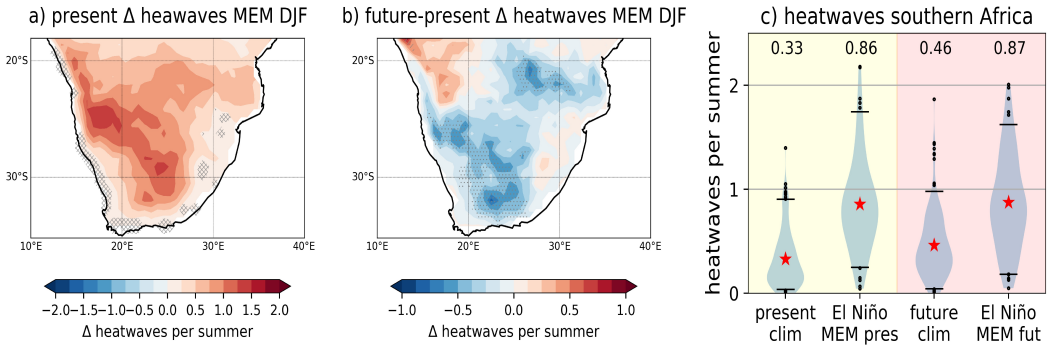

Figure 4.8: Anomalous heatwaves per summer (DJF) during very strong El Niño in Southern Africa in a) present-day and b) future - present. The hatching convention is the same as in Figs. 4.3 and 4.4. c) Violin plots of heatwave frequency in the present-day climatology, during very strong El Niño in the present, in the future climatology and during very strong El Niño in the future. Violin plots show the averaged heatwave frequency in the present-day climatology, during very strong El Niño in the present, in the future climatology and during very strong El Niño in the future.

Fig. 4.8c illustrates the mean heatwave frequency averaged over the Southern Africa region in the present and future conditions, as well as when very strong El Niño events occur in the present and future conditions, respectively. On average over Southern Africa, heatwaves increase in frequency by 62% when a very strong El Niño event occurs. Interestingly, this type of El Niño event will drive fewer heatwaves in the future over the region (Fig. 4.8b), relatively to the future averaged conditions, except for a slight increase in frequency of up to 0.5 heatwaves per summer in the south of Namibia. As shown in Fig 4.8c, there

is a negligible change in El Niño-driven heatwaves over South Africa in DJF in a warmer climate. However, heatwaves will be come 29% more frequent in the future compared to present-day climatology.

4.4. Discussion and conclusion

This study has used idealised pacemaker simulations with the EC-Earth3-CC model to quantify changes in the global impacts of strong El Niño events in a warmer climate. The observed 1982/83, 1997/98 and 2015/16 El Niño events were used as analogues of strong events in a future climate. This approach enables us to isolate the effects of strong El Niños and also the role of changing background climate conditions on the atmospheric response to El Niño from changes in ENSO dynamics, which has been a limitation of some previous studies (e.g., McGregor et al. (2022)).

Interestingly, the projected changes in El Niño teleconnections resemble those suggested by previous studies, suggesting that simulated changes in future impacts of El Niño in fully coupled models are dominated by changes in the mean state, rather than by changes in ENSO SSTs. In agreement with McGregor et al. (2022), we find a strengthening and southward shift of the North Atlantic jet stream in boreal winter during El Niño event in the future, highlighting the reinforcement of the El Niño-negative NAO relationship. This is also in agreement with previous literature (i.e. Drouard and Cassou (2019); Johnson et al. (2022)), although this response is not captured in CMIP5 models (Perry et al., 2020). Our results also align with the overall CMIP5 and CMIP6 trends in the northward shift of precipitation anomalies north of the La Plata Basin and the drying trend to the south of Brazil, although our pacemaker reveals a weakening of the dry anomalies driven by very strong El Niño event over the Amazon basin. Future work will assess whether there is any saturation of dry anomalies over this area during El Niño events of large amplitude such as the ones we are focusing on. Our results also agree with the overall CMIP5 and CMIP6 trend in the future weakening of dry anomalies over Southern Africa driven by El Niño events.

In terms of future changes in surface temperature anomalies driven by strong El Niño, we do find similarities between our results and the overall trend encompassing El Niño events of any amplitude. Some examples are a hot-gets hotter trend over western Brazil, and Northern Africa, and while CMIP5 projections do not show a significant change over Australia (Perry et al., 2020), our results agree with overall CMIP6 projections (McGregor et al., 2022) and large ensemble studies (Fasullo et al., 2018) in a significant amplification of hot anomalies over Australia.

Some additional features arise when focusing on very strong El Niño events that are not seen in the overall projections of ENSO impacts based on composite analysis, that indicate either a nonlinear climate response to strong El Niño events or a disagreement of the EC-Earth3-CC model with the overall CMIP6 mean (i.e. McGregor et al. (2022)). We find an intensification of cold anomalies driven by very strong El Niño over northeast North America and a significant weakening of warm anomalies over southern Africa. Interestingly, as shown in Fig. 4.4b, strong El Niño impacts in the present day drive cold anomalies over Alaska, which do not align with the composite impacts of El Niño shown in observations, probably due to nonlinearities in El Niño impacts over this region (Garfinkel et al., 2019).

We showed that the simulated modulation of the number of cool days per winter by strong El Niño is larger in the future over eastern North America. It is important to note that due to the overall background warming from climate change, the threshold for cool days increases from -2 K to 2 K from present to future. The number of cool days per winter slightly decreases in the future climatology, however there is a larger amount of cool days driven by El Niño in the future (13.82%) than in the present (6.77%), showing a larger negative anomaly in cool days during very strong El Niño events in the future. In agreement with Meehl and Teng (2007), we show an eastward shift of cold extremes in future El Niño events, with a decrease in cool days over the west coast of the US. This intensification might be linked to the strengthening of the teleconnection of El Niño to the North Atlantic sector (Johnson et al., 2022).

Regarding hot extremes, we have shown a mean state shift towards more heatwaves in Australia in the future climate (see Fig. 4.12) compared to the present one, and a further increase in heatwave frequency during the summer driven by strong El Niño events. This suggests an increase in the impacts of El Niño on Australian austral summer climate, which will further exacerbate the increased occurrence of hot anomalies induced by climate change. An increase in El Niño-driven heatwaves in the future will also increase the risk of wildfires during Australia's fire season (Fasullo et al., 2018), when high temperatures allow wildfires to spread rapidly (Abram et al., 2021).

Finally, we show that despite most of the regions with significant changes in very strong El Niño impacts, a limited number of areas, like southern Africa, experience a weakening of the signal driven by El Niño under future conditions. Fig. 4.8 suggests that El Niño-driven heatwaves during the summer will be half as frequent in the future as they are today, especially over southern Namibia, Botswana and central South Africa. While the climatological frequency of heatwaves per summer as simulated by EC-Earth3-CC increases from 0.33 in the present to 0.46 in the future, in agreement with future CORDEX-Africa climate projections over the region (Russo et al., 2016), the El Niño-driven heatwaves do not increase in frequency in a warmer climate. In absolute terms, the background warming induced by climate change will increase the frequency of heatwaves over Southern Africa, independent of whether there is a strong El Niño event happening or not. Therefore any increase in heatwave frequency over the region during strong El Niño years will be driven by the underlying trend imposed by climate change.

Our results reveal potential nonlinearities in the future climate response to El Niño events (e.g. the Amazon basin), where increasing SST anomalies in the Niño3.4 region do not further amplify the global surface impacts associated with a canonical El Niño event. This nonlinearities might be accompanied by shifts in circulation induced by climate change, with South America being the most illustrative example. According to our results, dry anomalies over the Amazon basin driven by very strong El Niño will get muted in the future, and wet and cool

anomalies over the La Plata Basin are expected to shift northwards in DJF. Further work is needed to assess the nature of these shifts and nonlinear behaviours.

We found that in our experiments, future El Niño events are slightly cooler in the eastern Pacific and have a warmer warm pool than their present-day analogues. We believe that this is caused by a feedback process triggered by the warm pool responding strongly to the imposed SST anomalies over the restoring region, which enhances a deeper convection over the warm pool and a strengthening of the Walker circulation that ultimately leads to weak cold SST anomalies in the restoring region. Furthermore, as is the case for most CMIP models (Cai et al., 2015; Maher et al., 2022), EC-Earth3-CC shows a trend towards an El Niño-like mean state warming in the tropical Pacific which does not appear to match observed trends over recent decades (Heede and Fedorov, 2021; Kociuba and Power, 2015). Future work could explore changes in strong El Niño teleconnections in the future, restoring SSTs in a wider area spanning through the whole equatorial Pacific ocean and potentially sampling a wider range of plausible background state changes.

Human-caused climate change is warming the planet at unprecedented rates. Natural climate variability can either amplify or mute the signature of climate change in the future. Strong El Niño events are projected to increase in frequency (Cai et al., 2014), and given the severity and reach of their impacts, it is crucial to understand how the impacts of these extreme events will change in the future to facilitate adaptation and mitigation policies in the areas affected. Future studies are needed to improve our understanding of the mechanisms of such amplification and dampening of the future impacts of very strong El Niño events. Additionally, a multi-model approach would allow to verify our results for a larger set of projections.

Another avenue for further study is identify regions where climate change will exhacerbate the surface climate response to El Niño in the future, examining the spatial constructive and destructive interferece of changes in strong El Niño impacts with the mean signal of climate change.

4.5. Supporting information

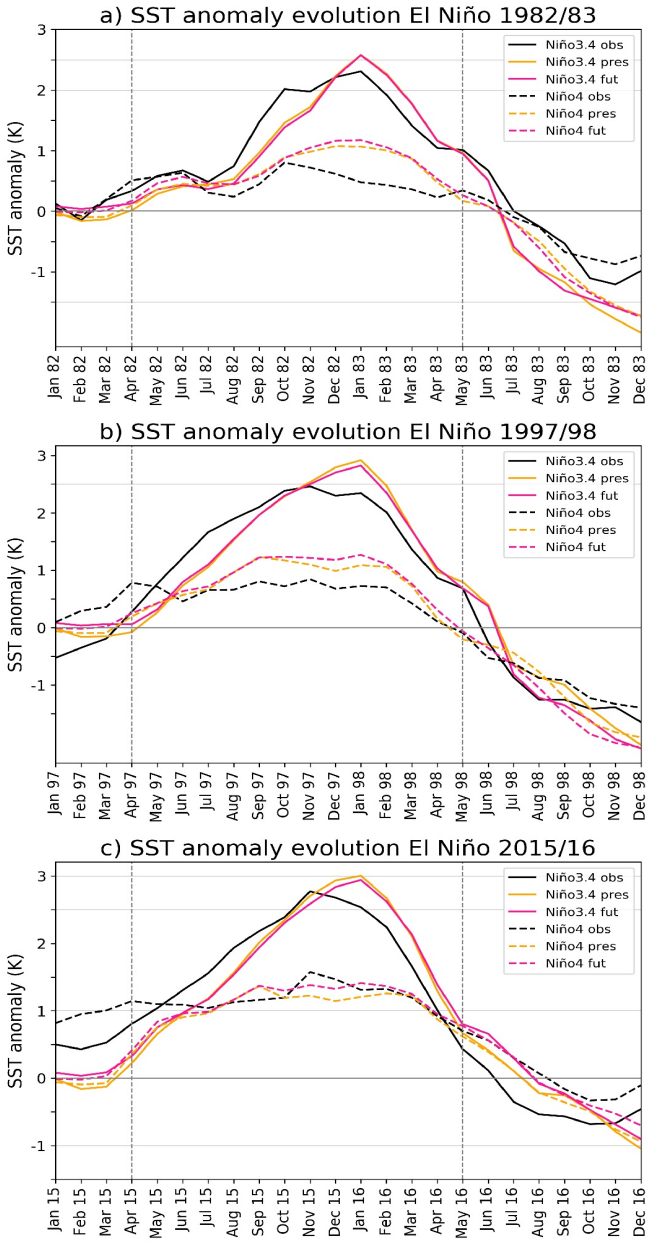

Figure 4.9: SST evolution during the 3 strong El Niño events (a) 1982/83, b) 1997/98 and c) 2015/16). Solid lines correspond to SST anomalies in the eastern (Niño3.4 region) and dashed lines to the western (Niño4 region) equatorial Pacific. Black lines show observations (ERSSTv5 (Huang et al., 2017)), colours show SST anomalies in the past (yellow), present (green) and future (purple) pacemaker simulations.

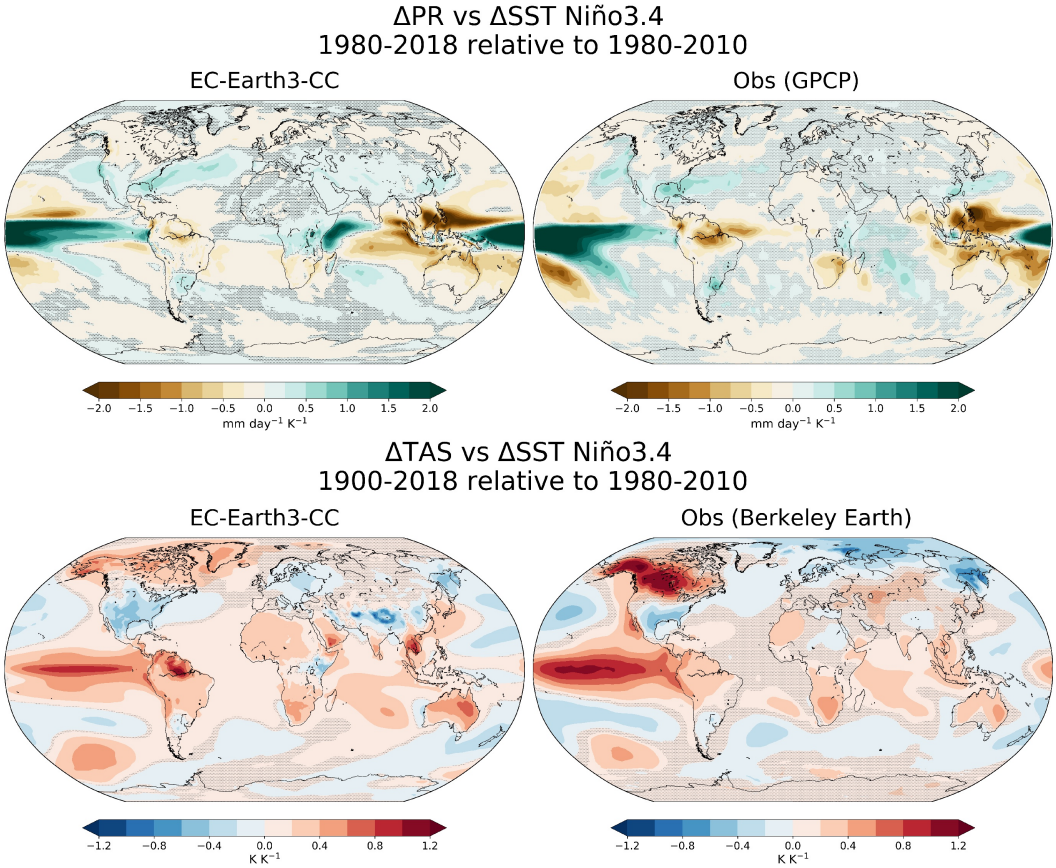

Figure 4.10: Model evaluation of mean precipitation (top) and surface temperature (bottom) anomalies regressed onto SST anomalies in the Niño3.4 region in DJF (left column), compared to observations (right column). Model data corresponds to output of tropical Pacific pacemaker simulations run with the EC-Earth3-CC model where observed SST anomalies in the tropical Pacific Ocean are imposed on top of the model's own climatology between 1900 and 2018. SST and TAS anomalies are computed relative to the 1980-2010 period, and the Berkeley Earth dataset (Rohde and Hausfather, 2020) is used as the reference observational dataset. For precipitation, the period used spans from 1980 to 2018, and GPCP v2.3 (Adler et al., 2018) is used as the observational dataset of reference. Stippling denotes lack of statistical significance at the 95% confidence level.

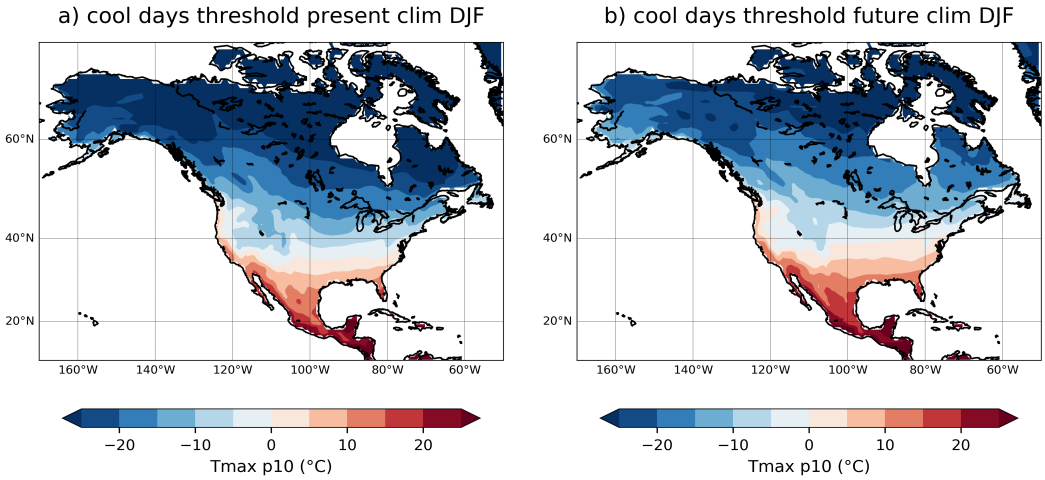

Figure 4.11: Cool day threshold in the present (a) and future (b) climatologies over North America, expressed as the value corresponding to the 10^{th} percentile of daily maximum winter temperature at each gridpoint.

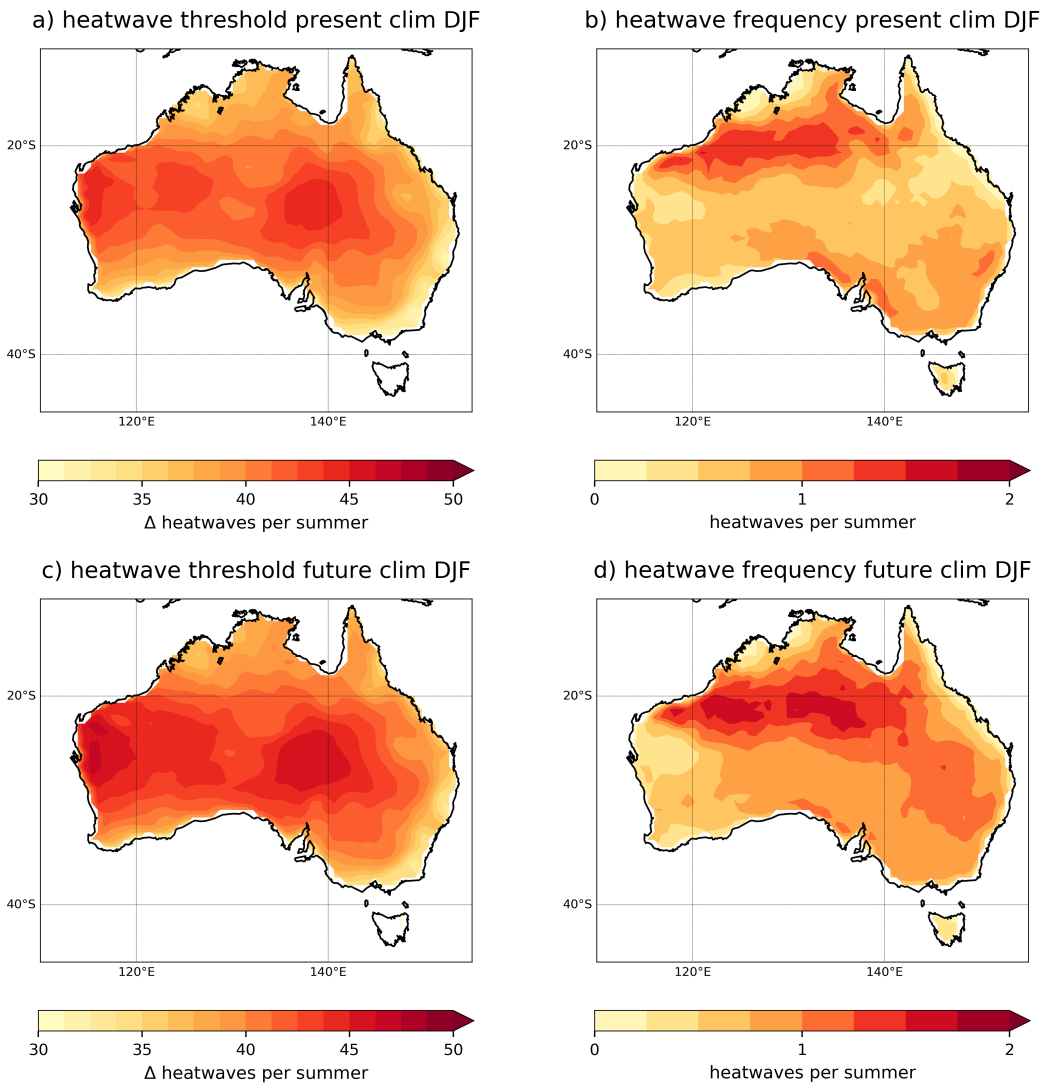

Figure 4.12: Heatwave thresholds in the a) present-day and c) future climatologies over Australia. Subpanels b) and d) show the average frequency of heatwaves per summer in the present and future climatologies, respectively.

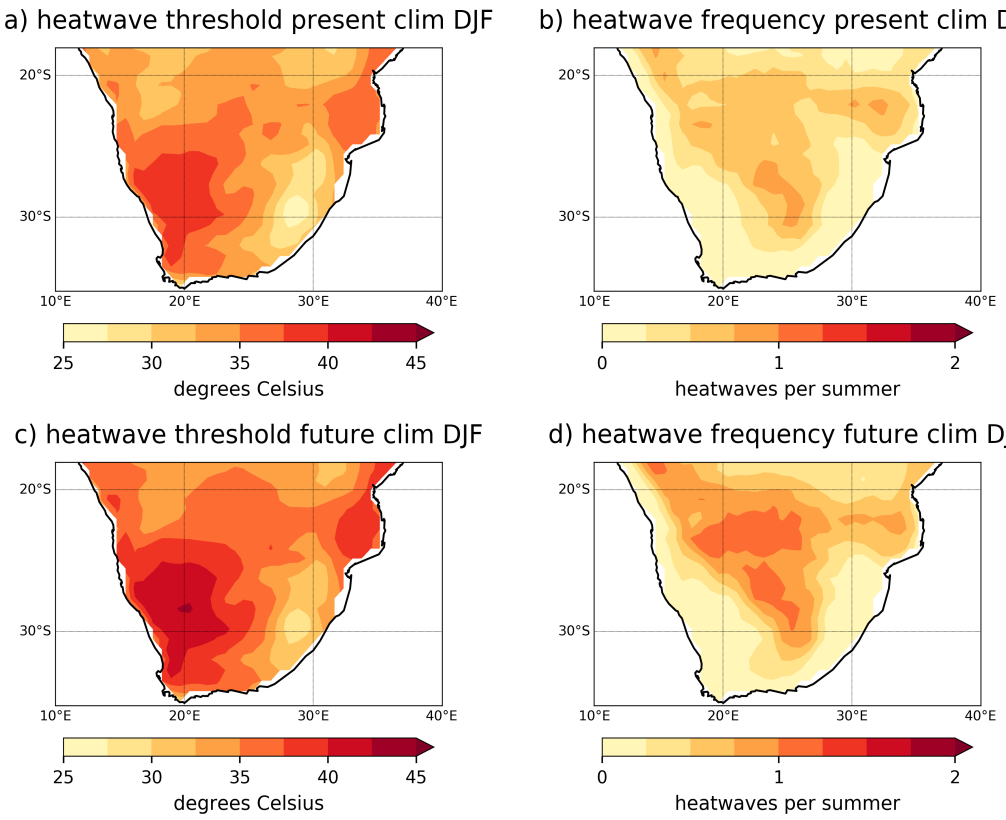

Figure 4.13: As in Fig. 4.12 but for Southern Africa.

References

N. J. Abram, B. J. Henley, A. S. Gupta, T. J. R. Lippmann, H. Clarke, A. J. Dowdy, J. J. Sharples, R. H. Nolan, T. Zhang, M. J. Wooster, J. B. Wurtzel, K. J. Meissner, A. J. Pitman, A. M. Ukkola, B. P. Murphy, N. J. Tapper, and M. M. Boer. Connections of climate change and variability to large and extreme forest fires in southeast australia. *Communications Earth Environment*, 2: 8, 2021. ISSN 2662-4435. doi: 10.1038/s43247-020-00065-8. URL https://doi.org/10.1038/s43247-020-00065-8. 157

R. F. Adler, M. R. P. Sapiano, G. J. Huffman, J.-J. Wang, G. Gu, D. Bolvin, L. Chiu, U. Schneider, A. Becker, E. Nelkin, P. Xie, R. Ferraro, and D.-B. Shin. The global precipitation climatology project (gpcp) monthly analysis (new version 2.3) and a review of 2017 global precipitation. *Atmosphere*, 9, 2018. ISSN 2073-4433. doi: 10.3390/atmos9040138. URL https://www.mdpi.com/2073-4433/9/4/138. 141, 160

J. K. Anttila-Hughes, A. S. Jina, and G. C. McCord. Enso impacts child undernutrition in the global tropics. *Nature Communications*, 12:5785, 2021. ISSN 2041-1723. doi: 10.1038/s41467-021-26048-7. URL https://doi.org/10.1038/s41467-021-26048-7. 138

J. M. Arblaster and L. V. Alexander. The impact of the el niño-southern oscillation on maximum temperature extremes. *Geophysical Research Letters*, 39, 2012. doi: https://doi.org/10.1029/2012GL053409. URL https://agupubs.onlinelibrary.wiley.com/doi/abs/10.1029/2012GL053409. 137, 143

S. Brönnimann. Impact of el niño–southern oscillation on european climate. *Reviews of Geophysics*, 45, 2007. doi: https://doi.org/10.1029/2006RG000199. URL https://agupubs.onlinelibrary.wiley.com/doi/abs/10.1029/2006RG000199. 145

W. Cai, S. Borlace, M. Lengaigne, P. van Rensch, M. Collins, G. Vecchi, A. Timmermann, A. Santoso, M. J. McPhaden, L. Wu, M. H. England, G. Wang, E. Guilyardi, and F.-F. Jin. Increasing frequency of extreme el niño events due to greenhouse warming. *Nature Climate Change*, 4:111–116, 2014. ISSN

1758-6798. doi: 10.1038/nclimate2100. URL https://doi.org/10.1038/nclimate2100. 138, 139, 158

W. Cai, A. Santoso, G. Wang, S.-W. Yeh, S.-I. An, K. M. Cobb, M. Collins, E. Guilyardi, F.-F. Jin, J.-S. Kug, M. Lengaigne, M. J. McPhaden, K. Takahashi, A. Timmermann, G. Vecchi, M. Watanabe, and L. Wu. Enso and greenhouse warming. *Nature Climate Change*, 5:849–859, 2015. ISSN 1758-6798. doi: 10.1038/nclimate2743. URL https://doi.org/10.1038/nclimate2743. 158

W. Cai, G. Wang, A. Santoso, X. Lin, and L. Wu. Definition of extreme el niño and its impact on projected increase in extreme el niño frequency. *Geophysical Research Letters*, 44:11, 111–184, 190, 2017. doi: https://doi.org/10.1002/2017GL075635. URL https://agupubs.onlinelibrary.wiley.com/doi/abs/10.1002/2017GL075635. 138

W. Cai, M. J. McPhaden, A. M. Grimm, R. R. Rodrigues, A. S. Taschetto, R. D. Garreaud, B. Dewitte, G. Poveda, Y.-G. Ham, A. Santoso, B. Ng, W. Anderson, G. Wang, T. Geng, H.-S. Jo, J. A. Marengo, L. M. Alves, M. Osman, S. Li, L. Wu, C. Karamperidou, K. Takahashi, and C. Vera. Climate impacts of the el niño–southern oscillation on south america. *Nature Reviews Earth Environment*, 1:215–231, 2020. ISSN 2662-138X. doi: 10.1038/s43017-020-0040-3. URL https://doi.org/10.1038/s43017-020-0040-3. 137

W. Cai, B. Ng, G. Wang, A. Santoso, L. Wu, and K. Yang. Increased enso sea surface temperature variability under four ipcc emission scenarios. *Nature Climate Change*, 12:228–231, 2022. ISSN 1758-6798. doi: 10.1038/s41558-022-01282-z. URL https://doi.org/10.1038/s41558-022-01282-z. 139

C. T. Y. Chung, S. B. Power, J. M. Arblaster, H. A. Rashid, and G. L. Roff. Nonlinear precipitation response to el niño and global warming in the indo-pacific. *Climate Dynamics*, 42:1837–1856, 2014. ISSN 1432-0894. doi: 10.1007/s00382-013-1892-8. URL https://doi.org/10.1007/s00382-013-1892-8. 138

L. Dhage and M. J. Widlansky. Assessment of 21st century changing sea surface temperature, rainfall, and sea surface height patterns in the tropical pacific islands using cmip6 greenhouse warming projections. *Earth's Future*, 10, 5 2022. ISSN 23284277. doi: 10.1029/2021EF002524. 144

M. G. Donat, L. V. Alexander, H. Yang, I. Durre, R. Vose, R. J. H. Dunn, K. M. Willett, E. Aguilar, M. Brunet, J. Caesar, B. Hewitson, C. Jack, A. M. G. K. Tank, A. C. Kruger, J. Marengo, T. C. Peterson, M. Renom, C. O. Rojas, M. Rusticucci, J. Salinger, A. S. Elrayah, S. S. Sekele, A. K. Srivastava, B. Trewin, C. Villarroel, L. A. Vincent, P. Zhai, X. Zhang, and S. Kitching. Updated analyses of temperature and precipitation extreme indices since the beginning of the twentieth century: The hadex2 dataset. *Journal of Geophysical Research Atmospheres*, 118:2098–2118, 5 2013. ISSN 21698996. doi: 10.1002/jgrd.50150. 143

M. Drouard and C. Cassou. A modeling- and process-oriented study to investigate the projected change of enso-forced wintertime teleconnectivity in a warmer world. *Journal of Climate*, 32:8047 – 8068, 2019. doi: https://doi.org/10.1175/JCLI-D-18-0803.1. URL https://journals.ametsoc.org/view/journals/clim/32/23/jcli-d-18-0803.1.xml. 140, 155

N. C. Duke, J. M. Kovacs, A. D. Griffiths, L. Preece, D. J. E. Hill, P. van Oosterzee, J. Mackenzie, H. S. Morning, and D. Burrows. Large-scale dieback of mangroves in australia's gulf of carpentaria: a severe ecosystem response, coincidental with an unusually extreme weather event. *Marine and Freshwater Research*, 68:1816–1829, 2017. URL https://doi.org/10.1071/MF16322. 138

R. Döscher, M. Acosta, A. Alessandri, P. Anthoni, T. Arsouze, T. Bergman, R. Bernardello, S. Boussetta, L.-P. Caron, G. Carver, M. Castrillo, F. Catalano, I. Cvijanovic, P. Davini, E. Dekker, F. J. Doblas-Reyes, D. Docquier, P. Echevarria, U. Fladrich, R. Fuentes-Franco, M. Gröger, J. v. Hardenberg, J. Hieronymus, M. P. Karami, J.-P. Keskinen, T. Koenigk, R. Makkonen, F. Massonnet, M. Ménégoz, P. A. Miller, E. Moreno-Chamarro, L. Nieradzik, T. van Noije, P. Nolan, D. O'Donnell, P. Ollinaho, G. van den Oord, P. Ortega, O. T. Prims, A. Ramos, T. Reerink, C. Rousset, Y. Ruprich-Robert, P. L.

Sager, T. Schmith, R. Schrödner, F. Serva, V. Sicardi, M. S. Madsen, B. Smith, T. Tian, E. Tourigny, P. Uotila, M. Vancoppenolle, S. Wang, D. Wårlind, U. Willén, K. Wyser, S. Yang, X. Yepes-Arbós, and Q. Zhang. The ec-earth3 earth system model for the coupled model intercomparison project 6. *Geoscientific Model Development*, 15:2973–3020, 2022. doi: 10.5194/gmd-15-2973-2022. URL https://gmd.copernicus.org/articles/15/2973/2022/. 140

J. T. Fasullo, B. L. Otto-Bliesner, and S. Stevenson. Enso's changing influence on temperature, precipitation, and wildfire in a warming climate. *Geophysical Research Letters*, 45:9216–9225, 2018. doi: https://doi.org/10.1029/2018GL079022. URL https://agupubs.onlinelibrary.wiley.com/doi/abs/10.1029/2018GL079022. 139, 156, 157

H.-B. Fredriksen, J. Berner, A. C. Subramanian, and A. Capotondi. How does el niño–southern oscillation change under global warming—a first look at cmip6. *Geophysical Research Letters*, 47:e2020GL090640, 2020. doi: https://doi.org/10.1029/2020GL090640. URL https://agupubs.onlinelibrary.wiley.com/doi/abs/10.1029/2020GL090640. e2020GL090640 2020GL090640. 139

C. Funk, F. Davenport, L. Harrison, T. Magadzire, G. Galu, G. A. Artan, S. Shukla, D. Korecha, M. Indeje, C. Pomposi, D. Macharia, G. Husak, and F. D. Nsadisa. Anthropogenic enhancement of moderate-to-strong el niño events likely contributed to drought and poor harvests in southern africa during 2016. *Bulletin of the American Meteorological Society*, 99:S91 – S96, 2018. doi: https://doi.org/10.1175/BAMS-D-17-0112.1. URL https://journals.ametsoc.org/view/journals/bams/99/1/bams-d-17-0112.1.xml. 138

C. I. Garfinkel, I. Weinberger, I. P. White, L. D. Oman, V. Aquila, and Y.-K. Lim. The salience of nonlinearities in the boreal winter response to enso: North pacific and north america. *Climate Dynamics*, 52:4429–4446, 2019. ISSN 1432-0894. doi: 10.1007/s00382-018-4386-x. URL https://doi.org/10.1007/s00382-018-4386-x. 156

M. Glantz. Currents of change: Impacts of el niño and la niña on climate and society. *Disaster Prevention and Management: An International Journal*, 10:

197–199, 1 2001. ISSN 0965-3562. doi: 10.1108/dpm.2001.10.3.197.5. URL https://doi.org/10.1108/dpm.2001.10.3.197.5. 138, 143

L. Goddard and N. E. Graham. Importance of the indian ocean for simulating rainfall anomalies over eastern and southern africa. *Journal of Geophysical Research Atmospheres*, 104:19099–19116, 8 1999. ISSN 01480227. doi: 10.1029/1999JD900326. 138

U. K. Heede and A. V. Fedorov. Eastern equatorial pacific warming delayed by aerosols and thermostat response to co2 increase. *Nature Climate Change*, 11:696–703, 2021. ISSN 1758-6798. doi: 10.1038/s41558-021-01101-x. URL https://doi.org/10.1038/s41558-021-01101-x. 158

U. K. Heede and A. V. Fedorov. Towards understanding the robust strengthening of enso and more frequent extreme el niño events in cmip6 global warming simulations. *Climate Dynamics*, 61:3047–3060, 2023. ISSN 1432-0894. doi: 10.1007/s00382-023-06856-x. URL https://doi.org/10.1007/s00382-023-06856-x. 139

K. Hu, G. Huang, P. Huang, Y. Kosaka, and S.-P. Xie. Intensification of el niño-induced atmospheric anomalies under greenhouse warming. *Nature Geoscience*, pages 1–6, 5 2021. ISSN 1752-0894. doi: 10.1038/s41561-021-00730-3. URL http://www.nature.com/articles/s41561-021-00730-3. 139

B. Huang, P. W. Thorne, V. F. Banzon, T. Boyer, G. Chepurin, J. H. Lawrimore, M. J. Menne, T. M. Smith, R. S. Vose, and H. M. Zhang. Extended reconstructed sea surface temperature, version 5 (ersstv5): Upgrades, validations, and intercomparisons. *Journal of Climate*, 30:8179–8205, 5 2017. ISSN 0894-8755. doi: 10.1175/JCLI-D-16-0836.1. URL https://journals.ametsoc.org/view/journals/clim/30/20/jcli-d-16-0836.1.xml. 141, 159

N. C. Johnson, A. T. Wittenberg, A. J. Rosati, T. L. Delworth, and W. Cooke. Future changes in boreal winter enso teleconnections in a large ensemble of high-resolution climate simulations. *Frontiers in Climate*, 4, 2022. ISSN 2624-9553. doi: 10.3389/fclim.2022.941055. URL https://www.frontiersin.org/articles/10.3389/fclim.2022.941055. 155, 156

G. Kociuba and S. B. Power. Inability of cmip5 models to simulate recent strengthening of the walker circulation: Implications for projections. *Journal of Climate*, 28:20 – 35, 2015. doi: https://doi.org/10.1175/JCLI-D-13-00752.1. URL https://journals.ametsoc.org/view/journals/clim/28/1/jcli-d-13-00752.1.xml. 158

J.-Y. Lee, J. Marotzke, G. Bala, L. Cao, S. Corti, J. P. Dunne, F. Engelbrecht, E. Fischer, J. C. Fyfe, C. Jones, et al. Future global climate: scenario-based projections and near-term information. 2021. 139

S.-K. Lee, C. Wang, and B. E. Mapes. A simple atmospheric model of the local and teleconnection responses to tropical heating anomalies. *Journal of Climate*, 22:272 – 284, 2009. doi: https://doi.org/10.1175/2008JCLI2303.1. URL https://journals.ametsoc.org/view/journals/clim/22/2/2008jcli2303.1.xml. 150

M. Lengaigne and G. A. Vecchi. Contrasting the termination of moderate and extreme el niño events in coupled general circulation models. *Climate Dynamics*, 35:299–313, 2010. ISSN 1432-0894. doi: 10.1007/s00382-009-0562-3. URL https://doi.org/10.1007/s00382-009-0562-3. 138

N. Maher, J. E. Kay, and A. Capotondi. Modulation of enso teleconnections over north america by the pacific decadal oscillation. *Environmental Research Letters*, 17:114005, 10 2022. doi: 10.1088/1748-9326/ac9327. URL https://dx.doi.org/10.1088/1748-9326/ac9327. 139, 158

S. McGregor, C. Cassou, Y. Kosaka, and A. S. Phillips. Projected enso teleconnection changes in cmip6. *Geophysical Research Letters*, 49:e2021GL097511, 2022. doi: https://doi.org/10.1029/2021GL097511. URL https://agupubs.onlinelibrary.wiley.com/doi/abs/10.1029/2021GL097511. e2021GL097511 2021GL097511. 139, 155, 156

G. A. Meehl and H. Teng. Multi-model changes in el niño teleconnections over north america in a future warmer climate. *Climate Dynamics*, 29:779–790, 2007. ISSN 1432-0894. doi: 10.1007/s00382-007-0268-3. URL https://doi.org/10.1007/s00382-007-0268-3. 143, 156

D. A. Mooley and B. Parthasarathy. Indian summer monsoon and el nino. *pure and applied geophysics*, 121:339–352, 1983. ISSN 1420-9136. doi: 10.1007/BF02590143. URL https://doi.org/10.1007/BF02590143. 138

S. E. Page, F. Siegert, J. O. Rieley, H.-D. V. Boehm, A. Jaya, and S. Limin. The amount of carbon released from peat and forest fires in indonesia during 1997. *Nature*, 420:61–65, 2002. ISSN 1476-4687. doi: 10.1038/nature01131. URL https://doi.org/10.1038/nature01131. 138

J. S. Panisset, R. Libonati, C. M. P. Gouveia, F. Machado-Silva, D. A. França, J. R. A. França, and L. F. Peres. Contrasting patterns of the extreme drought episodes of 2005, 2010 and 2015 in the amazon basin. *International Journal of Climatology*, 38:1096–1104, 2018. doi: https://doi.org/10.1002/joc.5224. URL https://rmets.onlinelibrary.wiley.com/doi/abs/10.1002/joc.5224. 138

P. K. Patra, D. Crisp, J. W. Kaiser, D. Wunch, T. Saeki, K. Ichii, T. Sekiya, P. O. Wennberg, D. G. Feist, D. F. Pollard, D. W. T. Griffith, V. A. Velazco, M. D. Maziere, M. K. Sha, C. Roehl, A. Chatterjee, and K. Ishijima. The orbiting carbon observatory (oco-2) tracks 2-3 peta-gram increase in carbon release to the atmosphere during the 2014-2016 el niño open. *Scientific Reports*, 7, 2017. doi: 10.1038/s41598-017-13459-0. URL www.nature.com/scientificreports. 138

S. J. Perry, S. McGregor, A. S. Gupta, M. H. England, and N. Maher. Projected late 21st century changes to the regional impacts of the el niño-southern oscillation. *Climate Dynamics*, 54:395–412, 2020. ISSN 1432-0894. doi: 10.1007/s00382-019-05006-6. URL https://doi.org/10.1007/s00382-019-05006-6. 139, 155, 156

C. L. Quéré, R. M. Andrew, P. Friedlingstein, S. Sitch, J. Hauck, J. Pongratz, P. A. Pickers, J. I. Korsbakken, G. P. Peters, J. G. Canadell, A. Arneth, V. K. Arora, L. Barbero, A. Bastos, L. Bopp, F. Chevallier, L. P. Chini, P. Ciais, S. C. Doney, T. Gkritzalis, D. S. Goll, I. Harris, V. Haverd, F. M. Hoffman, M. Hoppema, R. A. Houghton, G. Hurtt, T. Ilyina, A. K.

Jain, T. Johannessen, C. D. Jones, E. Kato, R. F. Keeling, K. K. Goldewijk, P. Landschützer, N. Lefèvre, S. Lienert, Z. Liu, D. Lombardozzi, N. Metzl, D. R. Munro, J. E. M. S. Nabel, S. Nakaoka, C. Neill, A. Olsen, T. Ono, P. Patra, A. Peregon, W. Peters, P. Peylin, B. Pfeil, D. Pierrot, B. Poulter, G. Rehder, L. Resplandy, E. Robertson, M. Rocher, C. Rödenbeck, U. Schuster, J. Schwinger, R. Séférian, I. Skjelvan, T. Steinhoff, A. Sutton, P. P. Tans, H. Tian, B. Tilbrook, F. N. Tubiello, I. T. van der Laan-Luijkx, G. R. van der Werf, N. Viovy, A. P. Walker, A. J. Wiltshire, R. Wright, S. Zaehle, and B. Zheng. Global carbon budget 2018. *Earth System Science Data*, 10:2141–2194, 2018. doi: 10.5194/essd-10-2141-2018. URL https://essd.copernicus.org/articles/10/2141/2018/. 138

J. V. Ratnam, S. K. Behera, Y. Masumoto, and T. Yamagata. Remote effects of el niño and modoki events on the austral summer precipitation of southern africa. *Journal of Climate*, 27:3802 – 3815, 2014. doi: https://doi.org/10.1175/JCLI-D-13-00431.1. URL https://journals.ametsoc.org/view/journals/clim/27/10/jcli-d-13-00431.1.xml. 138

R. A. Rohde and Z. Hausfather. The berkeley earth land/ocean temperature record. *Earth System Science Data*, 12:3469–3479, 2020. doi: 10.5194/essd-12-3469-2020. URL https://essd.copernicus.org/articles/12/3469/2020/. 141, 160

S. Russo, A. F. Marchese, J. Sillmann, and G. Immé. When will unusual heat waves become normal in a warming africa? *Environmental Research Letters*, 11:54016, 5 2016. doi: 10.1088/1748-9326/11/5/054016. URL https://dx.doi.org/10.1088/1748-9326/11/5/054016. 157

A. Santoso, S. McGregor, F.-F. Jin, W. Cai, M. H. England, S.-I. An, M. J. McPhaden, and E. Guilyardi. Late-twentieth-century emergence of the el niño propagation asymmetry and future projections. *Nature*, 504:126–130, 2013. ISSN 1476-4687. doi: 10.1038/nature12683. URL https://doi.org/10.1038/nature12683. 138

A. Santoso, M. J. Mcphaden, and W. Cai. The defining characteristics of enso extremes and the strong 2015/2016 el niño. *Reviews of Geophysics*, 55:1079–1129, 12 2017. ISSN 19449208. doi: 10.1002/2017RG000560. 138

R. Seager, N. Harnik, W. A. Robinson, Y. Kushnir, M. Ting, H.-P. Huang, and J. Velez. Mechanisms of enso-forcing of hemispherically symmetric precipitation variability. *Quarterly Journal of the Royal Meteorological Society*, 131:1501–1527, 2005. doi: https://doi.org/10.1256/qj.04.96. URL https://rmets.onlinelibrary.wiley.com/doi/abs/10.1256/qj.04.96. 138

A. S. Taschetto and M. H. England. El niño modoki impacts on australian rainfall. *Journal of Climate*, 22:3167 – 3174, 2009. doi: https://doi.org/10.1175/2008JCLI2589.1. URL https://journals.ametsoc.org/view/journals/clim/22/11/2008jcli2589.1.xml. 138

A. S. Taschetto, C. C. Ummenhofer, M. F. Stuecker, D. Dommenget, K. Ashok, R. R. Rodrigues, and S.-W. Yeh. Enso atmospheric teleconnections. *El Niño Southern Oscillation in a Changing Climate*, pages 309–335, 2020. doi: https://doi.org/10.1002/9781119548164.ch14. URL https://agupubs.onlinelibrary.wiley.com/doi/abs/10.1002/9781119548164.ch14. 137

P. Trascasa-Castro, A. C. Maycock, Y. Y. S. Yiu, and J. K. Fletcher. On the linearity of the stratospheric and euro-atlantic sector response to enso. *Journal of Climate*, 32:6607–6626, 10 2019. ISSN 0894-8755. doi: 10.1175/JCLI-D-18-0746.1. URL https://journals.ametsoc.org/view/journals/clim/32/19/jcli-d-18-0746.1.xml. 138

J. Wang, N. Zeng, M. Wang, F. Jiang, H. Wang, and Z. Jiang. Contrasting terrestrial carbon cycle responses to the 1997/98 and 2015/16 extreme el niño events. *Earth System Dynamics*, 9:1–14, 2018. doi: 10.5194/esd-9-1-2018. URL https://esd.copernicus.org/articles/9/1/2018/. 138

A. Wu, W. W. Hsieh, and A. Shabbar. The nonlinear patterns of north american winter temperature and precipitation associated with enso. *Journal of Climate*, 18:1736 – 1752, 2005. doi: https://doi.org/10.1175/

JCLI3372.1. URL https://journals.ametsoc.org/view/journals/clim/18/11/jcli3372.1.xml. 138

J. Ying, M. Collins, W. Cai, A. Timmermann, P. Huang, D. Chen, and K. Stein. Emergence of climate change in the tropical pacific. *Nature Climate Change*, 12:356–364, 2022. ISSN 1758-6798. doi: 10.1038/s41558-022-01301-z. URL https://doi.org/10.1038/s41558-022-01301-z. 139

Z.-Q. Zhou, S.-P. Xie, X.-T. Zheng, Q. Liu, and H. Wang. Global warming–induced changes in el niño teleconnections over the north pacific and north america. *Journal of Climate*, 27:9050 – 9064, 2014. doi: https://doi.org/10.1175/JCLI-D-14-00254.1. URL https://journals.ametsoc.org/view/journals/clim/27/24/jcli-d-14-00254.1.xml. 140

Chapter 5

Conclusions

"One never notices what has been done
one can only see what remains to be done.

Maria Salomea Skłodowska-Curie.

5.1. Key findings

This doctoral thesis has explored the effects of changes in the mean climate state on ENSO dynamics and teleconnections. Focusing on AMV as a key mode of decadal natural climate variability and a scenario for future anthropogenic forcing, the results chapters advance the overall scientific knowledge in how different drivers of variation in the background climate state modulate ENSO and its teleconnections.

The instrumental SST record is relatively short, spanning only to quantify 1 full AMV phase of each sign, which does not allow to robustly estimate the AMV impacts on climate. To overcome this issue, idealised modeling experiments similar to those performed for the DCPP project (Boer et al., 2016) are useful to robustly assess the global impacts of AMV and its interactions with other modes of climate variability. Chapter 2 investigates the AMV modulation of ENSO variability using idealised experiments run with the NCAR-CESM1 model, where North Atlantic SSTs are restored towards time independent patterns of the positive and negative phases of AMV. Positive AMV conditions were shown to weaken both El Niño and La Niña SST amplitude, as previously suggested (Dong and Sutton, 2007; Yu et al., 2015), although the mechanisms of this modulation were not clear. Warm AMV conditions strengthen the mean Walker circulation over the tropical Pacific, enhancing the zonal SST gradient and shifting ENSO SST and precipitation anomalies westwards.

With the aim of identifying the specific dynamical process behind the weakening of ENSO variability, the widely known method, the Bjerknes Stability Index was used (Jin et al., 2006), which decomposes the atmosphere-ocean processes contributing to ENSO growth and decay onto different feedback processes in the equatorial Pacific. This revealed a significant weakening of the thermocline feedback in AMV+ relative to AMV-, consisting of a less reactive thermocline to wind stress forcing. We point towards a confinement of the wind stress anomalies over the western-most part of the equatorial Pacific as the mechanism responsible for the thermocline feedback weakening. It is therefore key to consider not only

the strength of wind stress anomalies but also their location along the eastern equatorial Pacific, because the combination of these two factors determines how the thermocline reacts to changes in wind stress.

The weakened positive thermocline feedback under AMV+ delays ENSO growth, leading to El Niño and La Niña events whose SST anomalies are around 10% weaker in the EP compared to AMV- conditions. The role of AMV in muting ENSO variability highlights the importance of accounting for the combined effects of low frequency internal variability and greenhouse forcing in future climate projections.

Building on the findings in Chapter 2, Chapter 3 investigates if and how AMV modulates ENSO regional teleconnections. The fact that ENSO variability weakens under warm AMV conditions does not necessarily mean that ENSO teleconnections will also weaken. In fact, the sign of AMV modulation of ENSO impacts is highly region dependent. Australia is selected as the region of interest to study the AMV modulation of ENSO impacts, due to the good performance of CESM1 in capturing ENSO-driven impacts over Australia, and the well known influence of ENSO on climate conditions over Australia (Chung and Power, 2017). Additionally it has been suggested that other modes of climate variability interact with ENSO and help improve ENSO impacts prediction over Australia (Kiem and Franks, 2004; King et al., 2013; Power et al., 1999). The analysis separates the anomalies in climate impacts associated with the mean AMV climate response and the modulation of ENSO by AMV. In observations, one would observe the combined effects but the model experiments allow for these components to be separated.

Chapter 3 showed that AMV significantly modulates the climate response to ENSO over Australia. During austral summer, El Niño typically drives hot and dry anomalies in Australia, which get amplified over the west of the country and weakened over the east under warm AMV conditions. The results also show some asymmetry in the AMV modulation of ENSO impacts over Australia, with

a stronger weakening of the wet and cold anomalies driven by La Niña over eastern Australia and barely no AMV modulation of La Niña impacts over western Australia.

Under warm AMV conditions, the decrease in extreme precipitation over the central-west of Australia during El Niño summers is enhanced, and the amount of warm days increases over the country, especially in the North. While AMV+ overall intensifies El Niño-related extremes, it weakens the extreme precipitation response associated with La Niña, which leads to less wet days, and a large increase in warm days over eastern Australia, muting the impacts of La Niña.

Finally, the impacts of AMV on the ENSO-fire relationship under warm and cold AMV phases over southeastern Australia, the most populated area of the country, was investigated. Following the approach of Turco et al. (2018), the preconditioning by ENSO-driven precipitation and temperature anomalies precondition the extent of burned area during the fire season was explored. This approach has been proven to be very useful for seasonal prediction of global fire risk. The results show no significant modulation of ENSO-driven burned area by AMV, despite the large decrease in burned area during the positive phase of AMV, independent of the ENSO phase.

A decomposition of the large-scale atmospheric circulation into orthogonal local zonal Walker and Hadley components revealed that under warm AMV conditions there is a shift in tropical convection during El Niño from the western to the central equatorial Pacific, as shown in Trascasa-Castro et al. (2021). This shift mainly alters the Hadley circulation, which during El Niño translates into enhanced subsidence over western Australia (amplifying El Niño impacts) and upward motion over the north east (weakening El Niño impacts), which helps to explain the dipole of strengthening/weakening of El Niño impacts over the west/east of Australia under warm AMV conditions. During La Niña, the westward shift of deep convection in the equatorial Pacific under AMV+ projects onto enhanced subsidence over western Australia and a weaker enhancement of upward motion over eastern Australia, again repeating the amplification/weakening

dipole shown by the AMV modulation of the surface climate response to ENSO in Australia. The AMV modulation of the Hadley circulation explains most of the changes in ENSO-driven circulation over Australia, with a smaller contribution of changes in the Walker circulation.

The impacts of El Niño and La Niña events over Australia do not always have the same spatial structure or amplitude, they vary from event to event. Our study suggests that Atlantic Multidecadal Variability plays a role in explaining some percentage of the climate response to ENSO in Australia. In our work, we distinguish between "co-occurrence" and "modulation". The first term refers to the climate impact resulting of the combination of two modes of climate variability that co-occur in time, and is directly comparable to observations, being useful to develop storylines and understand what the climate impacts of different modes of variability might be over a certain region. On the other hand, by exploring the AMV modulation of ENSO, we are able to isolate the direct impacts of one mode over the other and understand the dynamical mechanisms of such modulation.

In the last decades, the unprecedented rise of global mean surface temperature due to human activities has brought scientists together in a mission to reduce uncertainties in future climate projections. Understanding the combined effects of changes in El Niño and changes in the mean climate state due to anthropogenic forcing will allow to reduce uncertainties in future climate impacts at a regional scale.

There is still a large disagreement within models in when and how ENSO variability might respond to greenhouse gas forcing (Maher et al., 2023). However, a number of studies suggest that the global impacts of El Niño will become amplified in high greenhouse gas forcing future climates (Bellenger et al., 2014; Cai et al., 2014, 2022; Johnson et al., 2022; McGregor et al., 2022; Perry et al., 2020). Models agree in that changes in ENSO-driven precipitation imposed by climate change are expected to emerge by the middle of the century, decades before any change in ENSO SST is discernible (Cai et al., 2021; Ying et al., 2022). The 1982/83, 1997/98 and 2015/16 El Niño events generated SST anomalies in the Niño3.4

region above 2°C, and caused devastating impacts such as droughts and floods that exposed several million people to food insecurity. Chapter 4 summarises the main results of an investigation that aims to understand how the impacts of very strong El Niño events, similar to those observed in the last decades, will alter in a warmer planet, assuming that ENSO-SST characteristics will remain unchanged. Pacemaker simulations were performed with the EC-Earth3-CC model (Döscher et al., 2022). Pacemaker experiments are historical simulations (following the CMIP nomenclature) in which the chronology of the SST is constrained in a sub-domain of the model. Comparing pacemaker simulations with the traditional historical simulations allow to isolate the impacts of the constrained SST anomalies on the climate. In this case, the ocean surface is restored to mimic SST anomalies from the aforementioned observed very strong El Niño events. This procedure was repeated using the same observed SST anomalies applied to present-day and future model climatologies, so that any difference in the absolute SST pattern obtained should reflect the change in the background state between the present and future. The future scenario is the SSP2-4.5, a middle-of-the road scenario, acknowledging that a more severe warming scenario might have changed the global teleconnections of very strong El Niño even further (McGregor et al., 2022).

In agreement with the multi-model CMIP6 trend, the EC-Earth3-CC model simulates a trend towards a weakening of the Walker circulation by the end of the 21st century under greenhouse gas forcing. This response consists of the eastern equatorial Pacific warming faster than the west, leading to a decrease of the zonal SST gradient of around 20% in the future relative to the present-day. This climatologically warmer eastern Pacific has implications for future ENSO teleconnections, since deep convection is shifted towards the eastern Pacific.

While pacemaker simulations are widely know and used within the scientific community, our approach of running observed analogue El Niño in the future is rather innovative. Opposite to atmosphere-only simulations, a coupled pacemaker approach allows to investigate the response of ocean variables and couple feedbacks to a specific forcing such as the one we imposed mimicking very strong El Niño

events, providing a more realistic comparison with the real world. In our very strong El Niño simulations, we found that the west Pacific warm pool, which lays outside the restoring region, responds strongly to the SST restoring over the eastern Pacific ocean, triggering an intensification of the Walker circulation in the future simulation relative to the present.

Over the tropical Pacific, the simulations show an anomalous precipitation response to very strong future El Niño events that accompanies the change in SST pattern. This response consists of an increase in precipitation over the warm pool that follows the anomalous El Niño-driven warm SST anomalies, and reduced precipitation in the central and eastern equatorial Pacific. It is striking that even having an anomalous SST pattern that reflects onto slightly milder El Niño events in the future, the global response to very strong El Niño in the future agrees with those works that exhibit an amplification of El Niño impacts towards the future in may regions (Fasullo et al., 2018; Johnson et al., 2022; McGregor et al., 2022; Perry et al., 2017). It is worth mentioning that in the aforementioned studies ENSO SST variability increases in the future. This suggests that even with a slightly weaker El Niño in the future, background changes driven by climate change will amplify the impacts of El Niño in the future in many regions of the planet.

The results of Chapter 4 reveal that very strong El Niño events analogous to those observed in the last decades would drive stronger impacts. Some examples are an intensification of cold anomalies over North America in boreal winter, and hot anomalies south of the Amazon and Congo basins, northern Africa and Australia in austral summer. The link between very strong El Niño and the negative phase of the North Atlantic Oscillation will intensify towards the future. Over the Amazon basin, there appears to be a nonlinear behaviour where future strong El Niño events do not lead to further drying. Additionally, shifts in atmospheric circulation in the future will weaken the response to El Niño, as it will be the case for La Plata Basin and southern Africa.

A more in-depth analysis on daily temperature extremes suggests that the amount

of cool days over North America in boreal winter will further increase towards the future, and summer heatwaves in Australia driven by very strong El Niño events will increase in frequency in the future, relative to the present. On the contrary, the amount of extreme El Niño-driven heatwaves in Southern Africa will be less frequent in the future.

With the results of this doctoral thesis, we have further proven that ENSO dynamics and teleconnections are sensitive to changes in the background state, which can be driven by internal climate variability or external forcing.

5.2. Future work

The results described in Chapters 2-4 offer several novel insights to the effects of the mean climate state on ENSO behaviour. Several avenues for further work have been highlighted as a consequence of the findings:

- The BJ index assumes linear relationships between all variables and SSTs. We know this is a simplication of ENSO processes. For instance the shortwave feedback, included in the thermodynamic feedback, is very nonlinear (Lloyd et al., 2012), and its magnitude largely varies between CMIP6 models due to the poor representation of tropical clouds (Bony and Dufresne, 2005). Future work, potentially with a multi-model approach using this method should also include a careful assessment of the dynamical processes involved in ENSO feedbacks.

- The results in this thesis rely on two climate models NCAR-CESM1 and EC-Earth3-CC. Differences in the performance and representation of ENSO, AMV and climate change in models are well documented. Overall, the suit of CMIP6 models that followed this protocol analogue to DCPP suggest a tropical Pacific cooling as a response to warm AMV conditions (Ruprich-Robert et al., 2021), however the impact of AMV on ENSO feedbacks might differ. Further investigation is needed to verify our results, ideally in a multi-model context and including atmospheric-only simulations, since it

has been recently suggested by O'Reilly et al. (2023) that idealised coupled AMV simulations might overestimate the effects of AMV.

- Building on the analysis of ENSO impacts over Australia in Chapter 3 extra work is needed to explore other world regions. Furthermore, as mentioned in the previous point, a multimodel study is needed to assess whether this modulation is verified in other CMIP models. Also, we have explored the DJF season because it is when ENSO variability is largest, however the strongest ENSO signal over Australia appears from October to December (Taschetto et al., 2020), so it would be insightful to analyse changes to teleconnections in other seasons.

- Regarding the very strong El Niño pacemaker simulations, additional experiments could be performed expanding the restoring region to cover the whole equatorial Pacific, including the warm pool. This way the time-evolution of SST anomalies over the tropical equatorial Pacific will be more strongly controlled, reducing feedback processes that lead to deviations of the SST response from the target state which might ultimately affect the global teleconnections of El Niño.

- Chapter 4 focuses on the modulation of El Nino impacts by climate change. It would be interesting to also look at the combination of changes in El Niño teleconnections and changes in the mean climate state to be able to say whether El Niño amplifies or masks the impacts of climate change in different regions. Also additional work is needed to examine models where the tropical eastern Pacific does not warm as much as the EC-Earth3-CC model (see Maher et al. (2022)).

- The results of Chapter 4 hint at the possibility of changes in the future response to very strong El Niño events, for example over the Amazon basin, where there seems to be a saturation of dry conditions during very strong El Niño events in the future. Further investigation is needed to explore whether the climate response to ENSO in the future gets saturated during very strong El Niño events.

- Further work will explore how strong El Niño events modulates the occurrence of extreme precipitation and temperature impacts in different regions in the present and future climates, using an absolute threshold for both climatological periods. In particular, I will quantify the relative contributions of changes in the mean state (due to climate change) and changes in the teleconnections of very strong El Niño events to absolute changes in the impacts of El Niño between present and future climates. That way, I will be able to identify regions where the global warming signal amplifies or weakens the future impacts of very strong El Niño events.

This thesis ends leaving more open questions than uncertainties solved. Nevertheless, it has made a contribution to the assembly of this beautiful global-scale jigsaw puzzle called El Niño-Southern Oscillation.

Life's a laugh and death's a joke, it's true
You'll see it's all a show
Keep 'em laughin' as you go
Just remember that the last laugh is on you
And
Always look on the bright side of life ♫♫♫♫♫
Always look on the right side of life ♫♫♫♫♫"

"Always look on the bright side of life", by Eric Idle, Monty Python.

References

H. Bellenger, E. Guilyardi, J. Leloup, M. Lengaigne, and J. Vialard. Enso representation in climate models: from cmip3 to cmip5. *Climate Dynamics*, 42: 1999–2018, 2014. ISSN 1432-0894. doi: 10.1007/s00382-013-1783-z. URL https://doi.org/10.1007/s00382-013-1783-z. 178

G. J. Boer, D. M. Smith, C. Cassou, F. Doblas-Reyes, G. Danabasoglu, B. Kirtman, Y. Kushnir, M. Kimoto, G. A. Meehl, R. Msadek, W. A. Mueller, K. E. Taylor, F. Zwiers, M. Rixen, Y. Ruprich-Robert, and R. Eade. The decadal climate prediction project (dcpp) contribution to cmip6. *Geoscientific Model Development*, 9:3751–3777, 2016. doi: 10.5194/gmd-9-3751-2016. URL https://gmd.copernicus.org/articles/9/3751/2016/. 175

S. Bony and J. L. Dufresne. Marine boundary layer clouds at the heart of tropical cloud feedback uncertainties in climate models. *Geophysical Research Letters*, 32:1–4, 5 2005. ISSN 00948276. doi: 10.1029/2005GL023851. 181

W. Cai, S. Borlace, M. Lengaigne, P. van Rensch, M. Collins, G. Vecchi, A. Timmermann, A. Santoso, M. J. McPhaden, L. Wu, M. H. England, G. Wang, E. Guilyardi, and F.-F. Jin. Increasing frequency of extreme el niño events due to greenhouse warming. *Nature Climate Change*, 4:111–116, 2014. ISSN 1758-6798. doi: 10.1038/nclimate2100. URL https://doi.org/10.1038/nclimate2100. 178

W. Cai, A. Santoso, M. Collins, B. Dewitte, C. Karamperidou, J.-S. Kug, M. Lengaigne, M. J. McPhaden, M. F. Stuecker, A. S. Taschetto, A. Timmermann, L. Wu, S.-W. Yeh, G. Wang, B. Ng, F. Jia, Y. Yang, J. Ying, X.-T. Zheng, T. Bayr, J. R. Brown, A. Capotondi, K. M. Cobb, B. Gan, T. Geng, Y.-G. Ham, F.-F. Jin, H.-S. Jo, X. Li, X. Lin, S. McGregor, J.-H. Park, K. Stein, K. Yang, L. Zhang, and W. Zhong. Changing el niño–southern oscillation in a warming climate. *Nature Reviews Earth Environment 2021*, pages 1–17, 5 2021. ISSN 2662-138X. doi: 10.1038/s43017-021-00199-z. URL https://www.nature.com/articles/s43017-021-00199-z. 178

W. Cai, B. Ng, G. Wang, A. Santoso, L. Wu, and K. Yang. Increased enso sea surface temperature variability under four ipcc emission scenarios. *Nature Climate Change*, 12:228–231, 2022. ISSN 1758-6798. doi: 10.1038/s41558-022-01282-z. URL https://doi.org/10.1038/s41558-022-01282-z. 178

C. T. Y. Chung and S. B. Power. The non-linear impact of el niño, la niña and the southern oscillation on seasonal and regional australian precipitation. *Journal of Southern Hemisphere Earth Systems Science*, 67:25–45, 2017. ISSN 22065865. doi: 10.22499/3.6701.003. 176

B. Dong and R. T. Sutton. Enhancement of enso variability by a weakened atlantic thermohaline circulation in a coupled gcm. *Journal of Climate*, 20: 4920 – 4939, 2007. doi: https://doi.org/10.1175/JCLI4284.1. URL https://journals.ametsoc.org/view/journals/clim/20/19/jcli4284.1.xml. 175

R. Döscher, M. Acosta, A. Alessandri, P. Anthoni, T. Arsouze, T. Bergman, R. Bernardello, S. Boussetta, L.-P. Caron, G. Carver, M. Castrillo, F. Catalano, I. Cvijanovic, P. Davini, E. Dekker, F. J. Doblas-Reyes, D. Docquier, P. Echevarria, U. Fladrich, R. Fuentes-Franco, M. Gröger, J. v. Hardenberg, J. Hieronymus, M. P. Karami, J.-P. Keskinen, T. Koenigk, R. Makkonen, F. Massonnet, M. Ménégoz, P. A. Miller, E. Moreno-Chamarro, L. Nieradzik, T. van Noije, P. Nolan, D. O'Donnell, P. Ollinaho, G. van den Oord, P. Ortega, O. T. Prims, A. Ramos, T. Reerink, C. Rousset, Y. Ruprich-Robert, P. L. Sager, T. Schmith, R. Schrödner, F. Serva, V. Sicardi, M. S. Madsen, B. Smith, T. Tian, E. Tourigny, P. Uotila, M. Vancoppenolle, S. Wang, D. Wårlind, U. Willén, K. Wyser, S. Yang, X. Yepes-Arbós, and Q. Zhang. The ec-earth3 earth system model for the coupled model intercomparison project 6. *Geoscientific Model Development*, 15:2973–3020, 2022. doi: 10.5194/gmd-15-2973-2022. URL https://gmd.copernicus.org/articles/15/2973/2022/. 179

J. T. Fasullo, B. L. Otto-Bliesner, and S. Stevenson. Enso's changing influence on temperature, precipitation, and wildfire in a warming climate. *Geophysical Research Letters*, 45:9216–9225, 2018. doi: https://doi.org/10.1029/2018GL079022. URL https://agupubs.onlinelibrary.wiley.com/doi/abs/10.1029/2018GL079022. 180

F. F. Jin, S. T. Kim, and L. Bejarano. A coupled-stability index for enso. *Geophysical Research Letters*, 33, 5 2006. ISSN 00948276. doi: 10.1029/2006GL027221. URL https://agupubs.onlinelibrary.wiley.com/doi/full/10.1029/2006GL027221https://agupubs.onlinelibrary.wiley.com/doi/abs/10.1029/2006GL027221https://agupubs.onlinelibrary.wiley.com/doi/10.1029/2006GL027221. 175

N. C. Johnson, A. T. Wittenberg, A. J. Rosati, T. L. Delworth, and W. Cooke. Future changes in boreal winter enso teleconnections in a large ensemble of high-resolution climate simulations. *Frontiers in Climate*, 4, 2022. ISSN 2624-9553. doi: 10.3389/fclim.2022.941055. URL https://www.frontiersin.org/articles/10.3389/fclim.2022.941055. 178, 180

A. S. Kiem and S. W. Franks. Multi-decadal variability of drought risk, eastern australia. *Hydrological Processes*, 18:2039–2050, 2004. doi: https://doi.org/10.1002/hyp.1460. URL https://onlinelibrary.wiley.com/doi/abs/10.1002/hyp.1460. 176

A. D. King, L. V. Alexander, and M. G. Donat. Asymmetry in the response of eastern australia extreme rainfall to low-frequency pacific variability. *Geophysical Research Letters*, 40:2271–2277, 2013. doi: https://doi.org/10.1002/grl.50427. URL https://agupubs.onlinelibrary.wiley.com/doi/abs/10.1002/grl.50427. 176

J. Lloyd, E. Guilyardi, and H. Weller. The role of atmosphere feedbacks during enso in the cmip3 models. part iii: The shortwave flux feedback. *Journal of Climate*, 25:4275 – 4293, 2012. doi: https://doi.org/10.1175/JCLI-D-11-00178.1. URL https://journals.ametsoc.org/view/journals/clim/25/12/jcli-d-11-00178.1.xml. 181

N. Maher, J. E. Kay, and A. Capotondi. Modulation of enso teleconnections over north america by the pacific decadal oscillation. *Environmental Research Letters*, 17:114005, 10 2022. doi: 10.1088/1748-9326/ac9327. URL https://dx.doi.org/10.1088/1748-9326/ac9327. 182

N. Maher, R. C. J. Wills, P. DiNezio, J. Klavans, S. Milinski, S. C. Sanchez, S. Stevenson, M. F. Stuecker, and X. Wu. The future of the el niño–southern oscillation: using large ensembles to illuminate time-varying responses and inter-model differences. *Earth System Dynamics*, 14:413–431, 2023. doi: 10.5194/esd-14-413-2023. URL https://esd.copernicus.org/articles/14/413/2023/. 178

S. McGregor, C. Cassou, Y. Kosaka, and A. S. Phillips. Projected enso teleconnection changes in cmip6. *Geophysical Research Letters*, 49:e2021GL097511, 2022. doi: https://doi.org/10.1029/2021GL097511. URL https://agupubs.onlinelibrary.wiley.com/doi/abs/10.1029/2021GL097511. e2021GL097511 2021GL097511. 178, 179, 180

C. H. O'Reilly, M. Patterson, J. Robson, P. A. Monerie, D. Hodson, and Y. Ruprich-Robert. Challenges with interpreting the impact of atlantic multidecadal variability using sst-restoring experiments. *npj Climate and Atmospheric Science*, 6:14, 2023. ISSN 2397-3722. doi: 10.1038/s41612-023-00335-0. URL https://doi.org/10.1038/s41612-023-00335-0. 182

S. J. Perry, S. McGregor, A. S. Gupta, and M. H. England. Future changes to el niño–southern oscillation temperature and precipitation teleconnections. *Geophysical Research Letters*, 44:10, 608–610, 616, 2017. doi: https://doi.org/10.1002/2017GL074509. URL https://agupubs.onlinelibrary.wiley.com/doi/abs/10.1002/2017GL074509. 180

S. J. Perry, S. McGregor, A. S. Gupta, M. H. England, and N. Maher. Projected late 21st century changes to the regional impacts of the el niño-southern oscillation. *Climate Dynamics*, 54:395–412, 2020. ISSN 1432-0894. doi: 10.1007/s00382-019-05006-6. URL https://doi.org/10.1007/s00382-019-05006-6. 178

S. Power, T. Casey, C. Folland, A. Colman, and V. Mehta. Inter-decadal modulation of the impact of enso on australia. *Climate Dynamics*, 15:319–324, 1999. ISSN 1432-0894. doi: 10.1007/s003820050284. URL https://doi.org/10.1007/s003820050284. 176

Y. Ruprich-Robert, E. Moreno-Chamarro, X. Levine, A. Bellucci, C. Cassou, F. Castruccio, P. Davini, R. Eade, G. Gastineau, L. Hermanson, D. Hodson, K. Lohmann, J. Lopez-Parages, P.-A. Monerie, D. Nicolì, S. Qasmi, C. D. Roberts, E. Sanchez-Gomez, G. Danabasoglu, N. Dunstone, M. Martin-Rey, R. Msadek, J. Robson, D. Smith, and E. Tourigny. Impacts of atlantic multidecadal variability on the tropical pacific: a multi-model study. *npj Climate and Atmospheric Science*, 4:33, 12 2021. ISSN 2397-3722. doi: 10.1038/s41612-021-00188-5. URL http://www.nature.com/articles/s41612-021-00188-5. 181

A. S. Taschetto, C. C. Ummenhofer, M. F. Stuecker, D. Dommenget, K. Ashok, R. R. Rodrigues, and S.-W. Yeh. Enso atmospheric teleconnections. *El Niño Southern Oscillation in a Changing Climate*, pages 309–335, 2020. doi: https://doi.org/10.1002/9781119548164.ch14. URL https://agupubs.onlinelibrary.wiley.com/doi/abs/10.1002/9781119548164.ch14. 182

P. Trascasa-Castro, Y. Ruprich-Robert, F. Castruccio, and A. C. Maycock. Warm phase of amv damps enso through weakened thermocline feedback. *Geophysical Research Letters*, 48:e2021GL096149, 2021. doi: https://doi.org/10.1029/2021GL096149. URL https://agupubs.onlinelibrary.wiley.com/doi/abs/10.1029/2021GL096149. e2021GL096149 2021GL096149. 177

M. Turco, S. Jerez, F. J. Doblas-Reyes, A. Aghakouchak, M. C. Llasat, and A. Provenzale. Skilful forecasting of global fire activity using seasonal climate predictions. *Nature Communications*, 9, 2018. ISSN 20411723. doi: 10.1038/s41467-018-05250-0. URL http://dx.doi.org/10.1038/s41467-018-05250-0. 177

J. Ying, M. Collins, W. Cai, A. Timmermann, P. Huang, D. Chen, and K. Stein. Emergence of climate change in the tropical pacific. *Nature Climate Change*, 12:356–364, 2022. ISSN 1758-6798. doi: 10.1038/s41558-022-01301-z. URL https://doi.org/10.1038/s41558-022-01301-z. 178

J. Y. Yu, P. K. Kao, H. Paek, H. H. Hsu, C. W. Hung, M. M. Lu, and S. I. An. Linking emergence of the central pacific el niño to the atlantic multidecadal

oscillation. *Journal of Climate*, 28:651–662, 5 2015. ISSN 08948755. doi: 10.1175/JCLI-D-14-00347.1. URL https://journals.ametsoc.org/view/journals/clim/28/2/jcli-d-14-00347.1.xml. 175